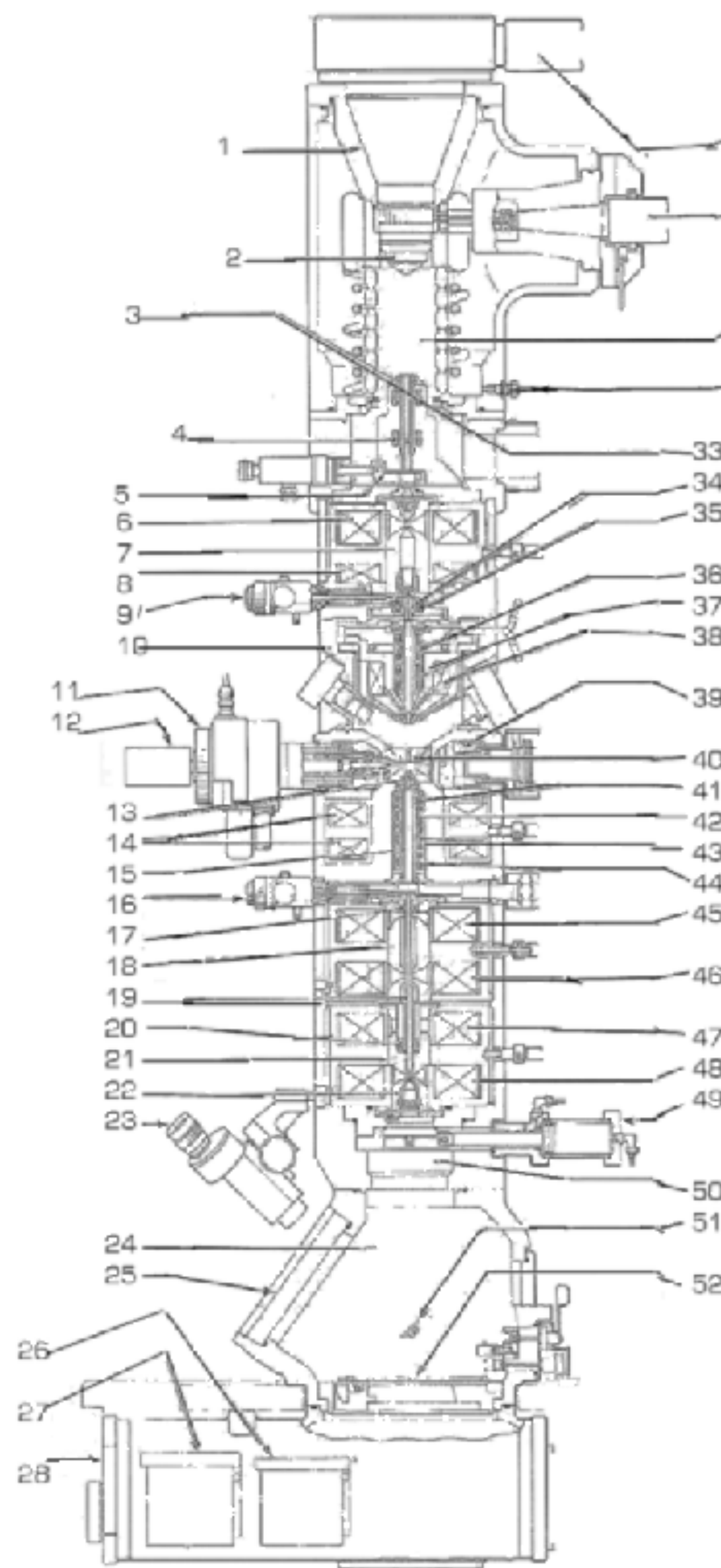
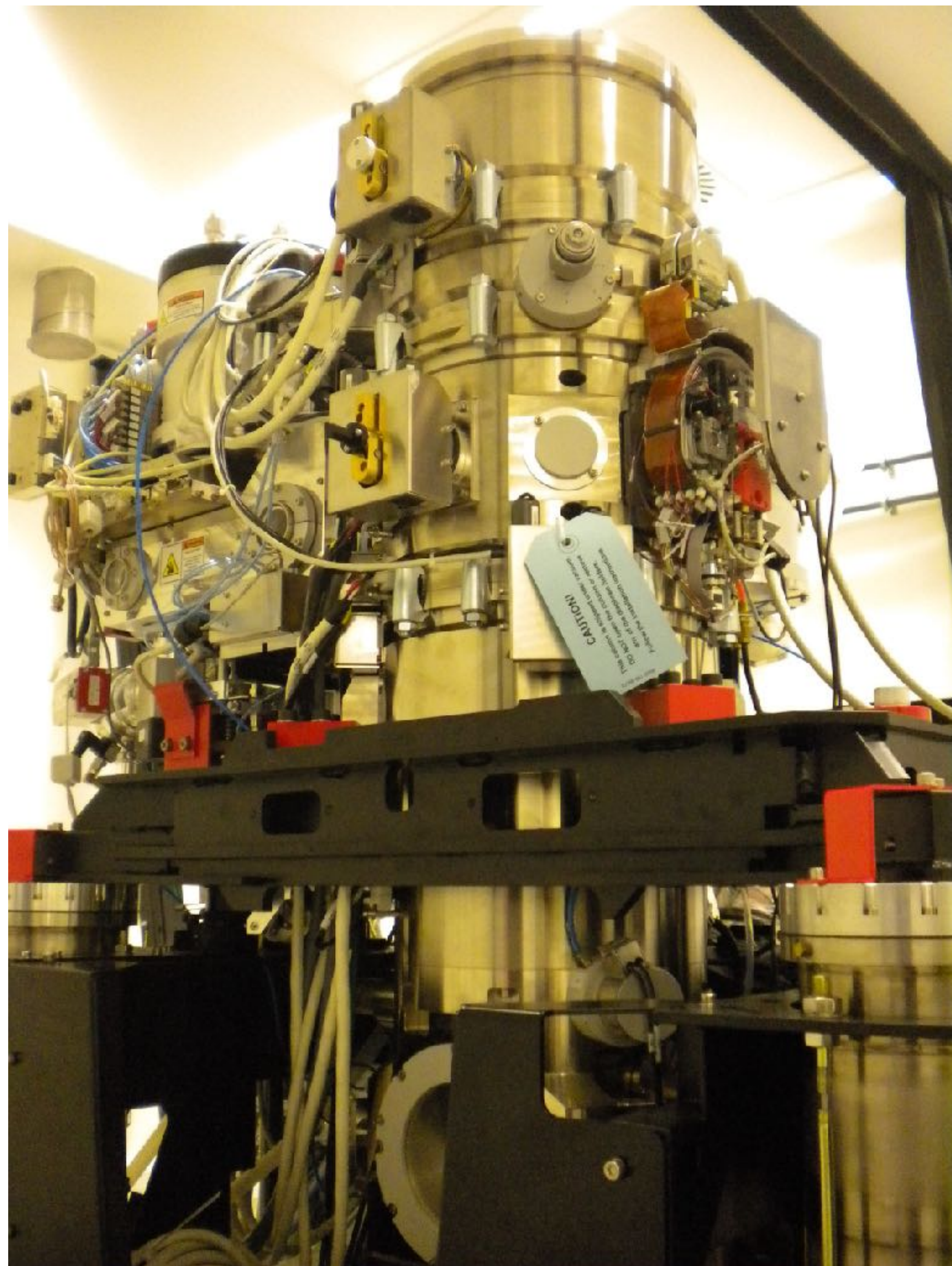


Electron microscope physics & optics

Chris Russo

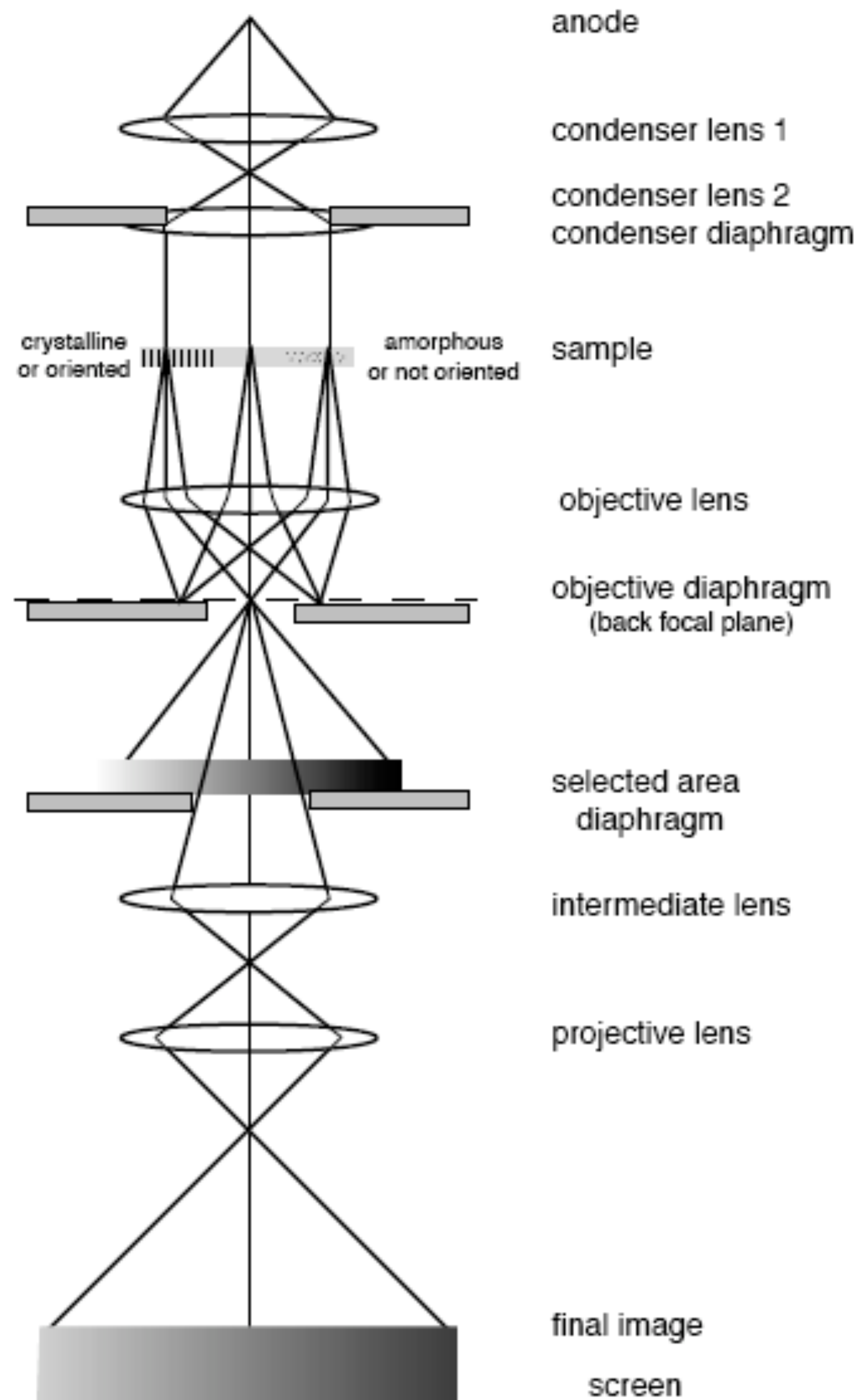
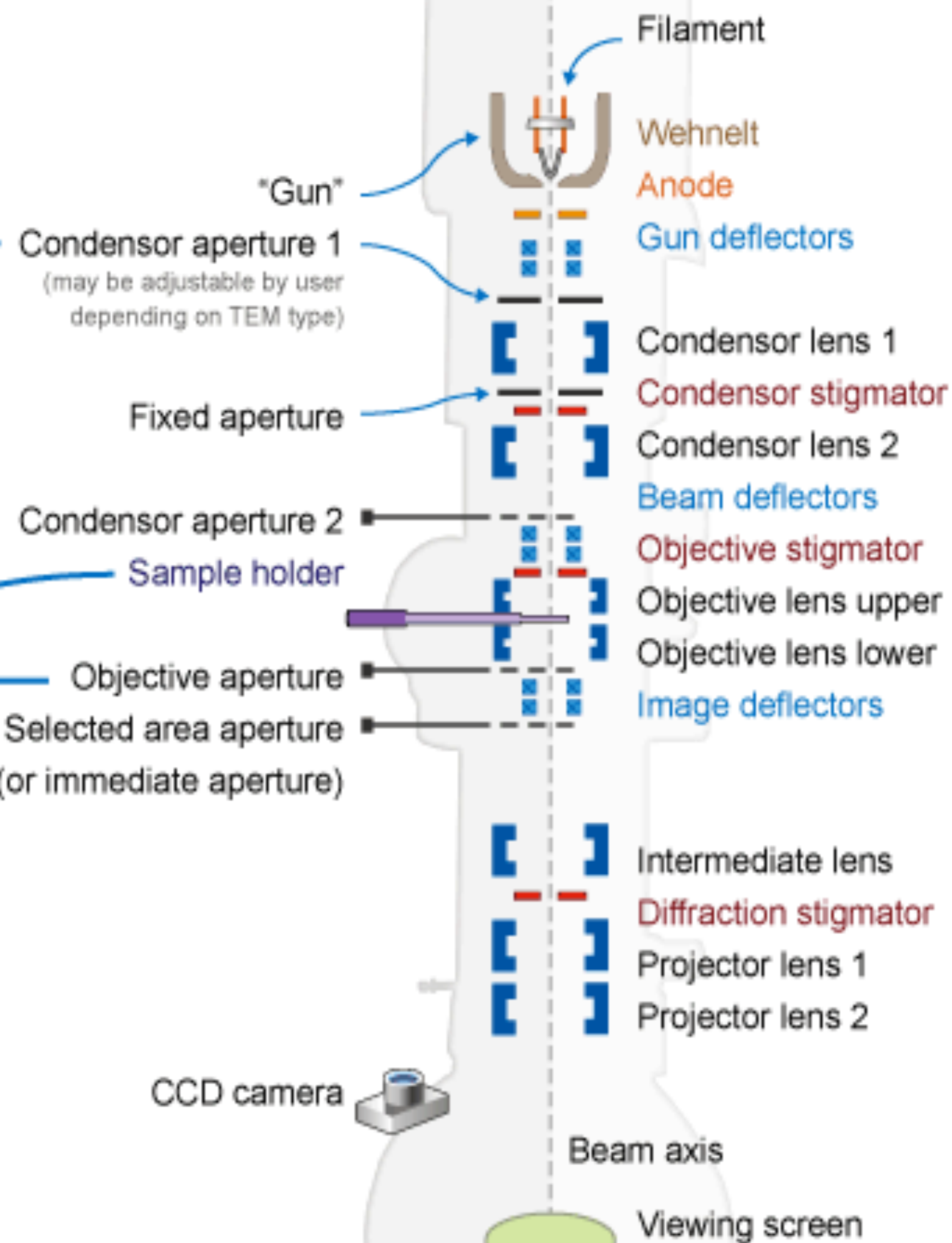
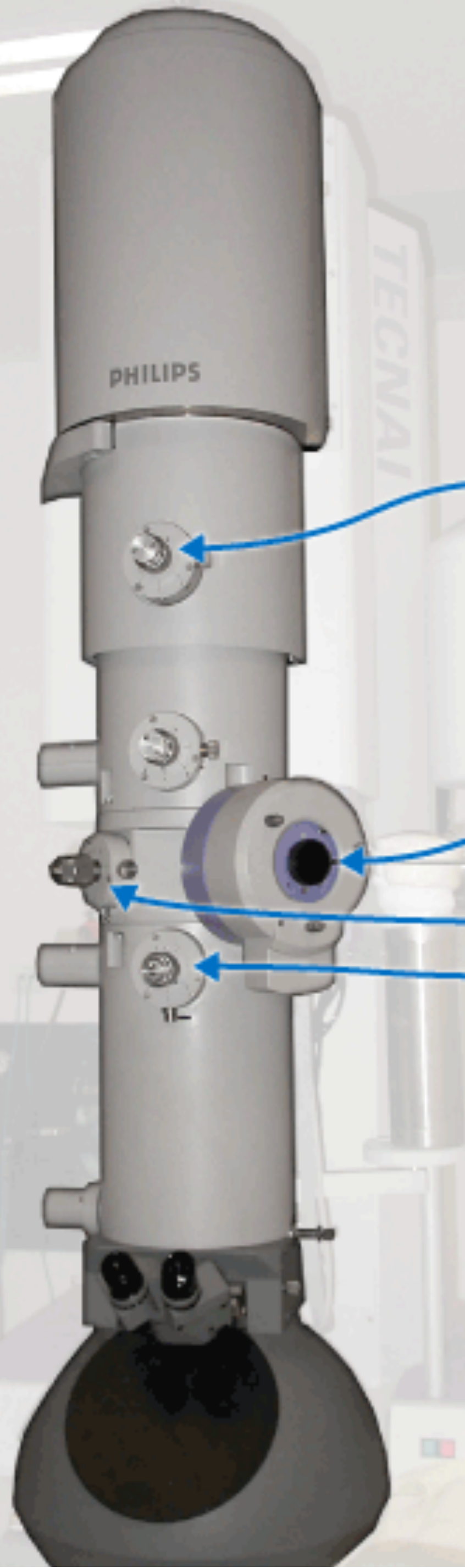




1. Electron Gun	14. Objective Lens Coil	27. Receiving Magazine	40. Objective Polepiece
2. Wehnelt Unit	15. Objective Lens Liner Tube	28. Camera Chamber	41. Objective Lens Stigmator Coil
3. Anode	16. Field Limiting Aperture	29. Lift Arm	42. 1st Image Shift Coil
4. Electron Gun Second Beam Deflector Coil	17. Intermediate Lens Stigmator Coil	30. HT Cable	43. Objective Minilens(OM Lens) Coil
5. Anode Chamber Isolation Valve	18. Intermediate Polepiece	31. Anode Chamber	44. 2nd Image Shift Coil
6. 1st Condenser Lens Coil	19. Intermediate Lens Linear Tube	32. Gas Inlet	45. 1st Intermediate Lens Coil
7. Condenser Polepiece	20. Projector Lens Beam Deflector Coil	33. Electron Gun 1st Beam Deflector Coil	46. 2nd Intermediate Lens Coil
8. 3rd Condenser Lens Coil	21. Projector Upper Polepiece	34. Condenser Lens Stigmator Coil	47. 3rd Intermediate Lens Coil
9. Condenser Aperture Assembly	22. Projector Lower Polepiece	35. Spot Alignment Coil	48. Projector Lens Coil
10. Specimen Chamber	23. Binoculars	36. Condenser Lens 1st Beam Deflector Coil	49. Viewing Chamber Isolation Valve
11. Goniometer	24. Viewing Chamber	37. Condenser Lens 2nd Beam Deflector Coil	50. High Resolution Diffraction Chamber
12. Specimen Holder	25. Viewing Window	38. Condenser Minilens(CM Lens) Coil	51. Small Screen
13. Stigmator Screening Cylinder	26. Dispensing Magazine	39. Stage Heater	52. Large Screen

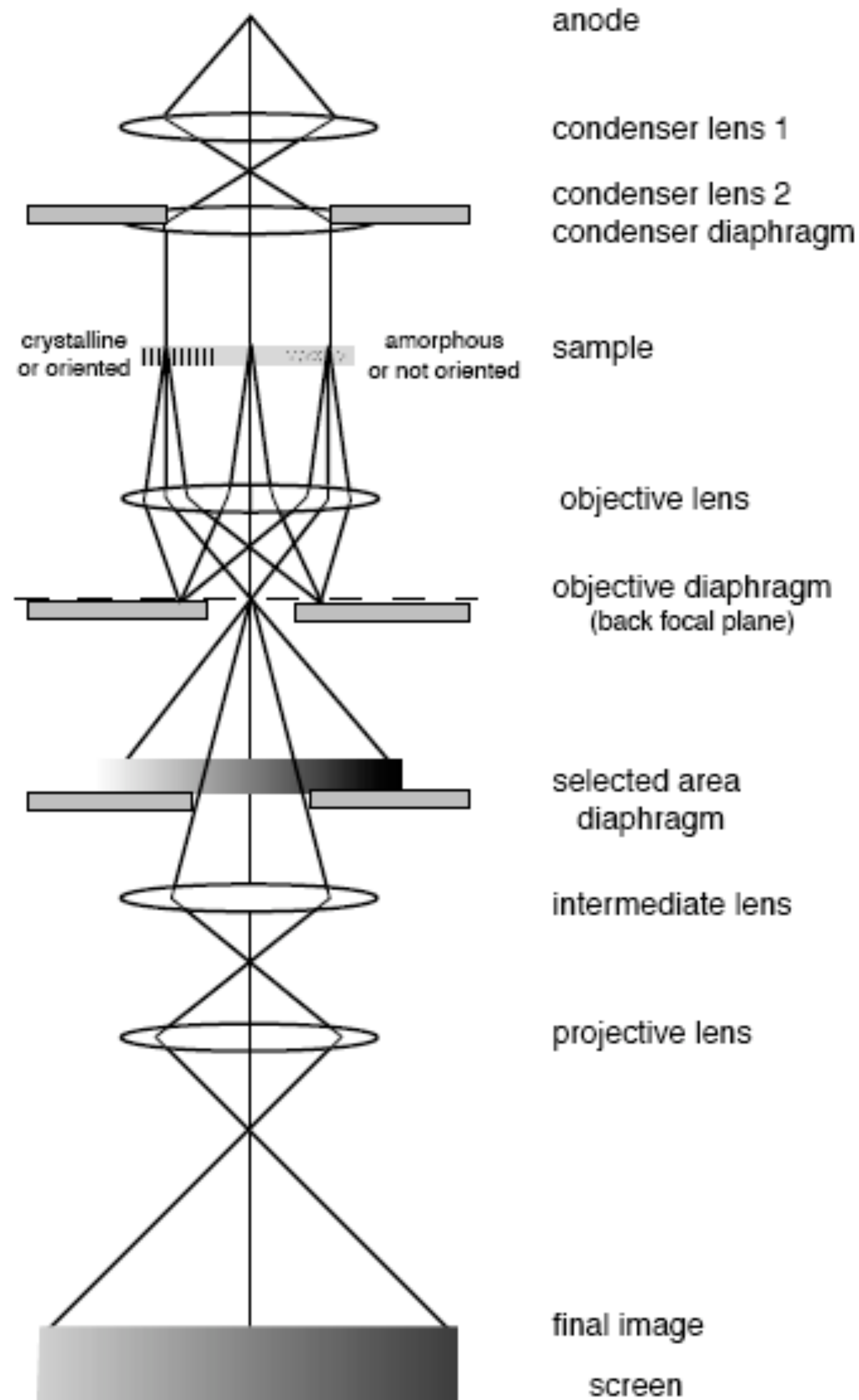
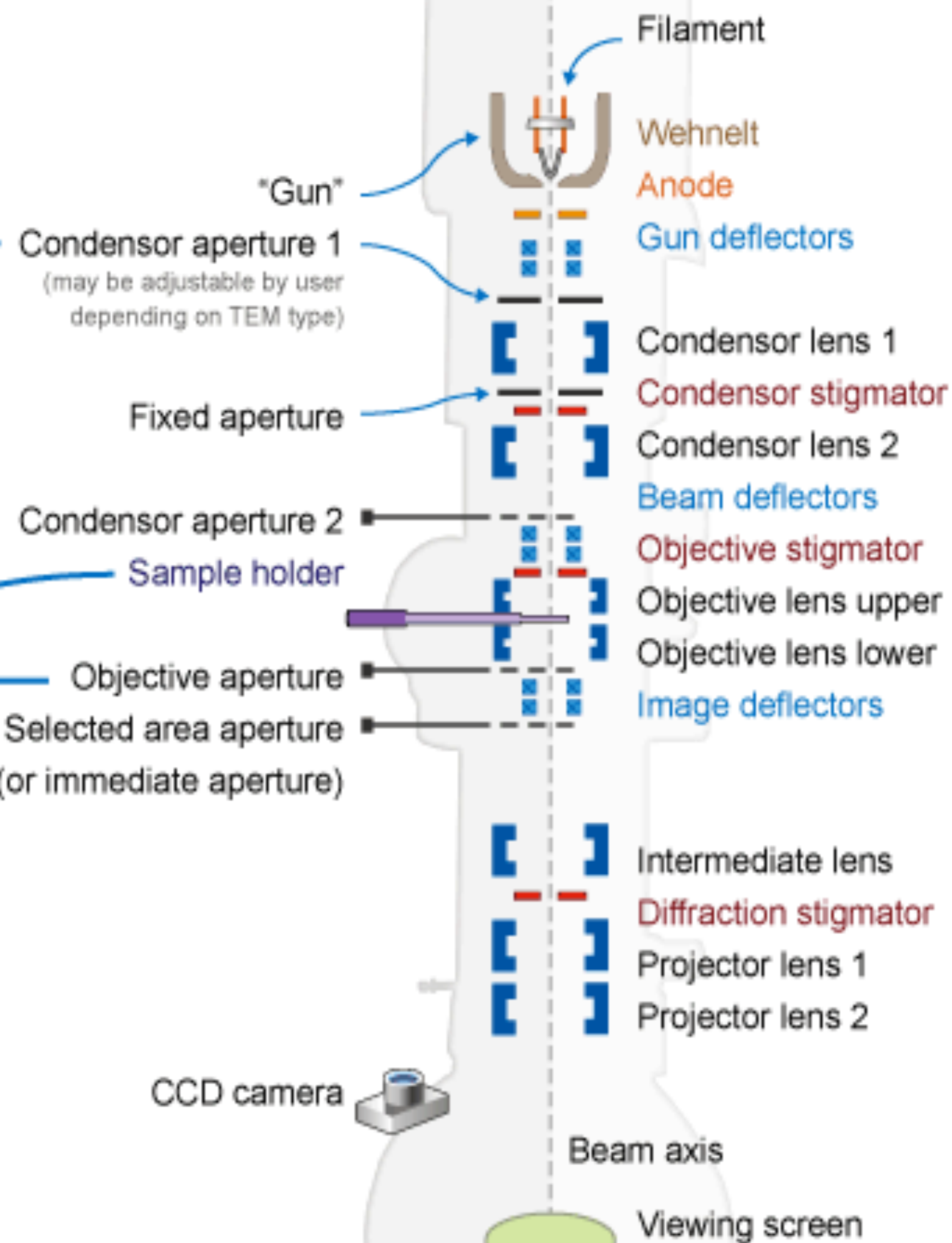
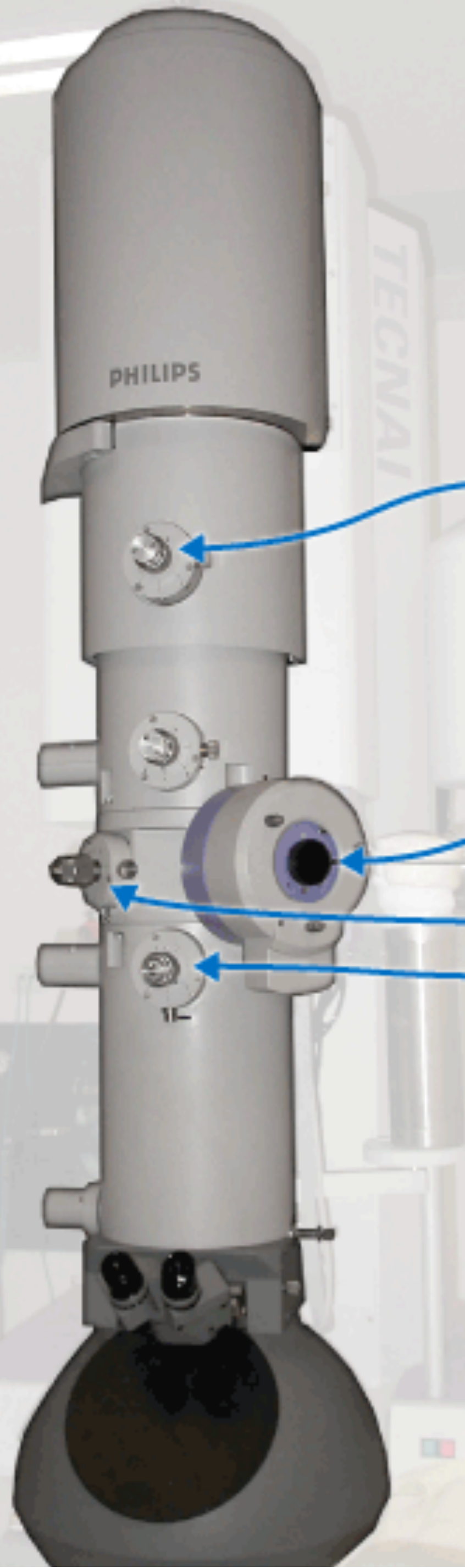
Example TEM schematic

One of many types of TEMs

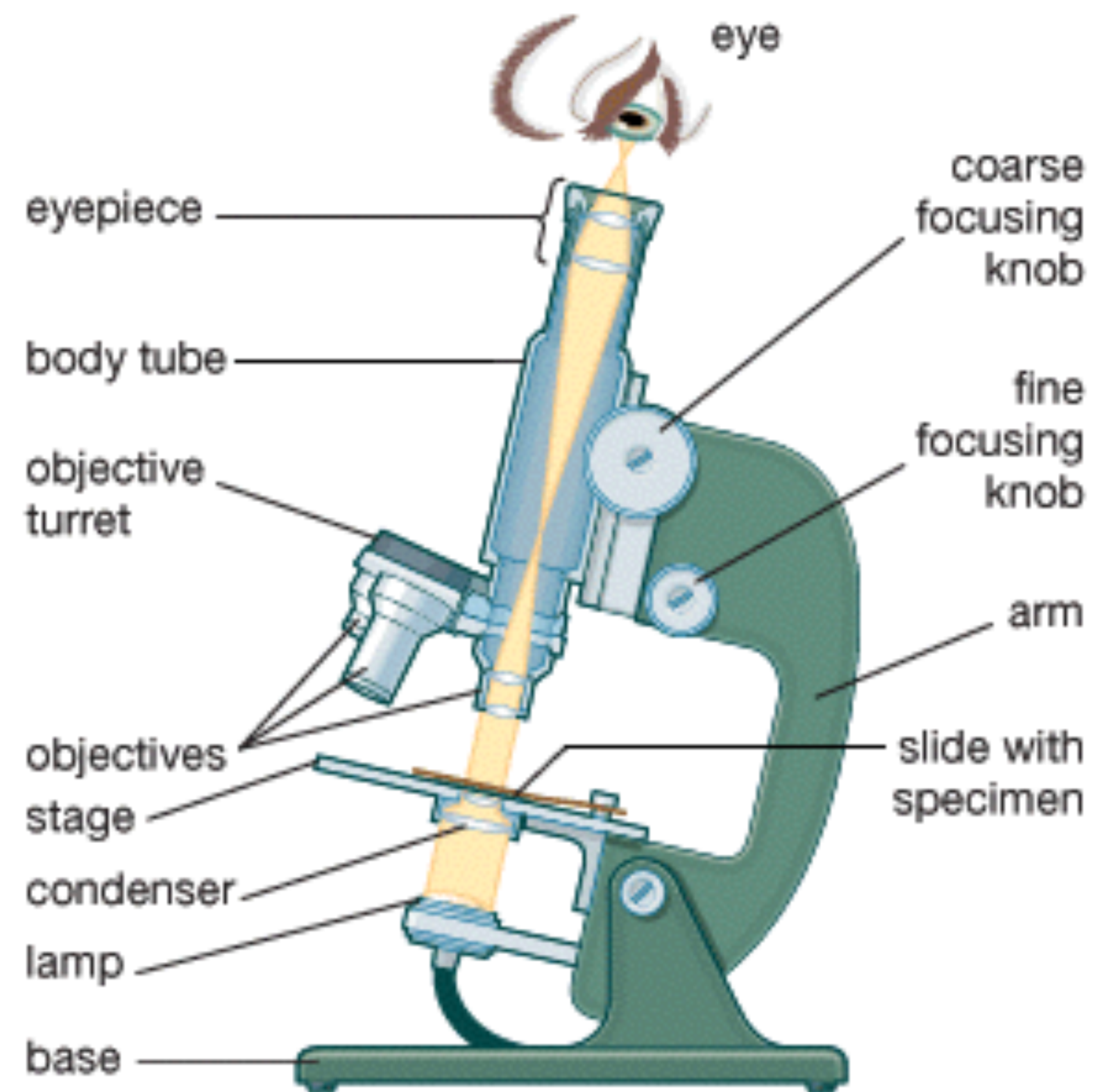


Example TEM schematic

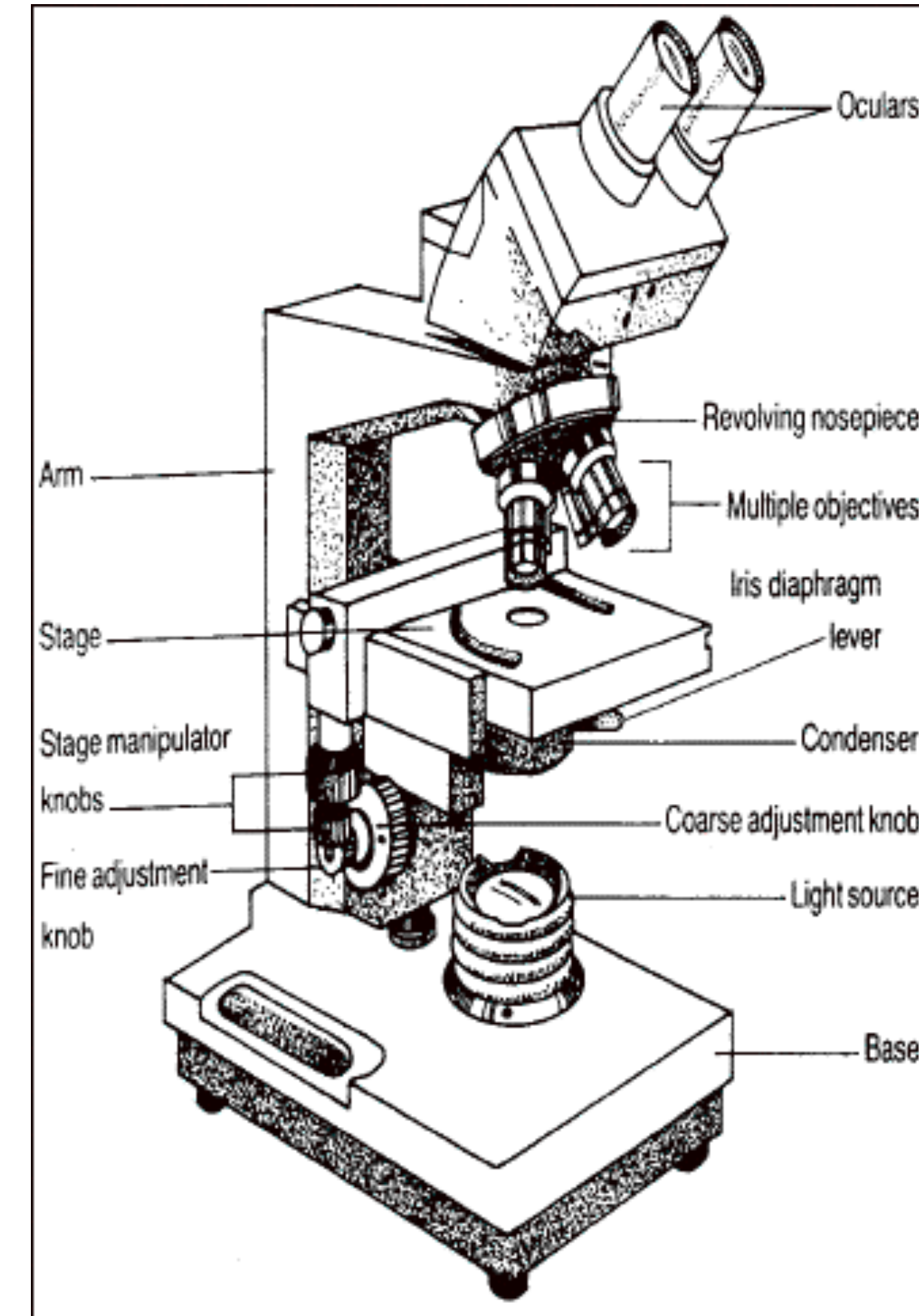
One of many types of TEMs



The Optical Microscope

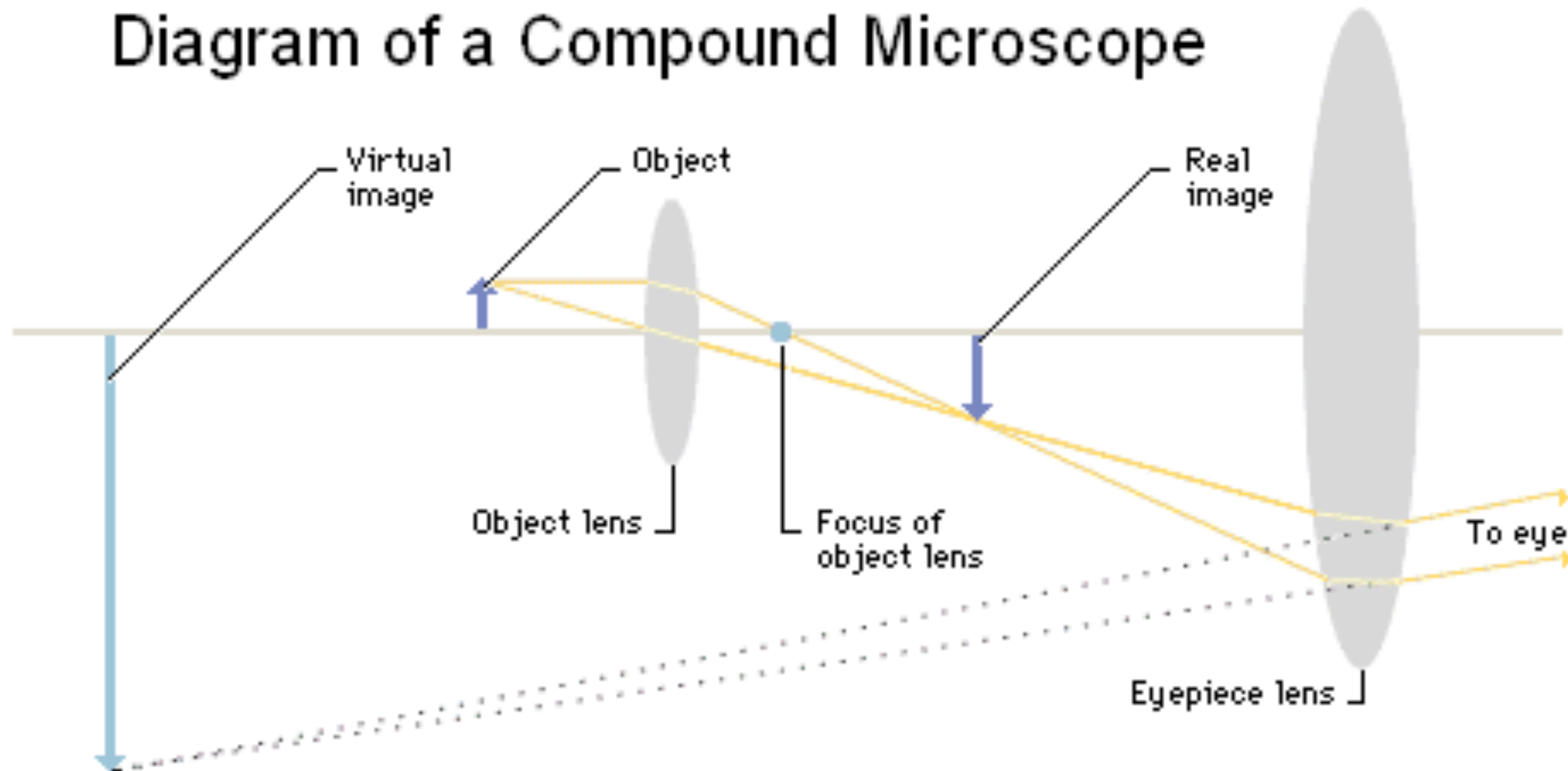


© 2006 Encyclopædia Britannica, Inc.

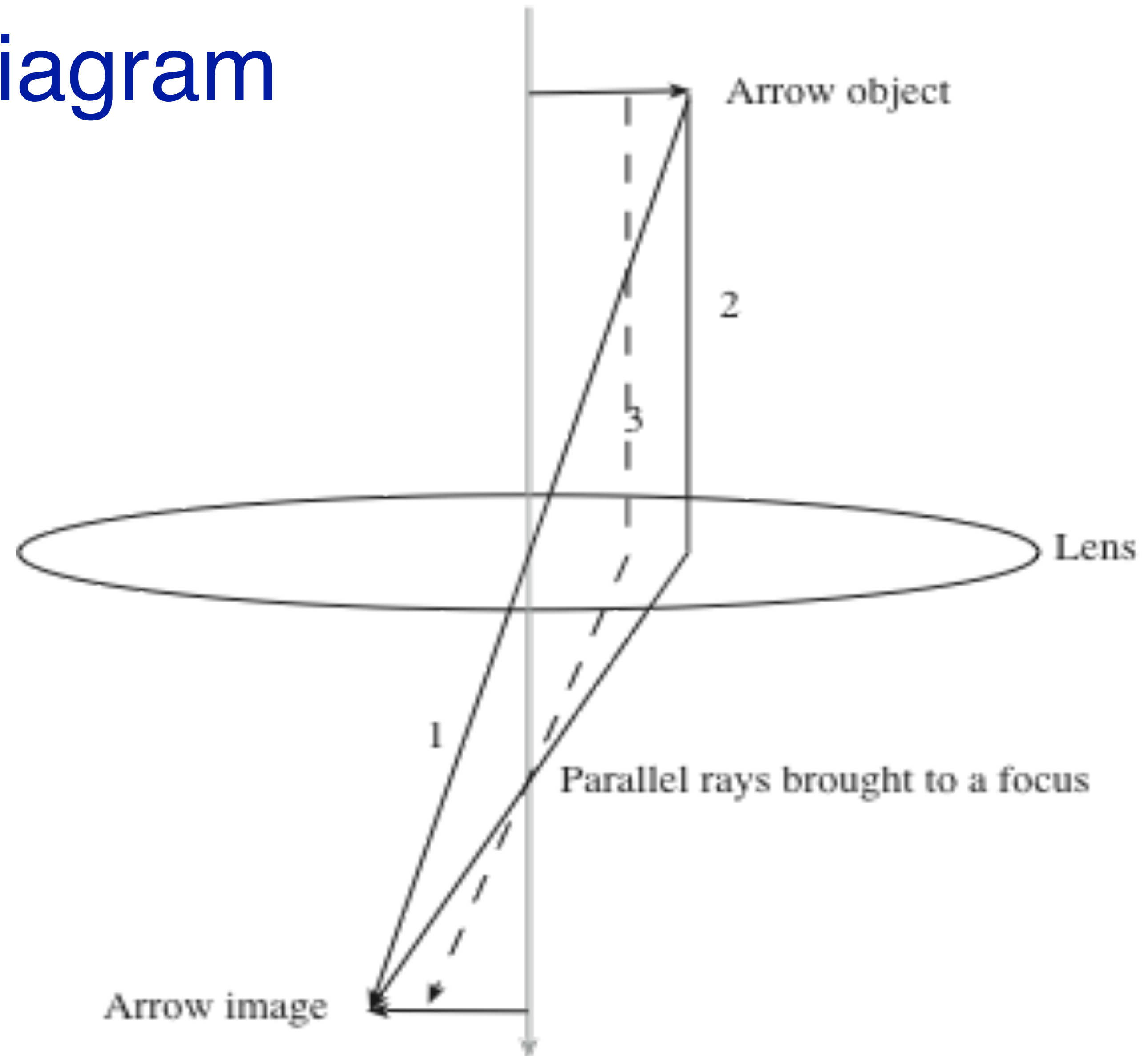


Optical Microscope Lens Diagram

Diagram of a Compound Microscope



Convex lens ray diagram



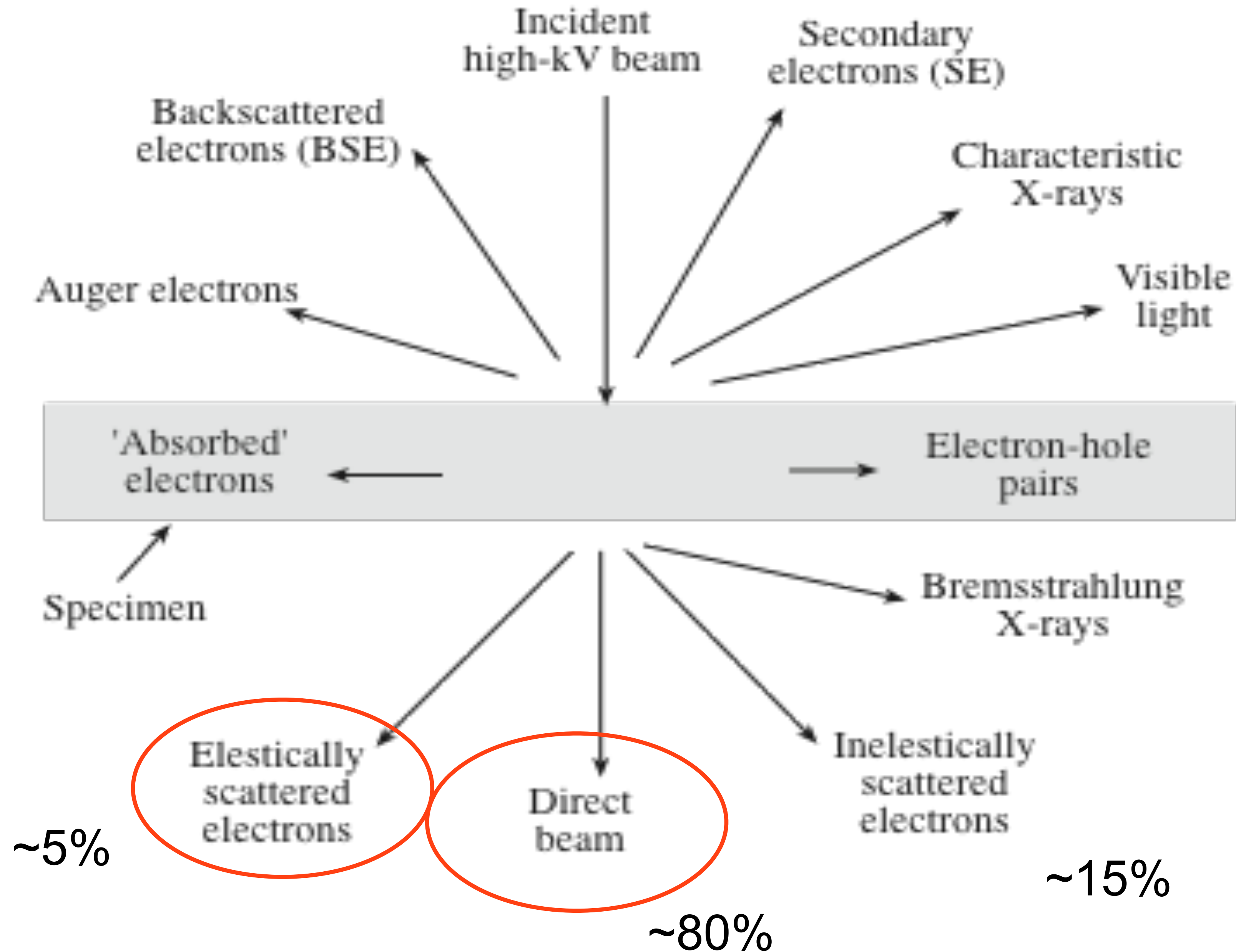
Important diagram
(Draw in ~10 seconds)

Steps are 1, 2, 3

Very basic electron image formation

- Part of the beam electrons hit the nuclei or electrons of the atoms in specimen, and they are “scattered”
- Scattered electrons can be removed using apertures
- Dense sections in the specimen (i.e. stained parts) cause more scattering and are dark in the image plane
- The most important factor in image formation in TEM is **scattering**
- (NOTE! In light microscopy: it's absorption, in phase contrast microscopy, it's photon scattering)

Large Number of Signals



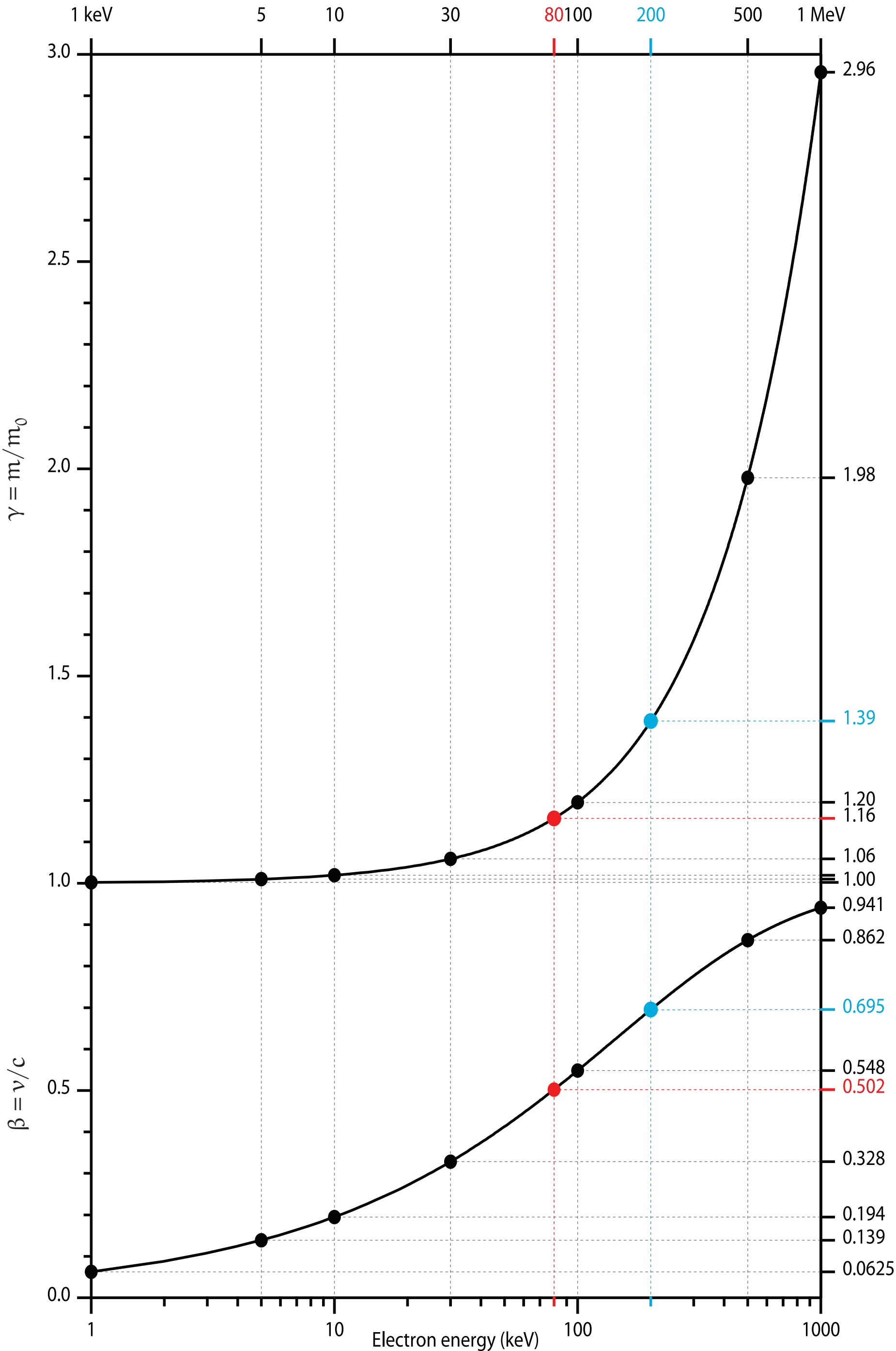
Properties of electrons are used for simple calculations

Reimer 2008

Table 2.1. Properties of the electron.			
Rest mass	m_0	$=$	$9.1091 \times 10^{-31} \text{ kg}$
Charge	e	$=$	$-1.602 \times 10^{-19} \text{ C}$
Kinetic energy	E	$=$	eU $1 \text{ eV} = 1.602 \times 10^{-19} \text{ J}$
Velocity of light	c	$=$	$2.9979 \times 10^8 \text{ m s}^{-1}$
Rest energy	E_0	$=$	$m_0 c^2 = 511 \text{ keV}$
Spin	s	$=$	$\hbar/4\pi$
Planck's constant	h	$=$	$6.6256 \times 10^{-34} \text{ J s} = 4.136 \times 10^{-15} \text{ eV} \cdot \text{s}$
Nonrelativistic ($E \ll E_0$)		Relativistic ($E \sim E_0$)	
Newton's law	$\mathbf{F} = \frac{d\mathbf{p}}{d\tau}$	$\mathbf{F} = \frac{d}{d\tau}(m\mathbf{v})$	(2.7)
Mass	$m = m_0$	$m = m_0 / \sqrt{1 - v^2/c^2}$	(2.8a)
Energy	$E = eU = \frac{1}{2} m_0 v^2$	$mc^2 = m_0 c^2 + eU = E_0 + E$	(2.9)
		$m = m_0 (1 + E/E_0)$	(2.8b)
Velocity	$v = \sqrt{2E/m_0}$	$v = c \sqrt{1 - \frac{1}{(1 + E/E_0)^2}}$	(2.10)
Momentum	$p = m_0 v = \sqrt{2m_0 E}$	$p = \sqrt{2m_0 E (1 + E/2E_0)}$	(2.11)
		$= \frac{1}{c} \sqrt{2EE_0 + E^2}$	
Wavelength	$\lambda = \frac{h}{p} = h/\sqrt{2m_0 E}$	$\lambda = h/\sqrt{2m_0 E (1 + E/2E_0)}$	(2.12)
		$= hc/\sqrt{2EE_0 + E^2}$	

Example: how many electrons are in the column at a time?

Some words: Volts vs. electron Volts
 dose, fluence, flux
 ~~electron density~~



Limitations of electron beam instruments

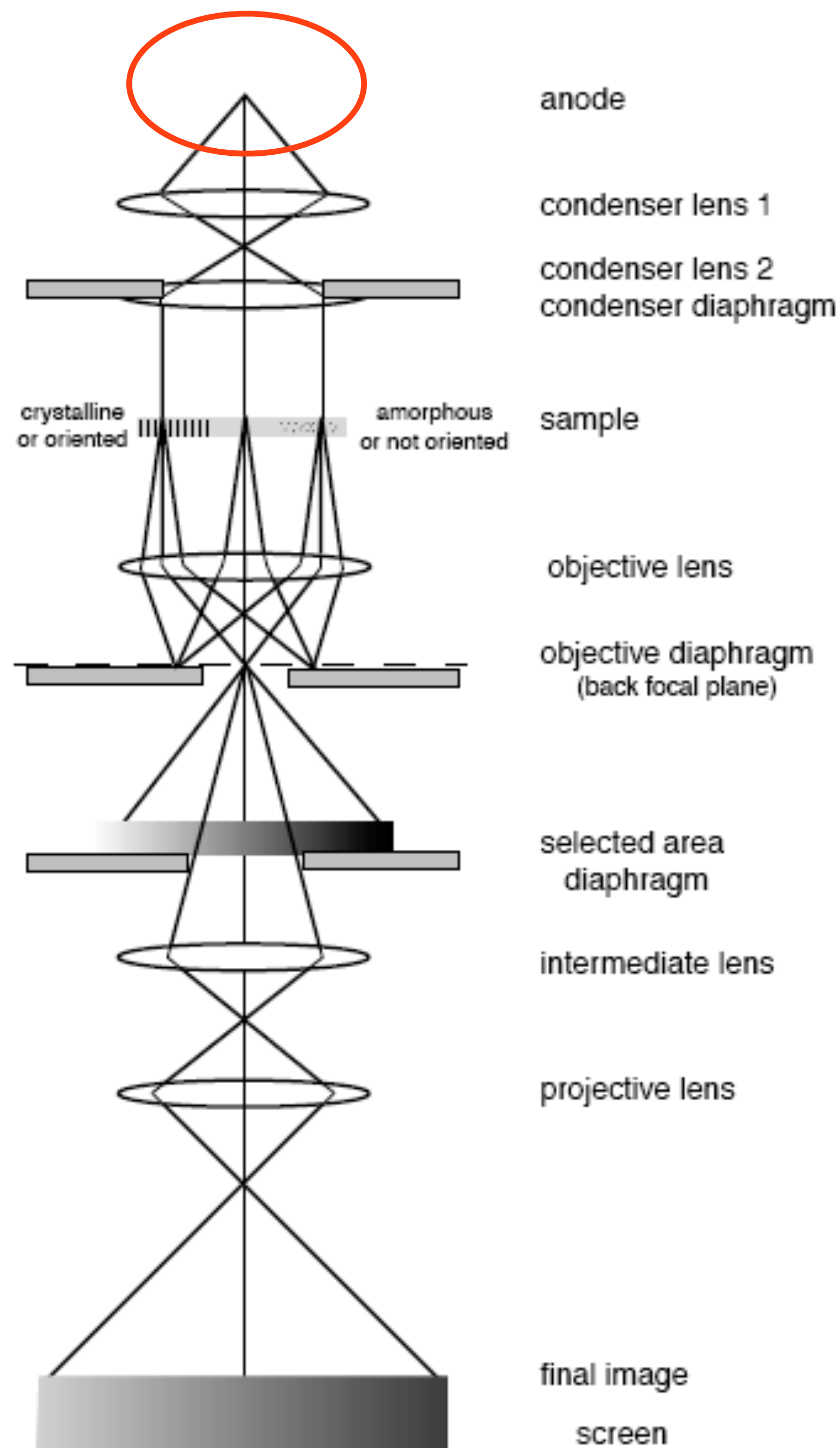
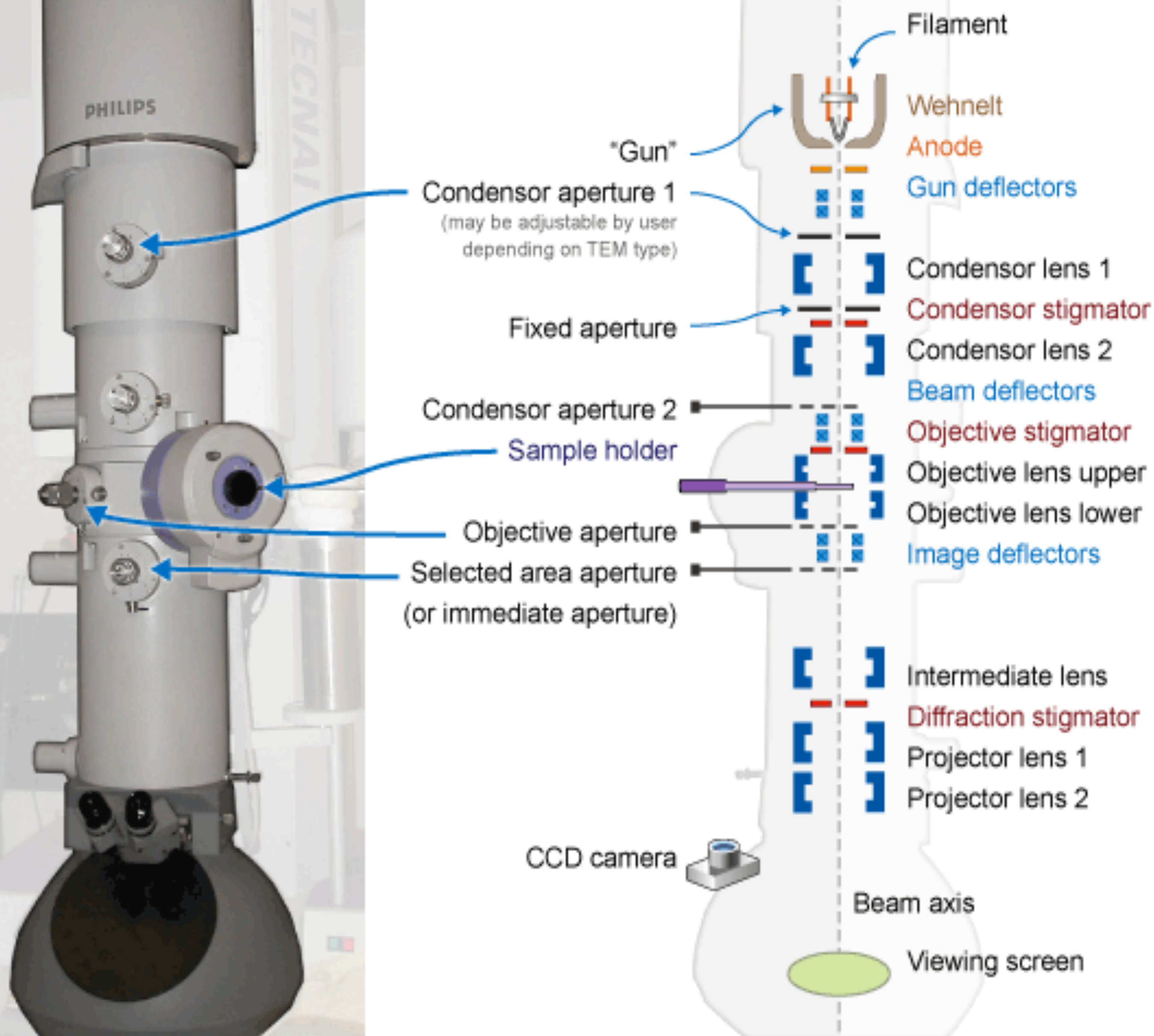
- Vacuum
- Damage Damage Damage Damage Damage Damage Damage Damage

Electron microscopes are used to simulate damage in the core of a nuclear reactor!

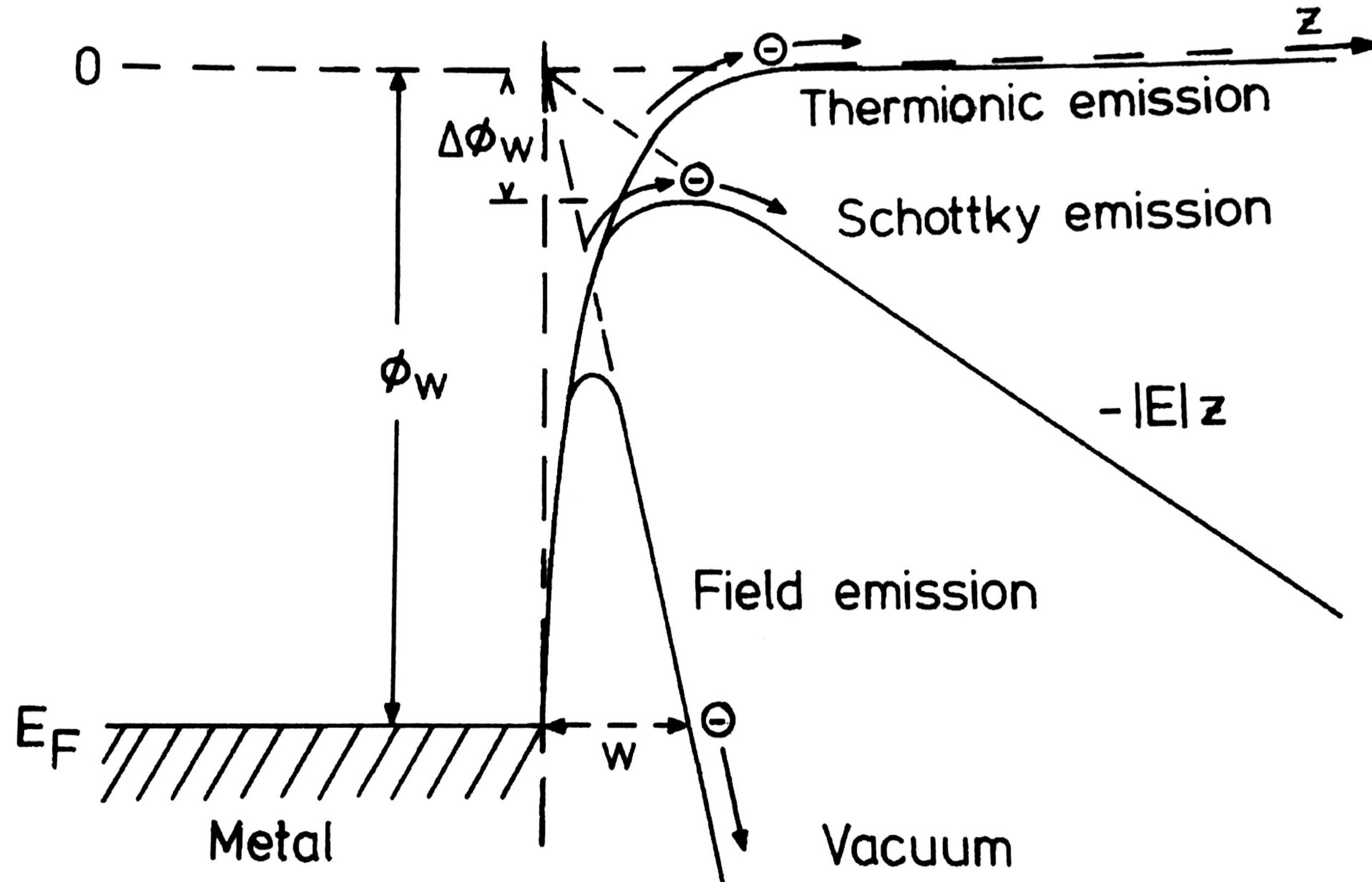
- Electron lenses terrible (relative to photon lenses) and hard to make
- Have to record many many noisy images, lots of data (just ask Jake & Toby!)
- Charging: non-conductive samples charge up and act like lenses
- Samples must be very thin and are quite fragile, move around in the beam and are often difficult to make
- Expensive (From £300k to £10M) Krios is £3000/day

Example TEM schematic

One of many types of TEMs



How to get electrons



Thermal Emission Source

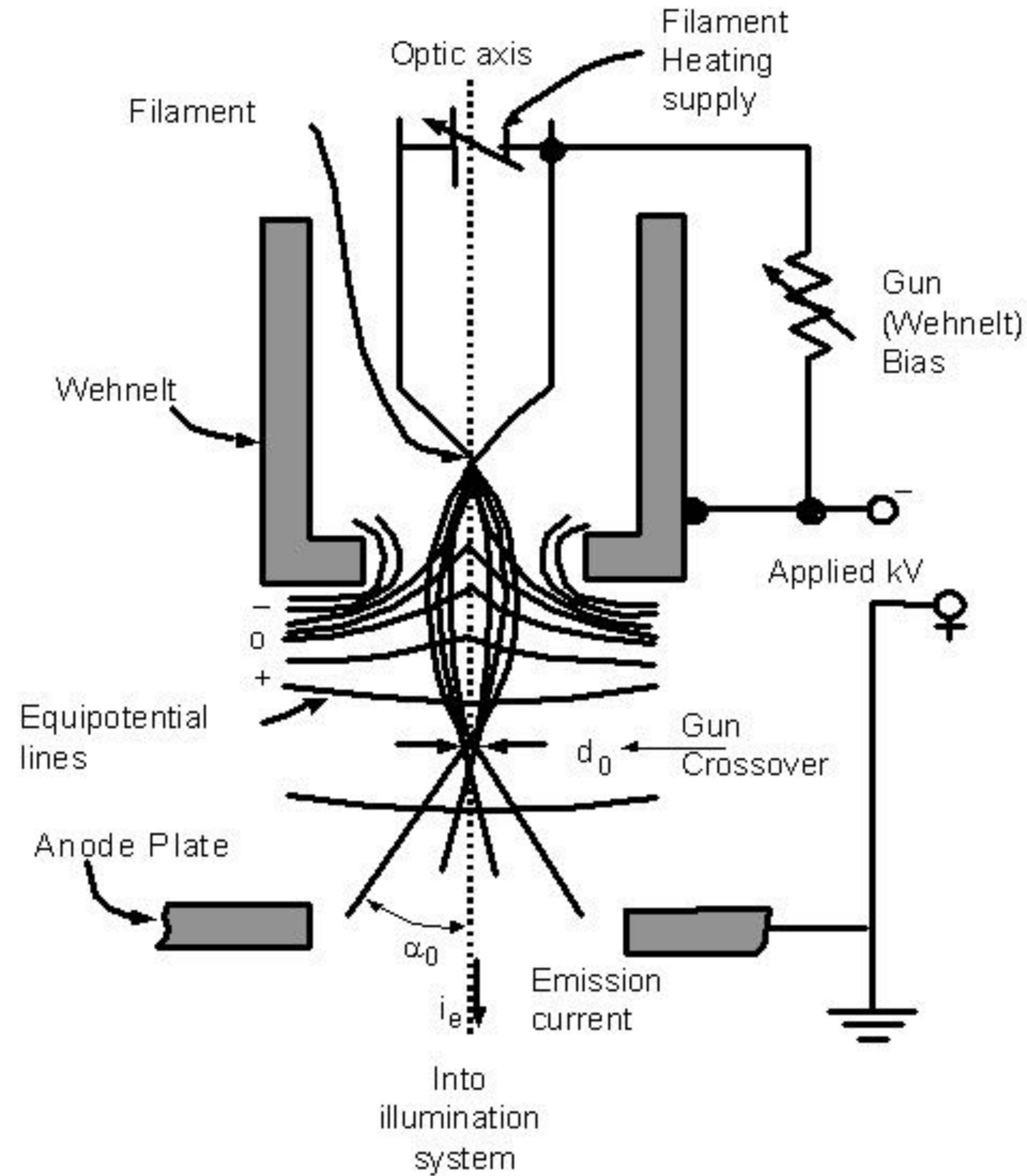
Important ideas

Wehnelt is the first lens

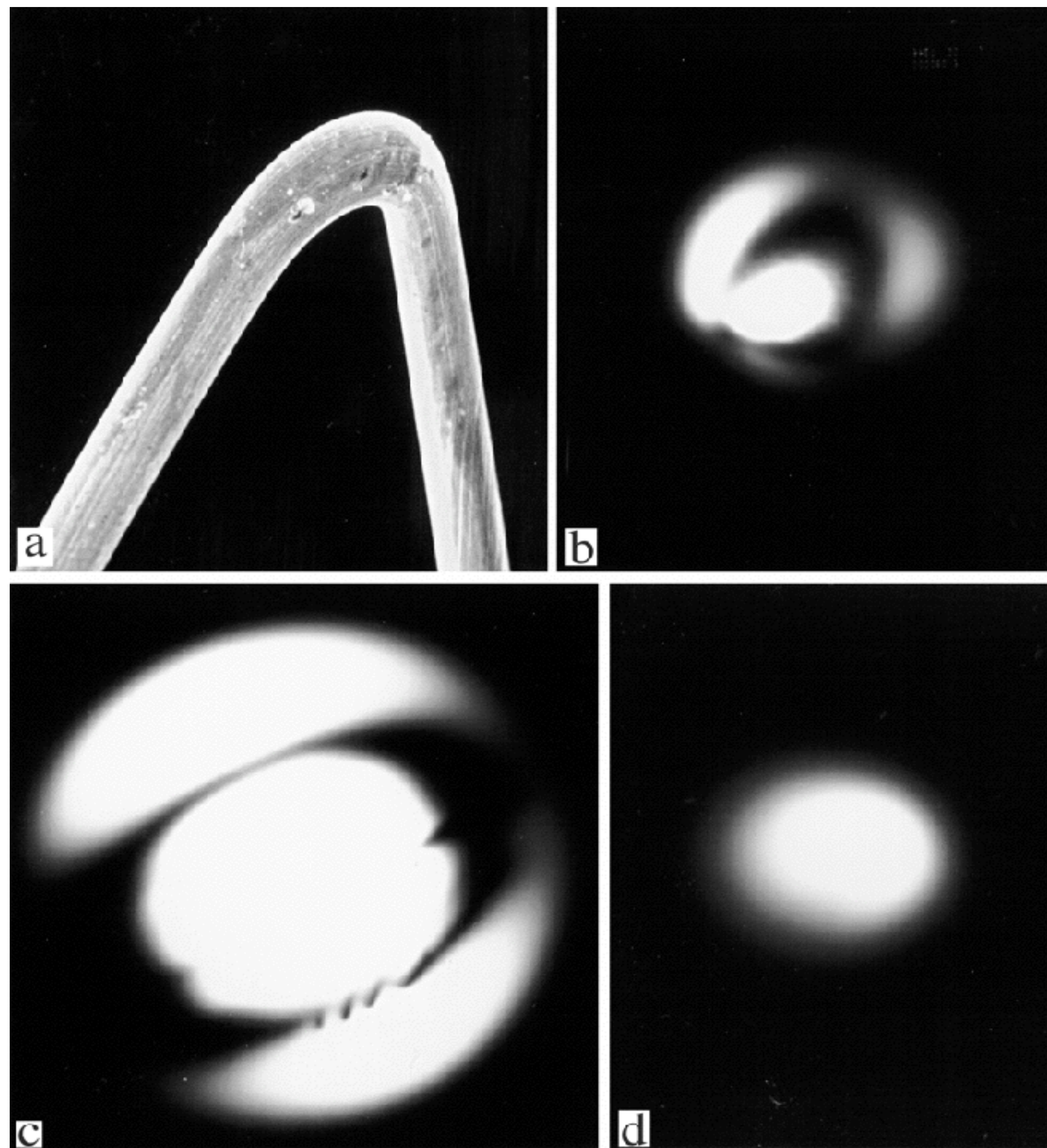
Anode plate

Dimensions

Cross-over



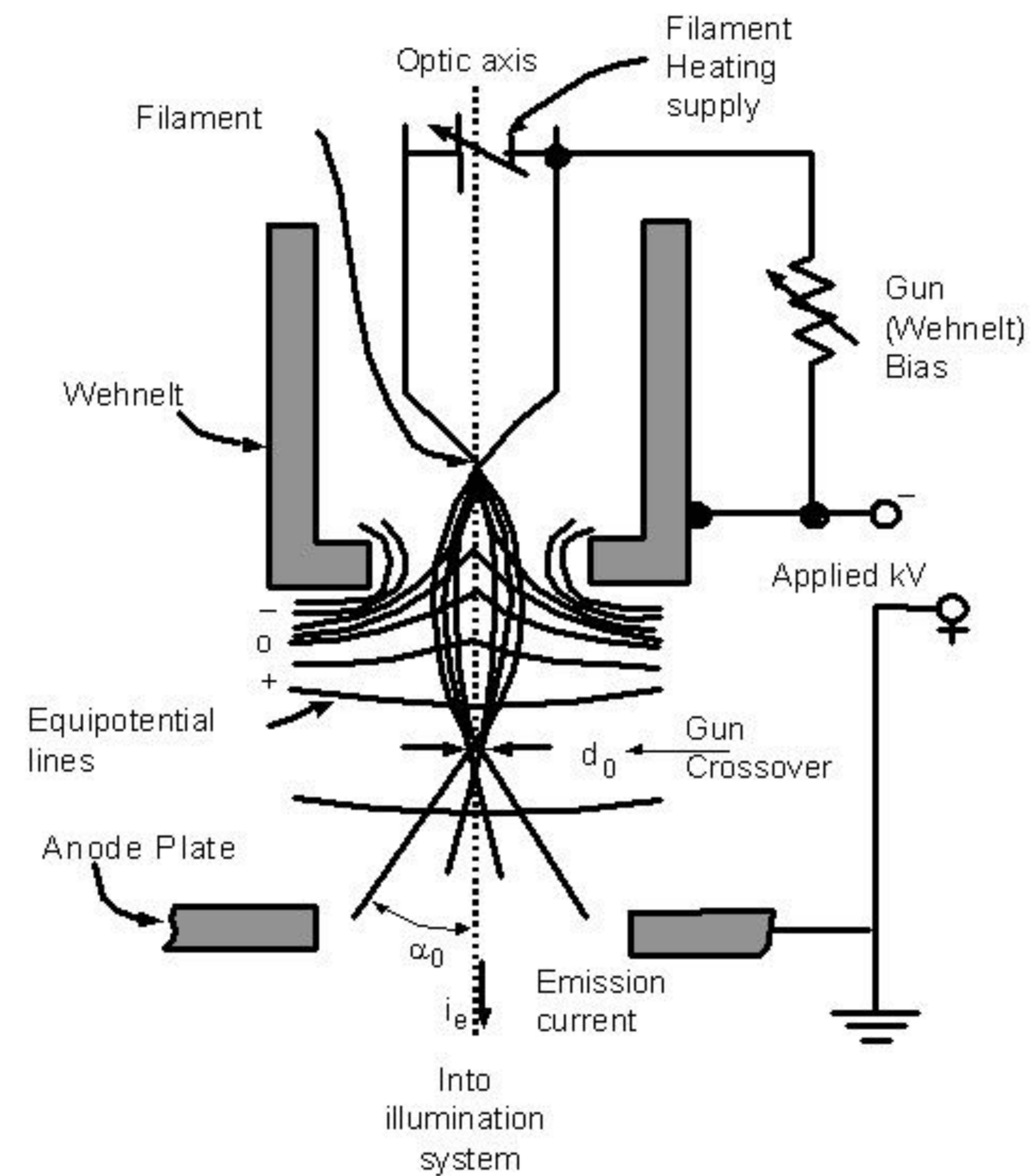
Hairpin filament



Underfocused but centered

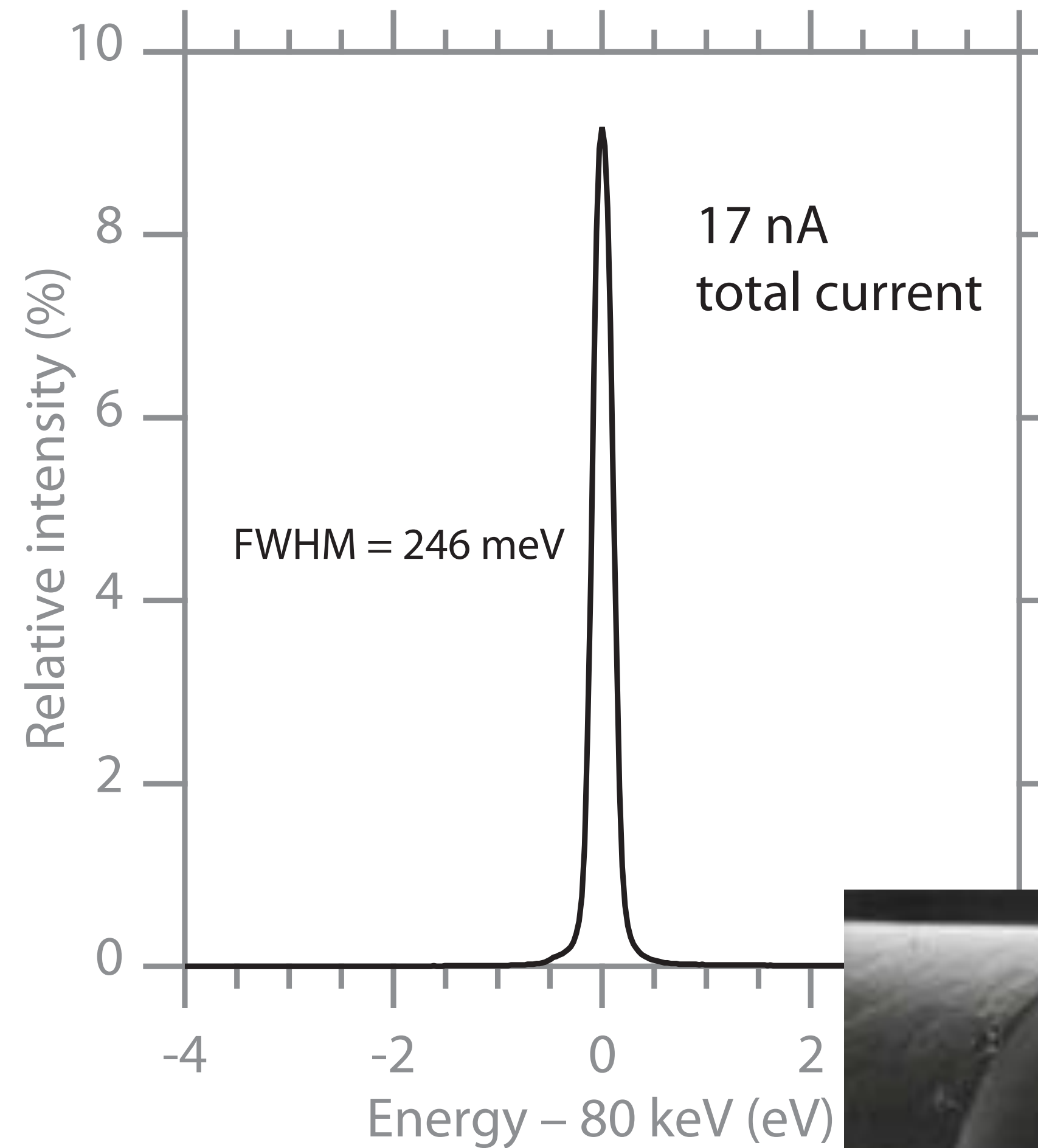
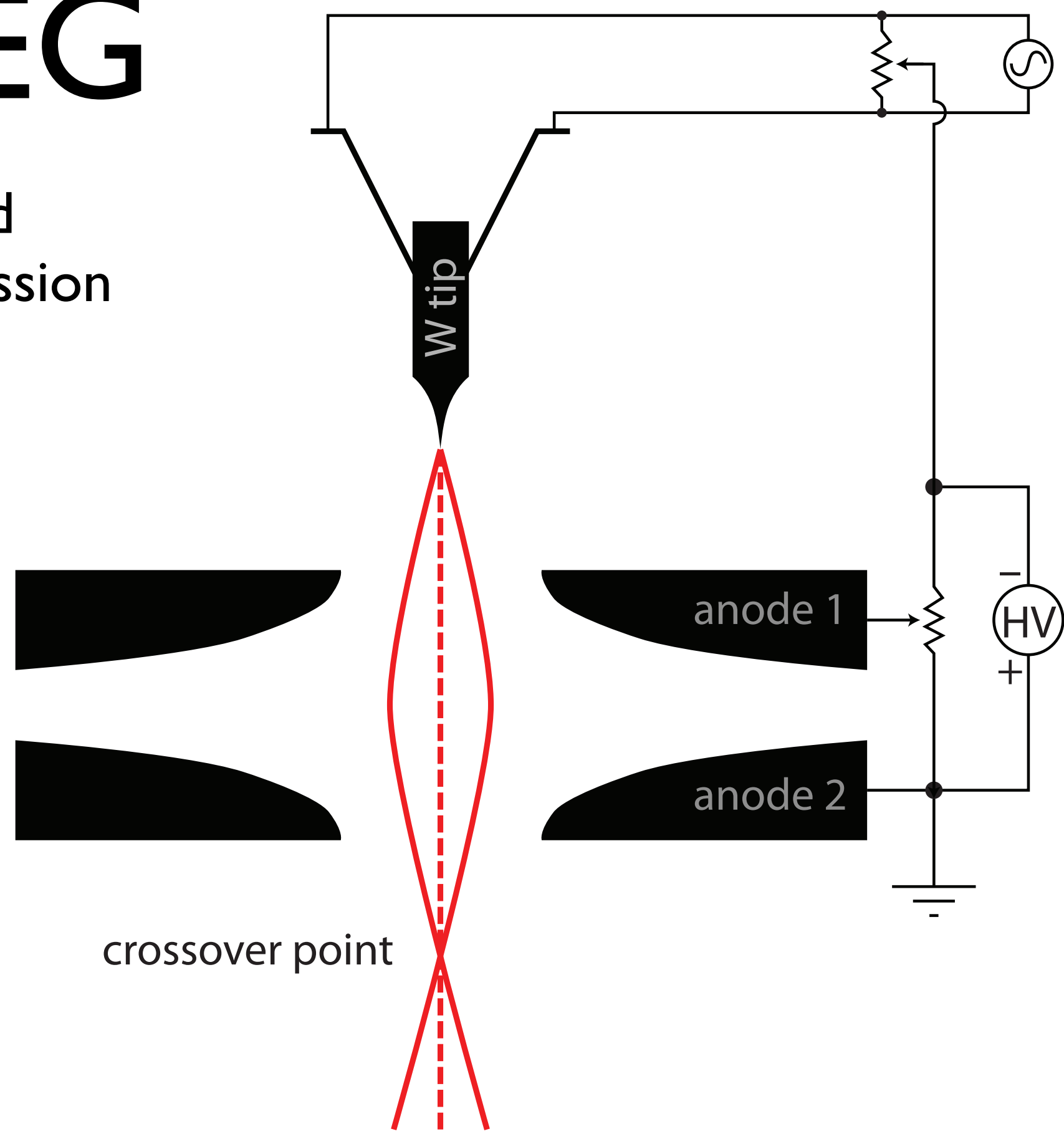
Underfocused & off center

Centered & focused

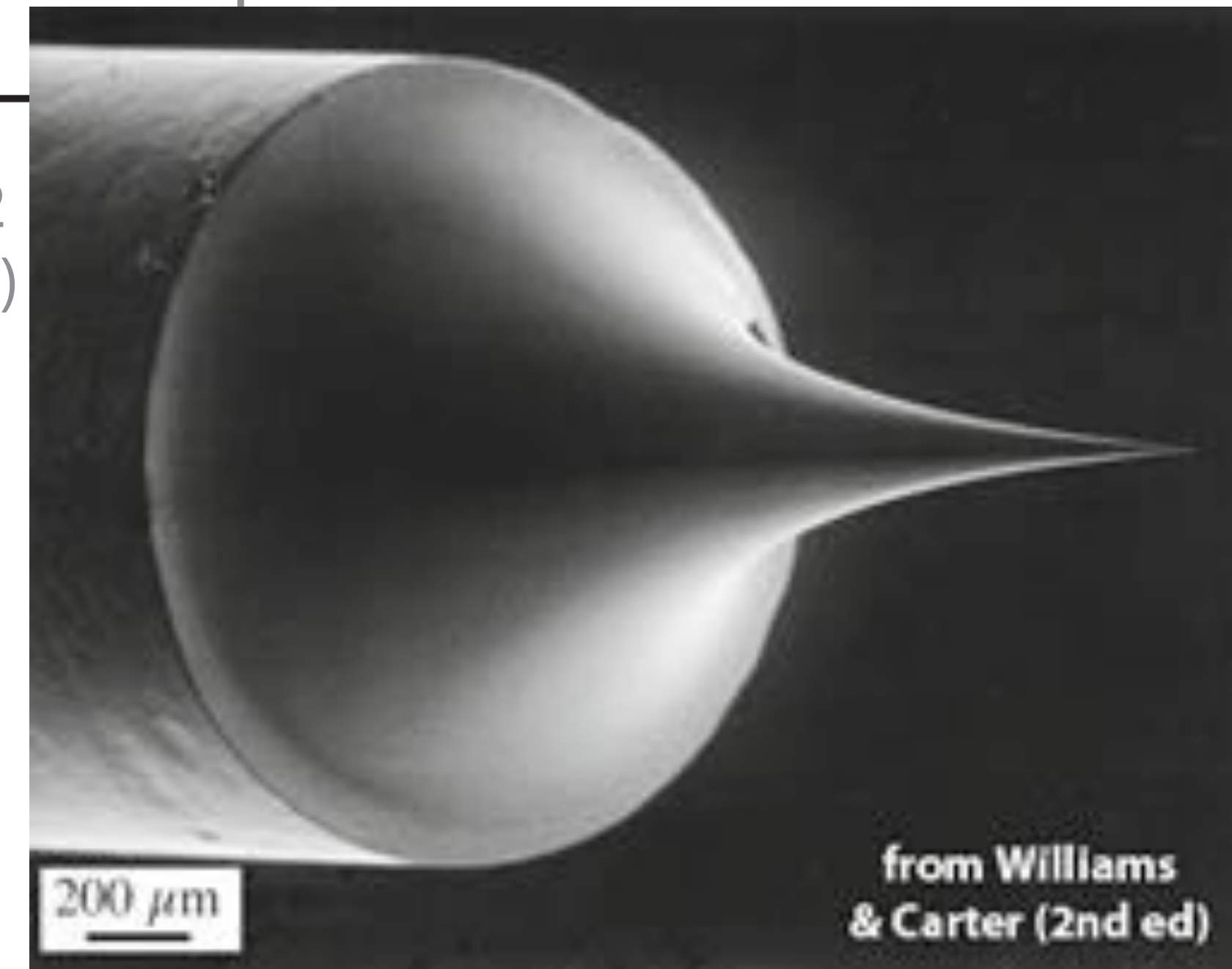


FEG

Field
Emission
Gun

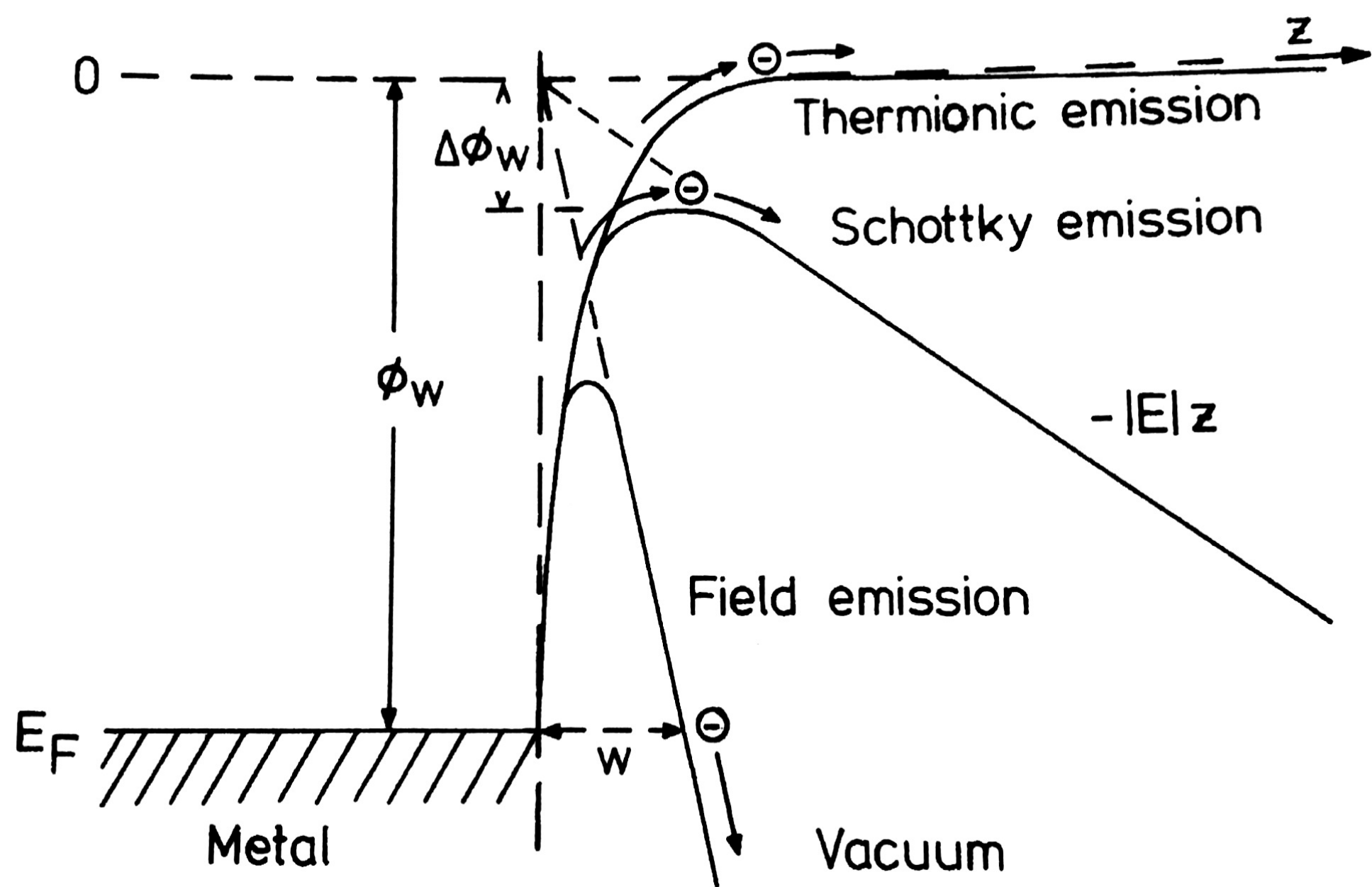


Brighter,
More coherent
More monochromatic source
crudely, think 'laser vs. light bulb'



from Williams
& Carter (2nd ed)

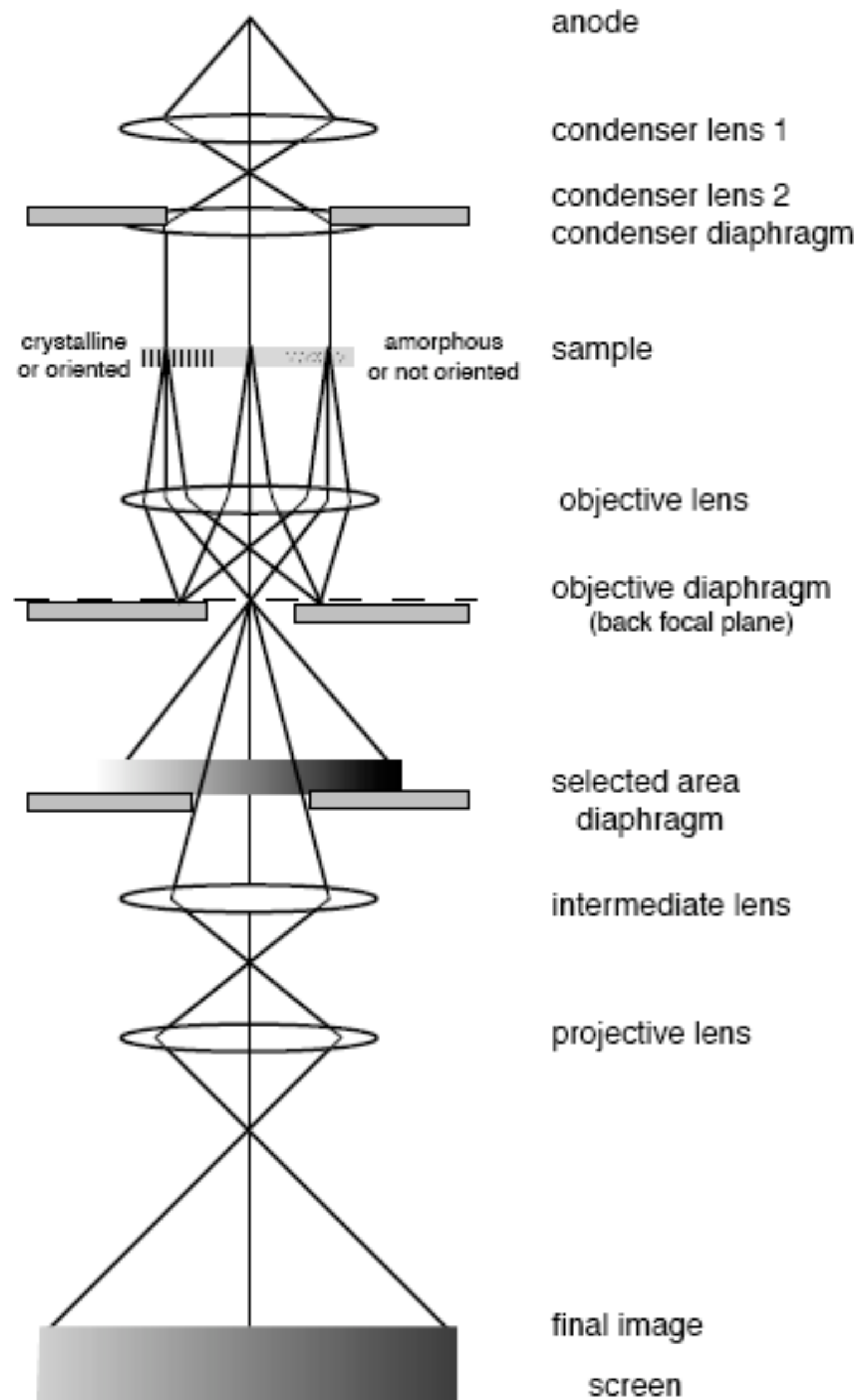
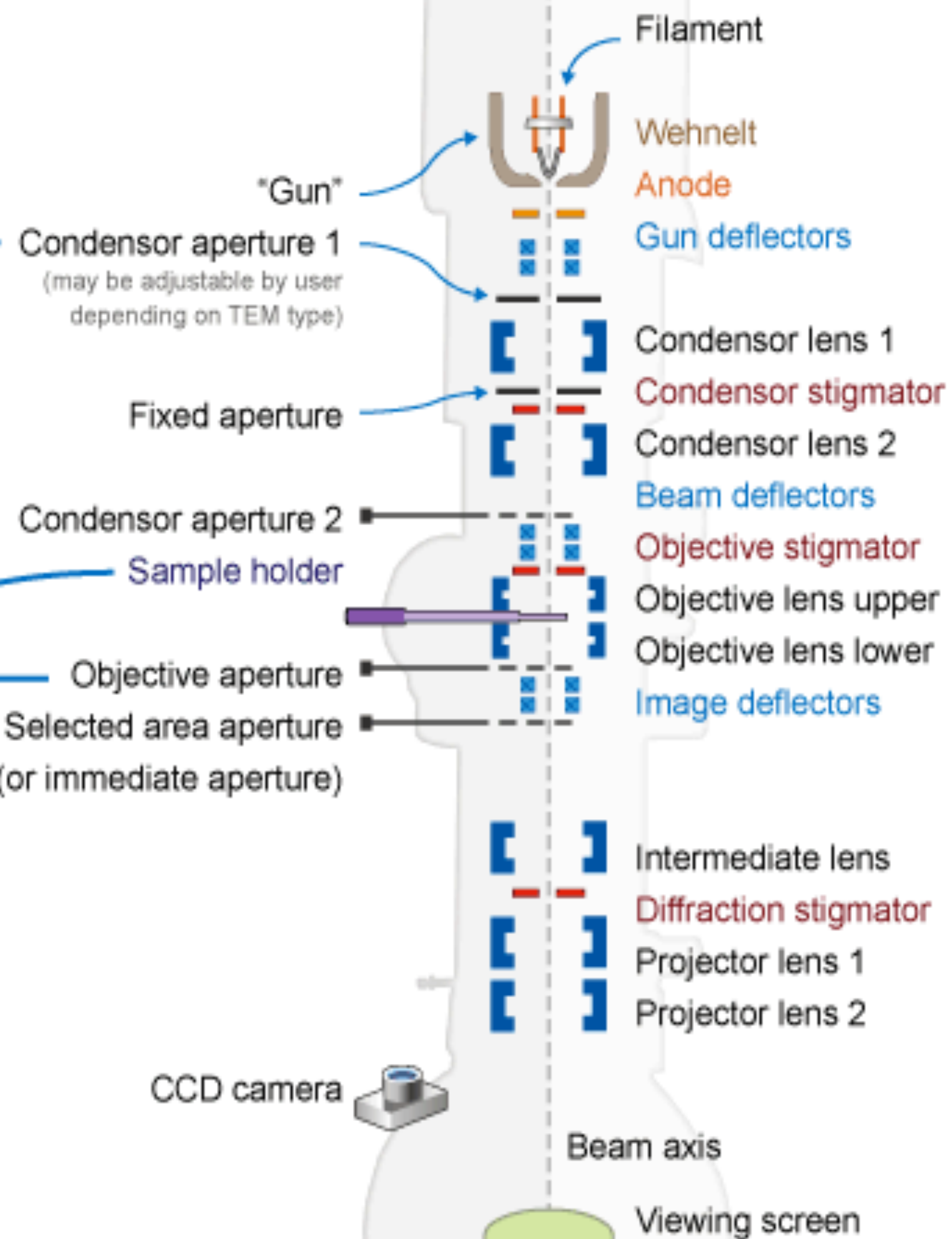
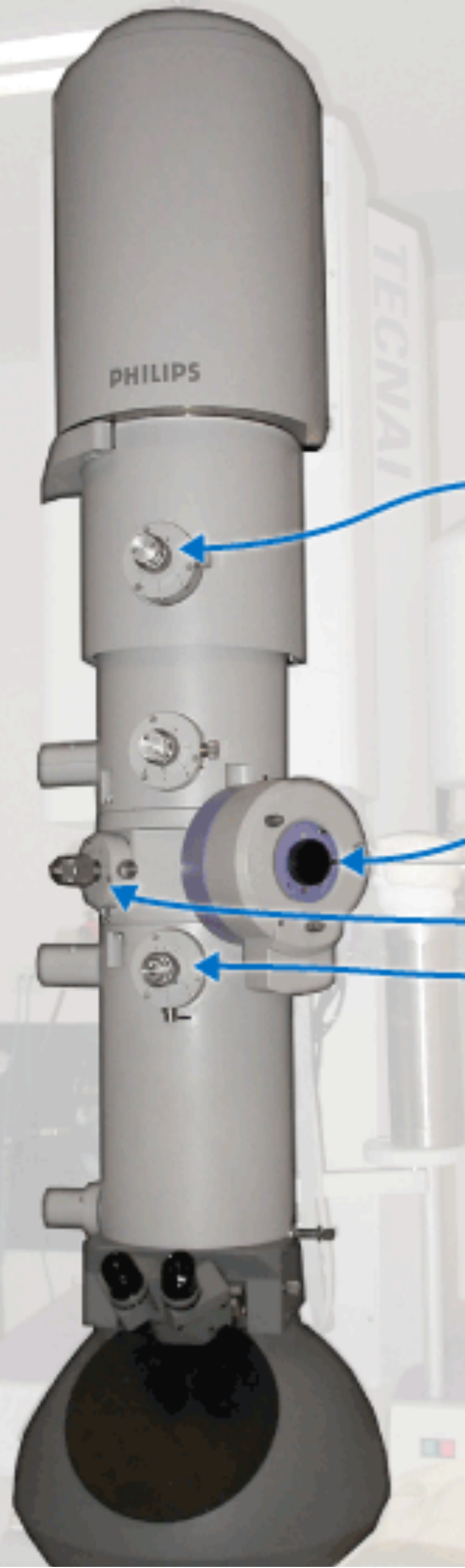
Characteristics of Electron Sources



	Units	Tungsten	LaB ₆	FEG
Operating Temperature	K	2700	1700	300
Current Density	A/m ²	5x10 ⁴	10 ⁶	10 ¹⁰
Crossover size	μm	50	10	<0.01
Energy spread	eV	3	1.5	0.3
Stability	% / hr	<1	<1	5
Vacuum	Pa	10 ⁻²	10 ⁻⁴	10 ⁻⁸
Lifetime	hr	100	500	>1000

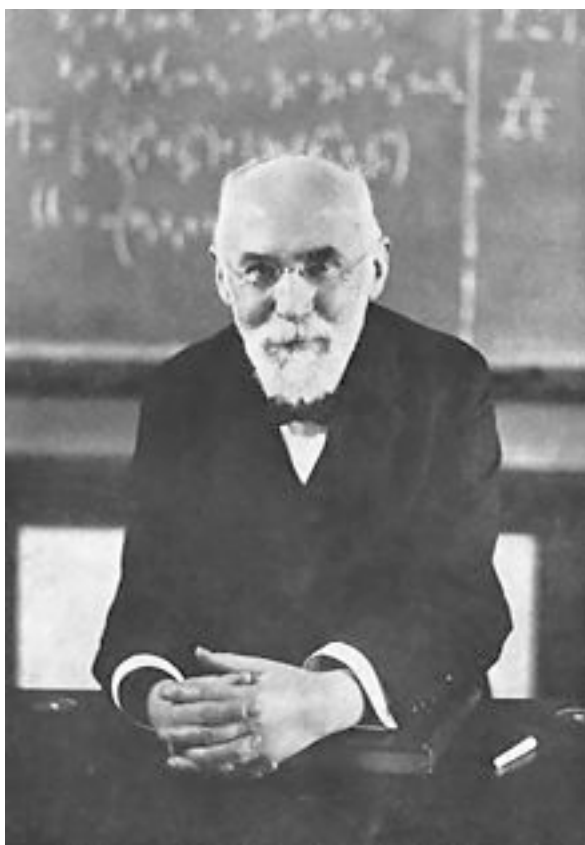
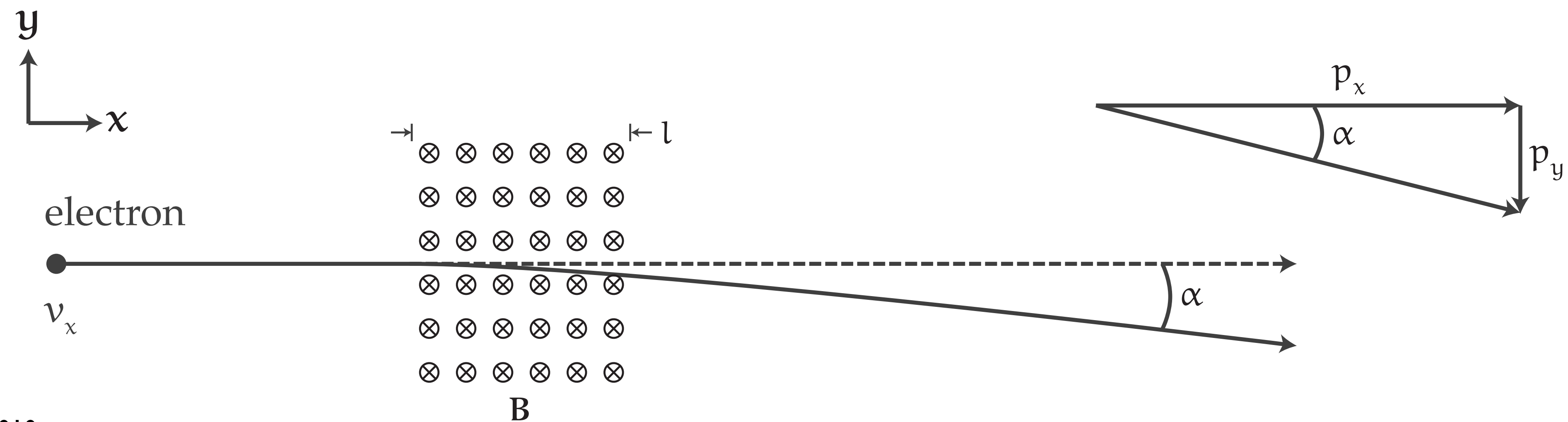
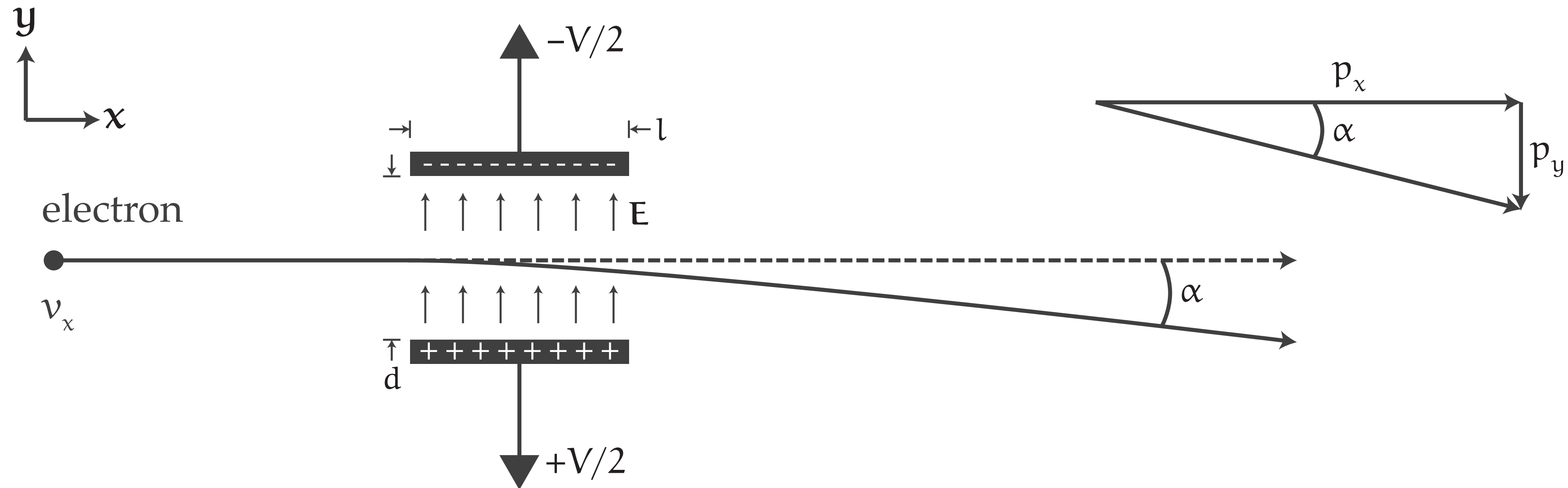
Example TEM schematic

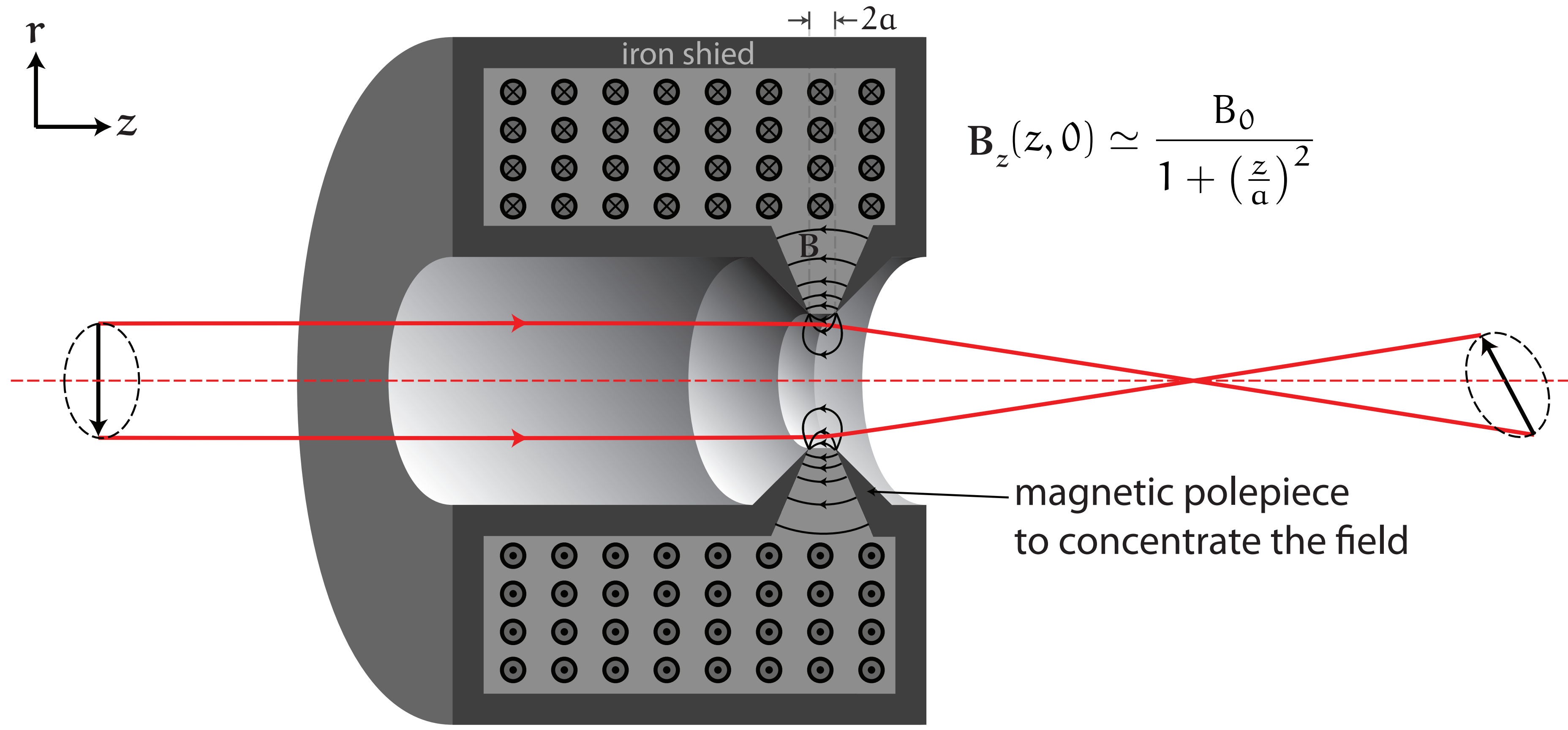
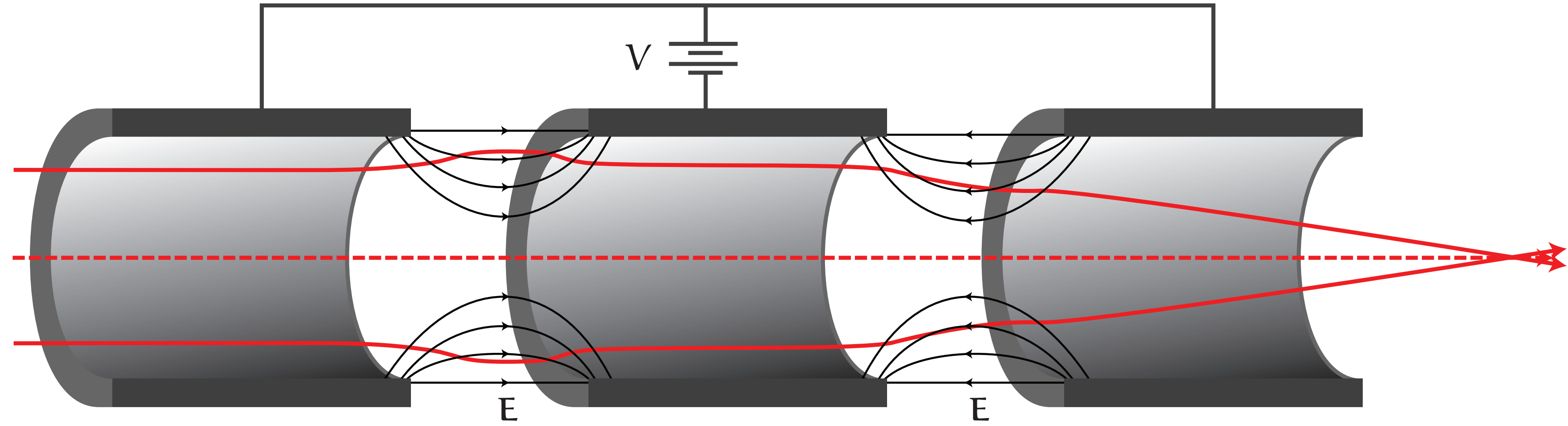
One of many types of TEMs



The Lorentz force

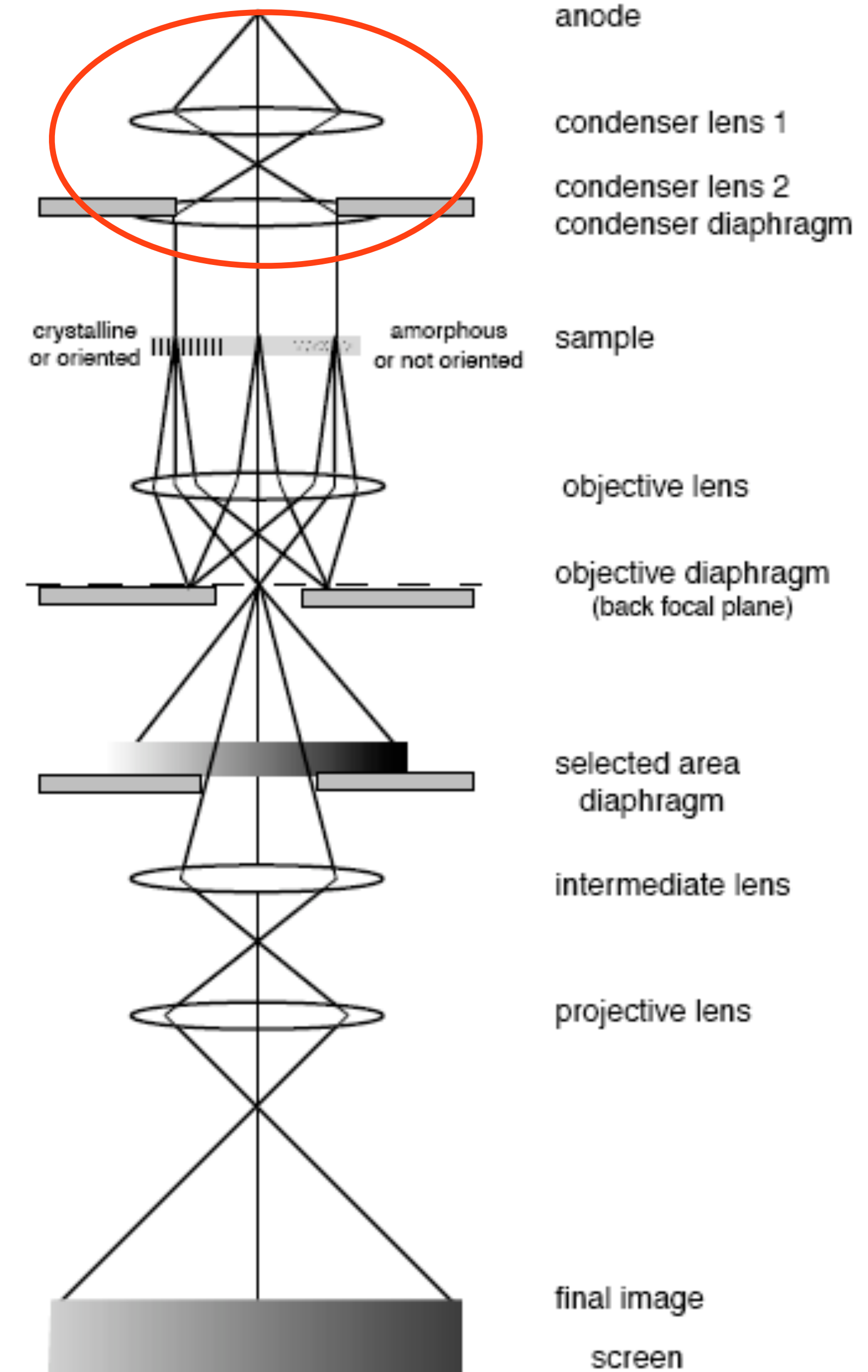
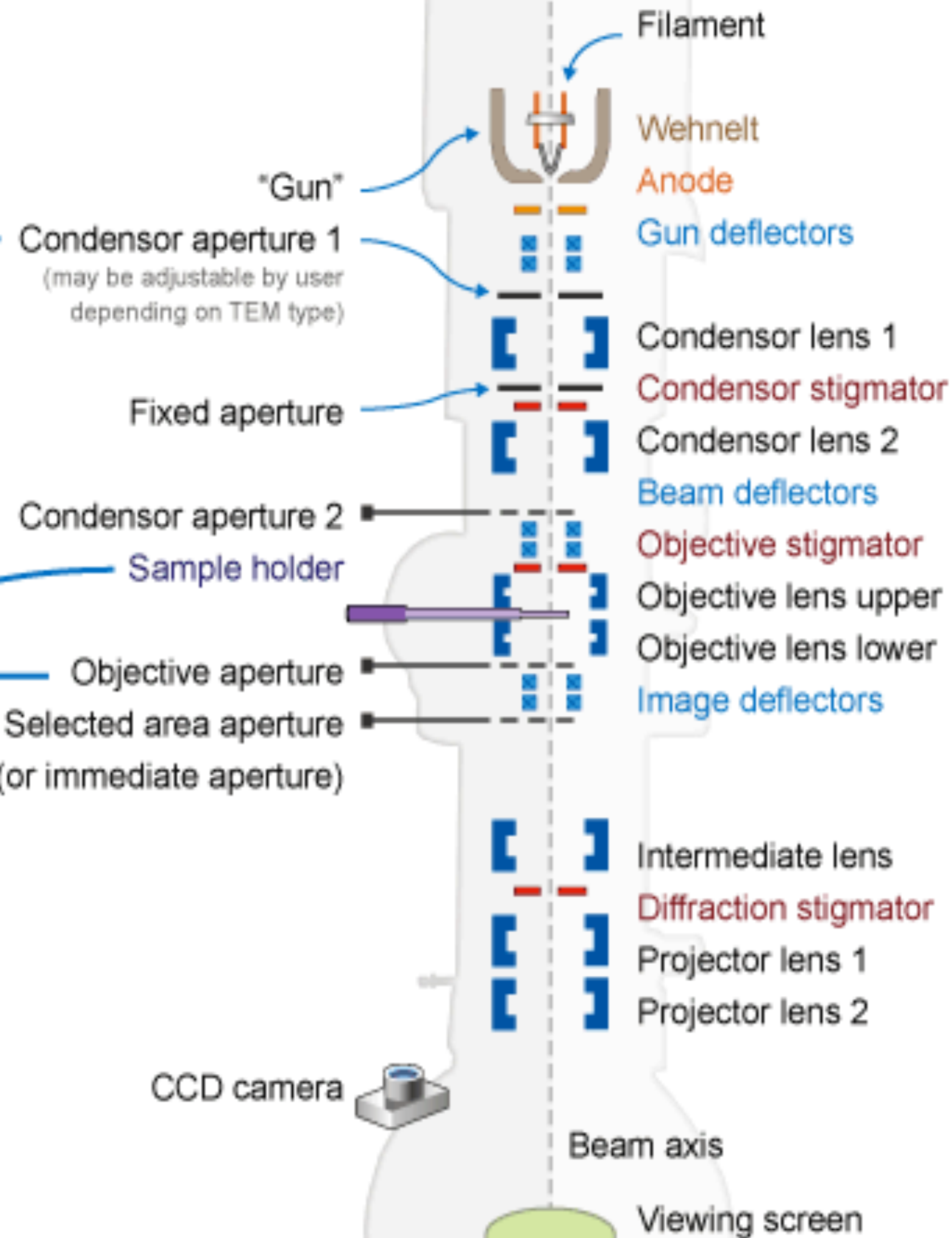
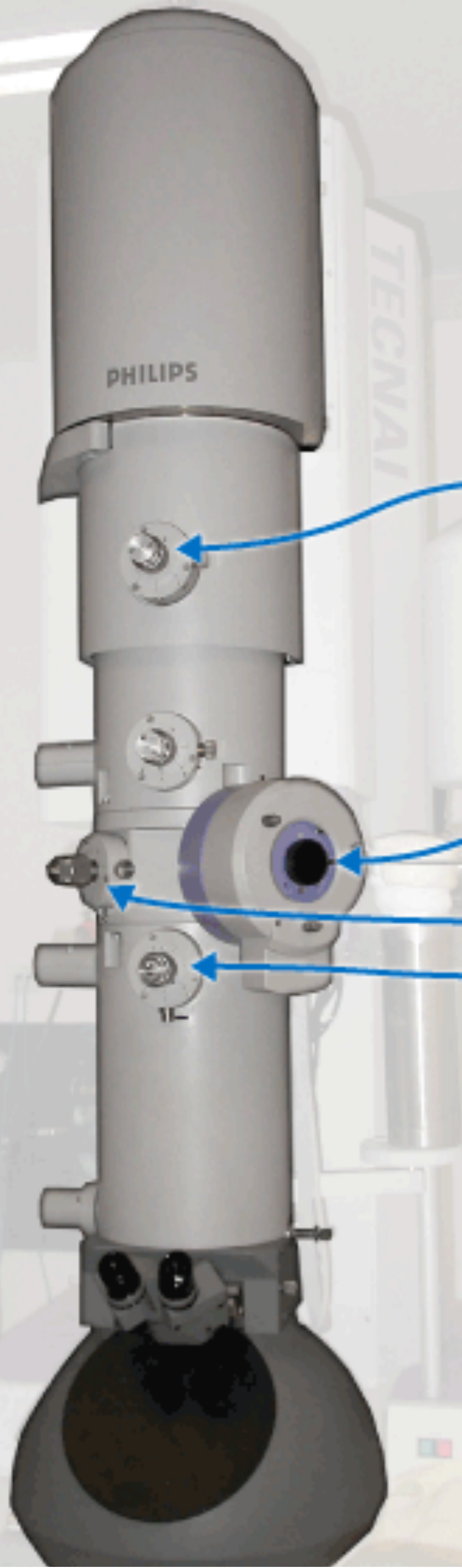
$$\mathbf{F} = -q_e(\mathbf{E} + \mathbf{v} \times \mathbf{B})$$



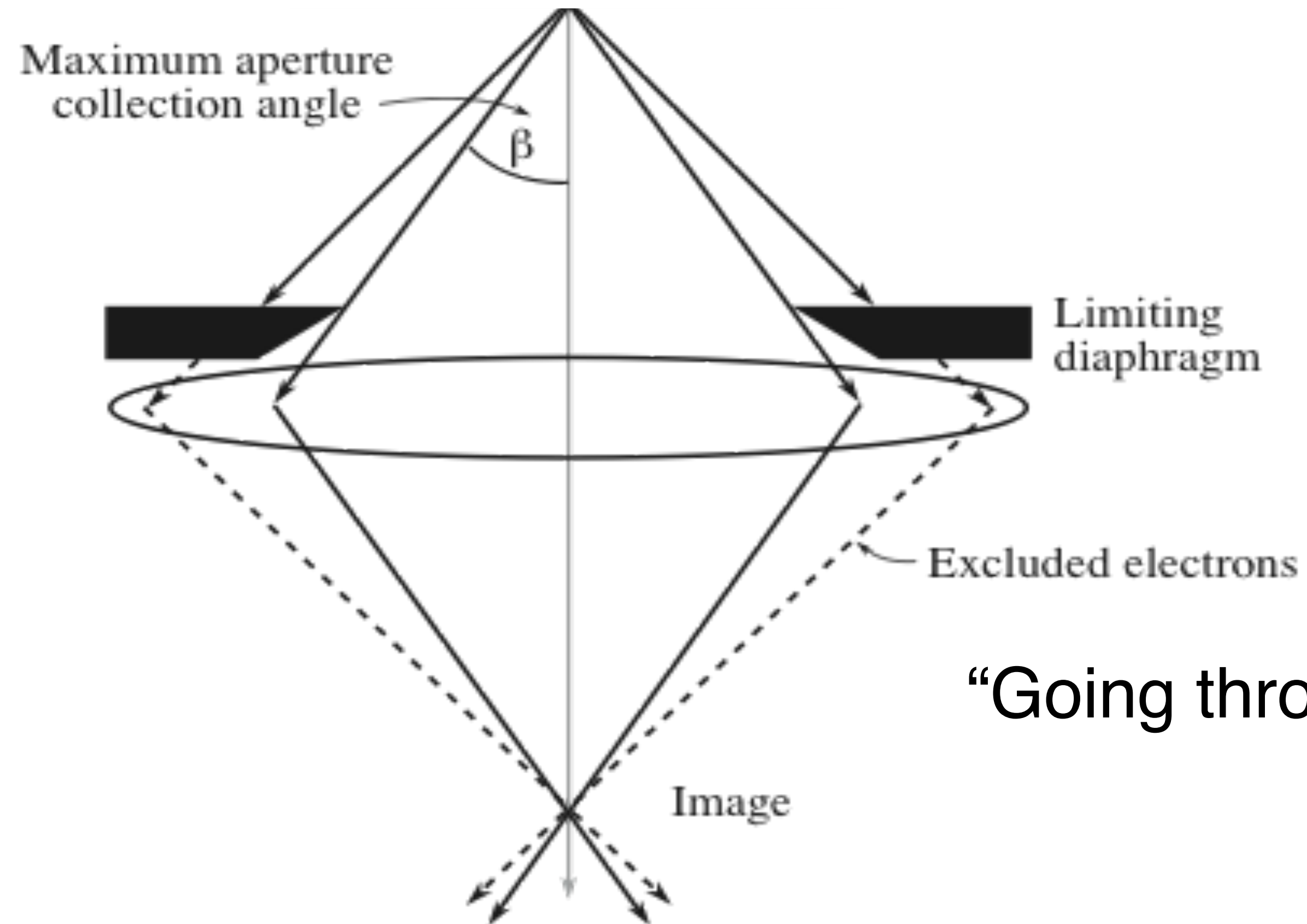


Example TEM schematic

One of many types of TEMs



Diaphragms & Apertures

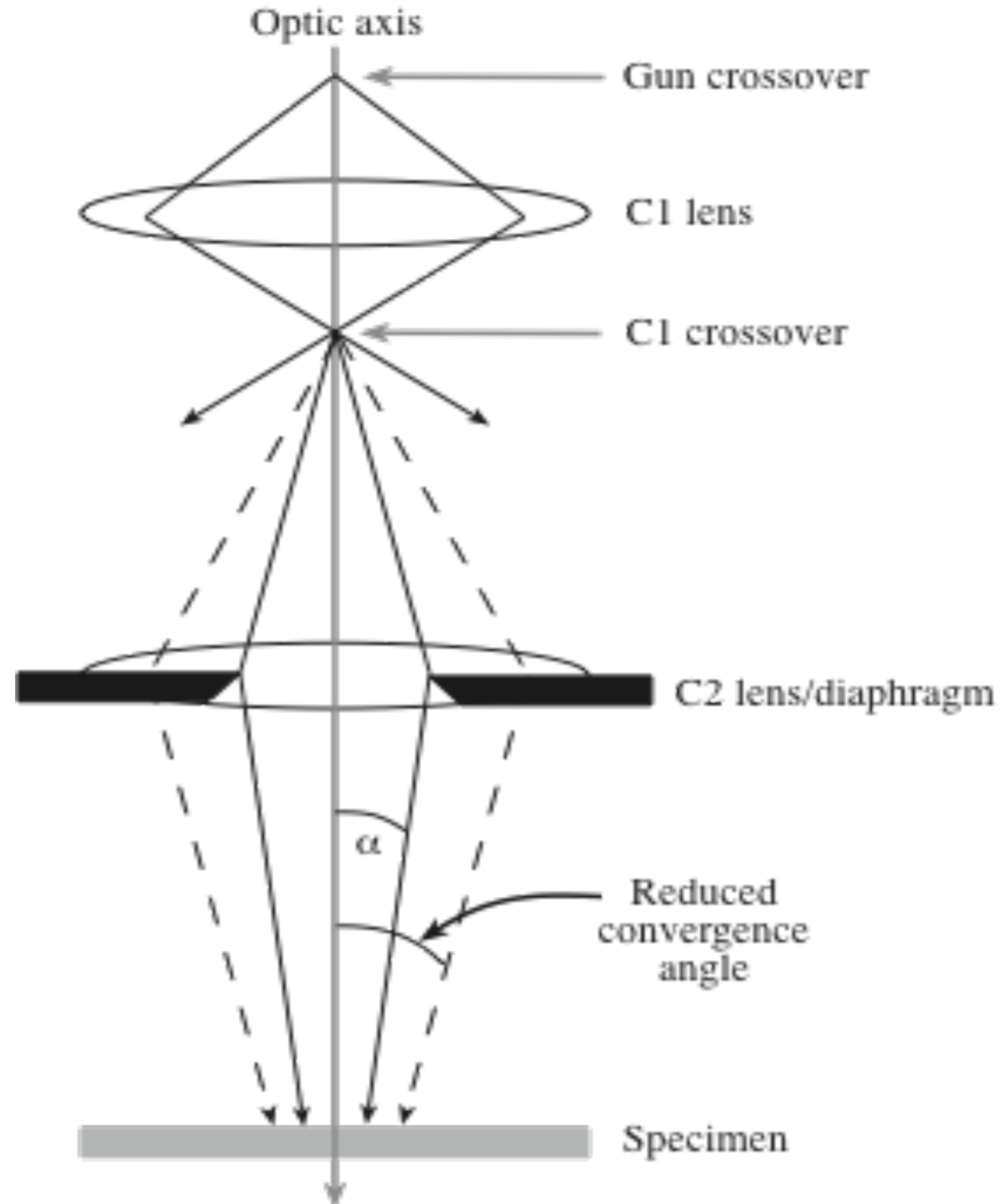


“Going through the door”

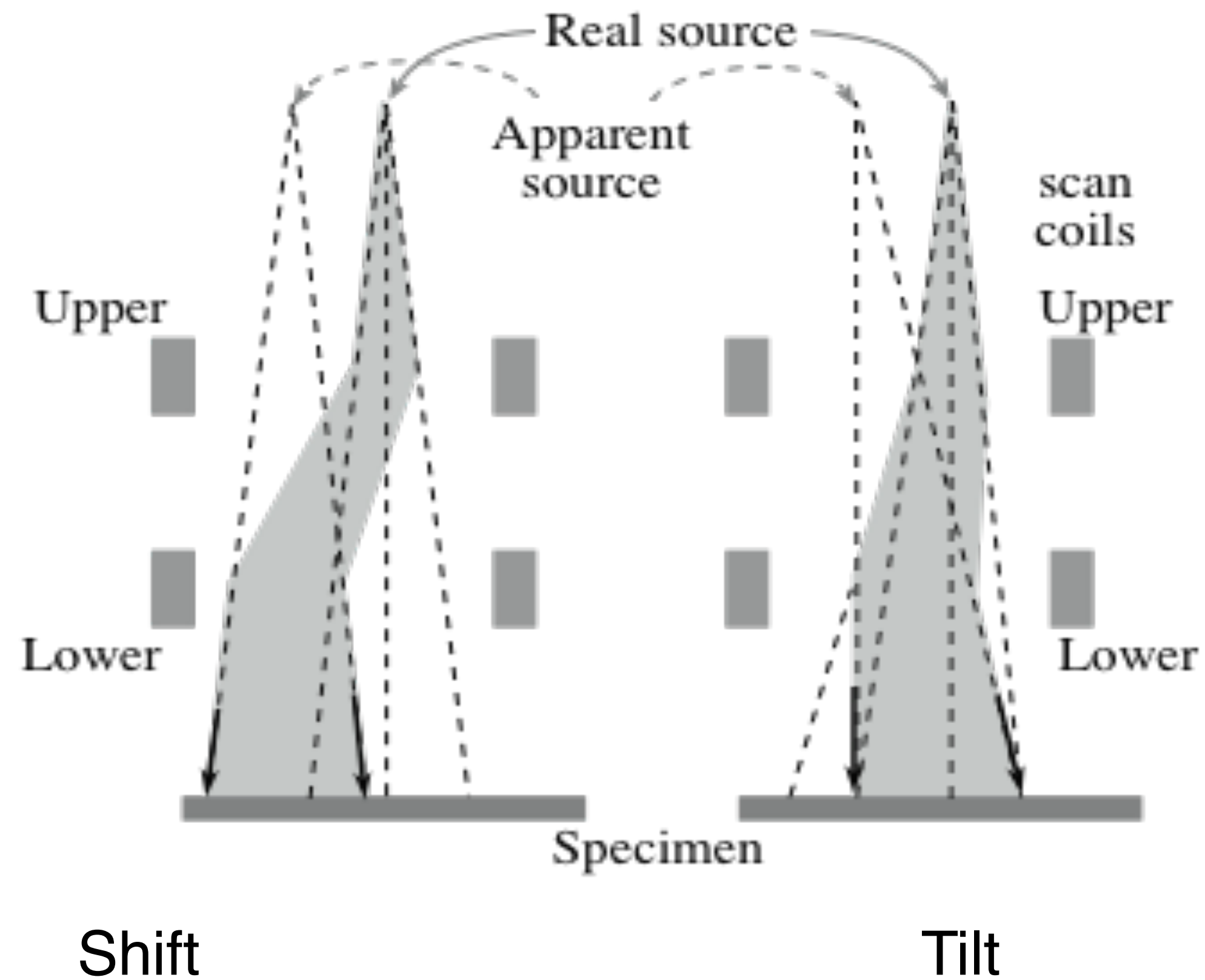
The Basic Electron Condenser System

Most TEMs 2 lenses + 1 aperture

Krios: 3 lenses + 1 aperture



Shift and tilt through a lens

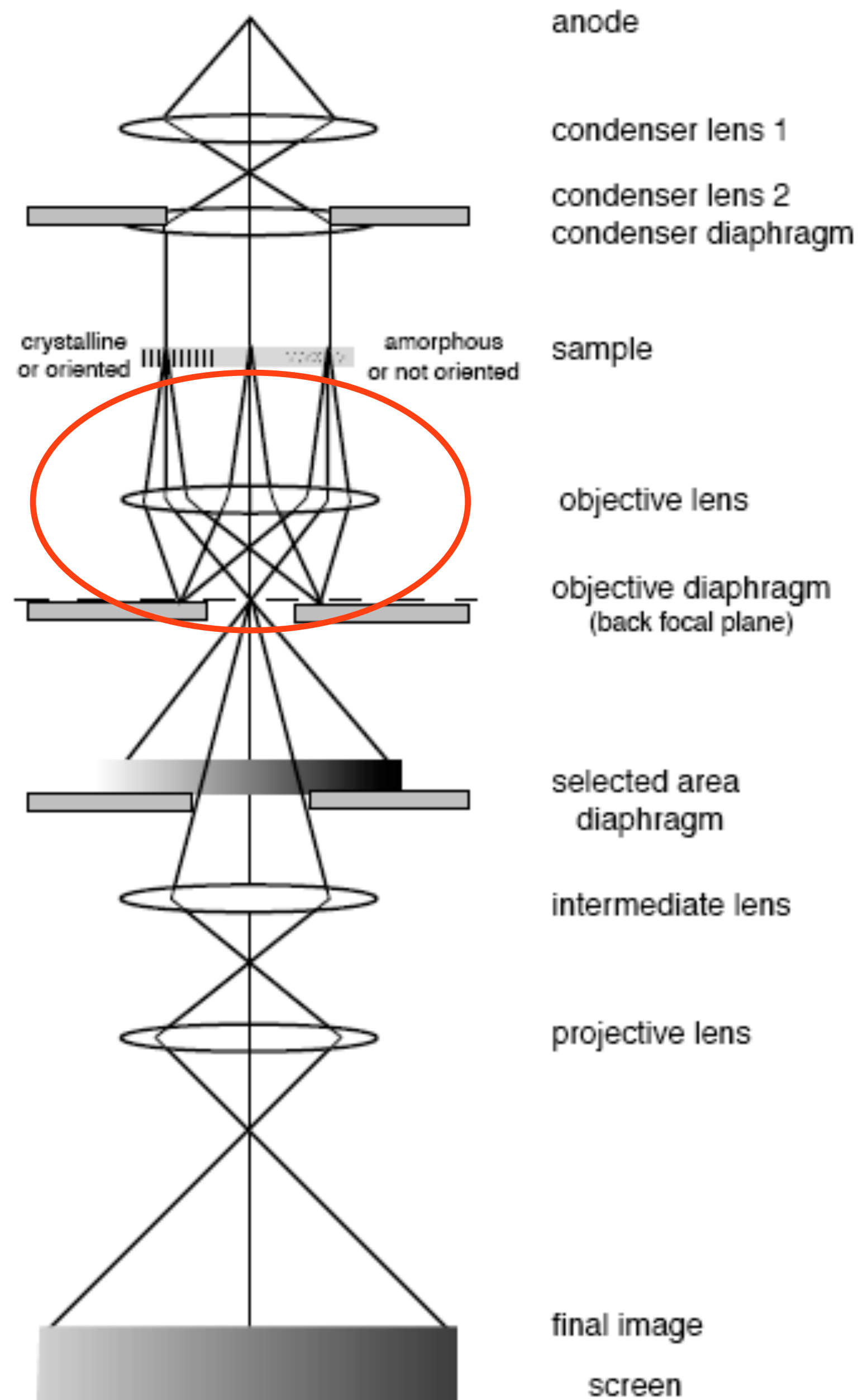
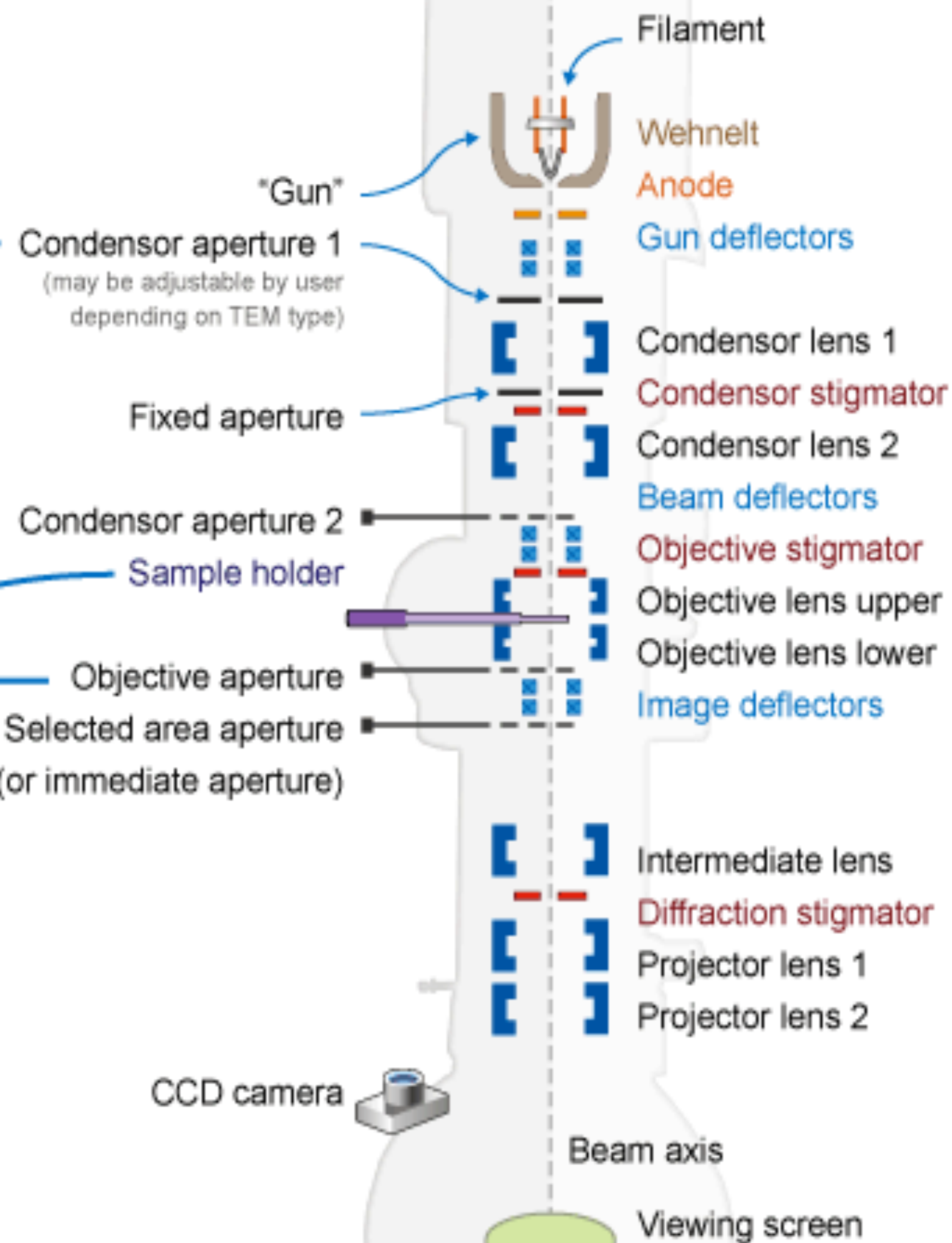
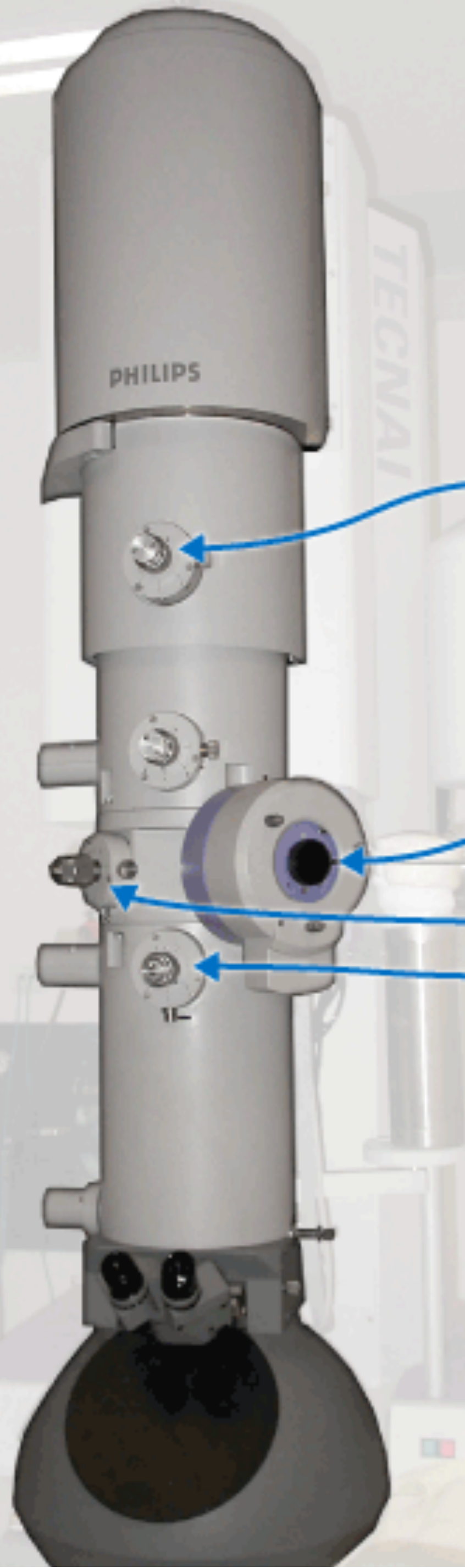


Same direction -> Different area

Same area -> Different direction

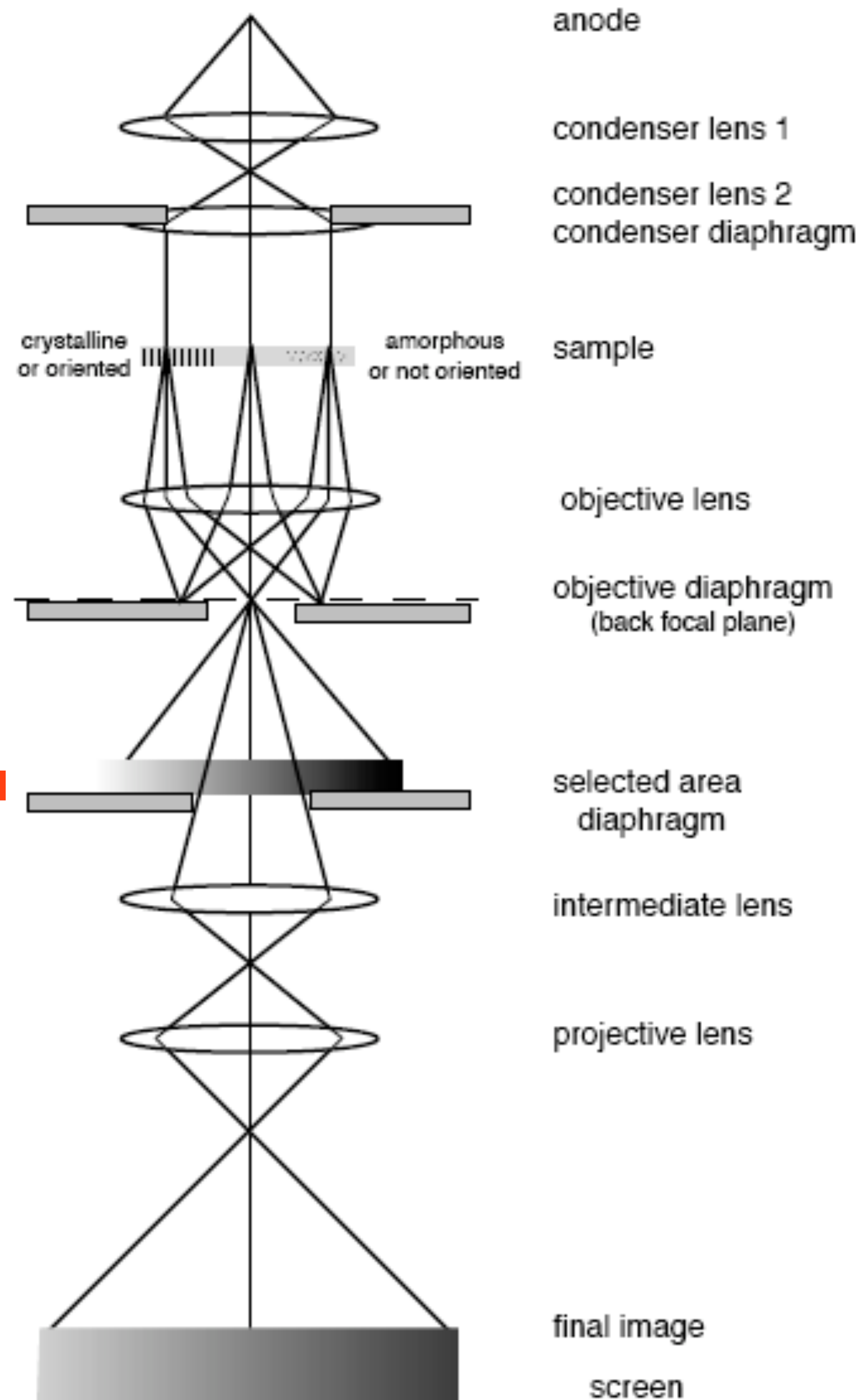
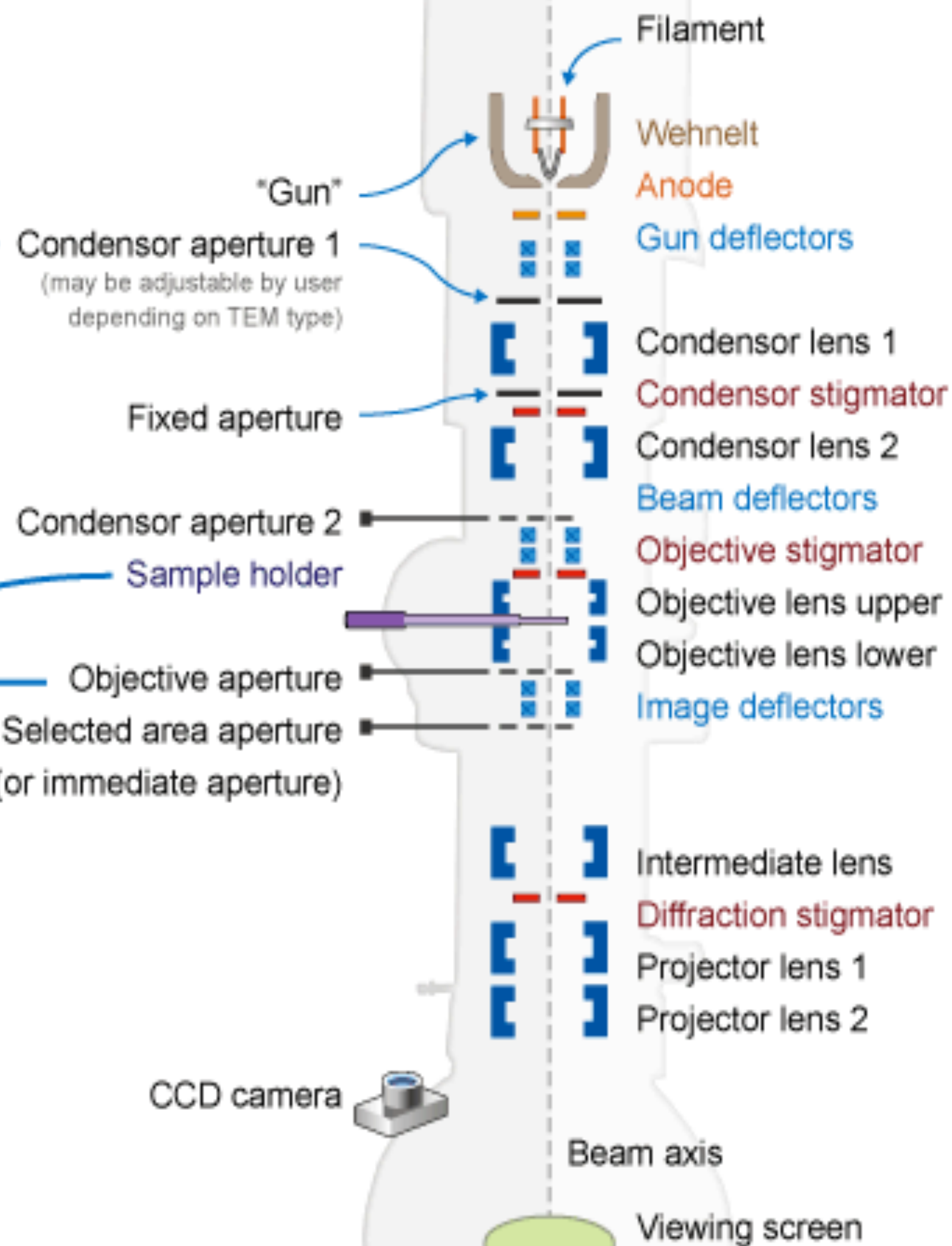
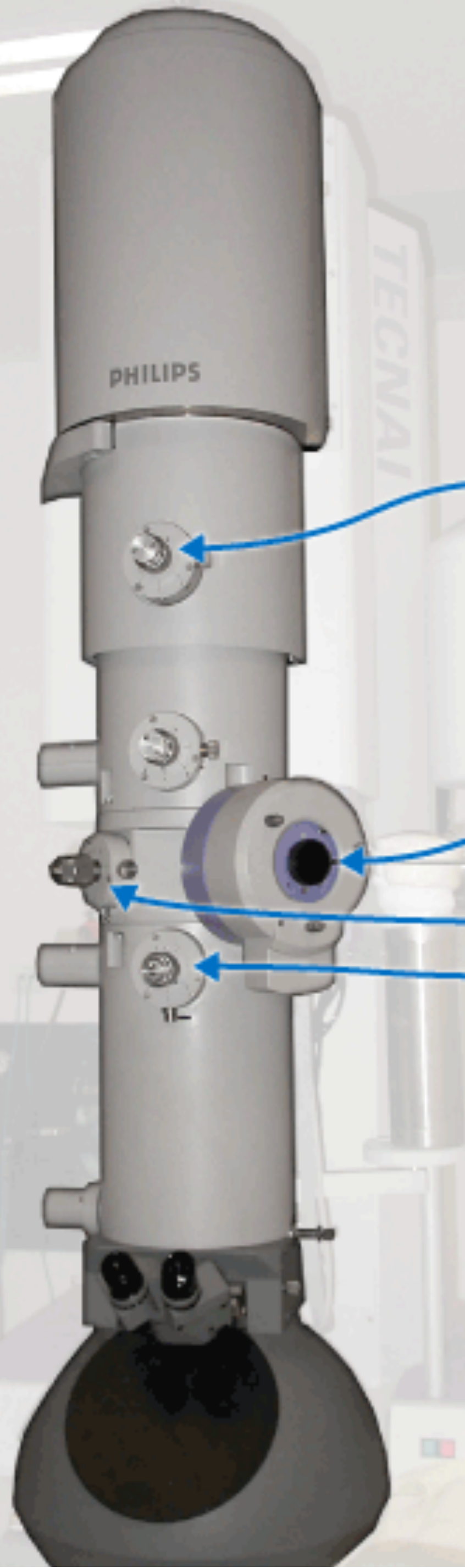
Example TEM schematic

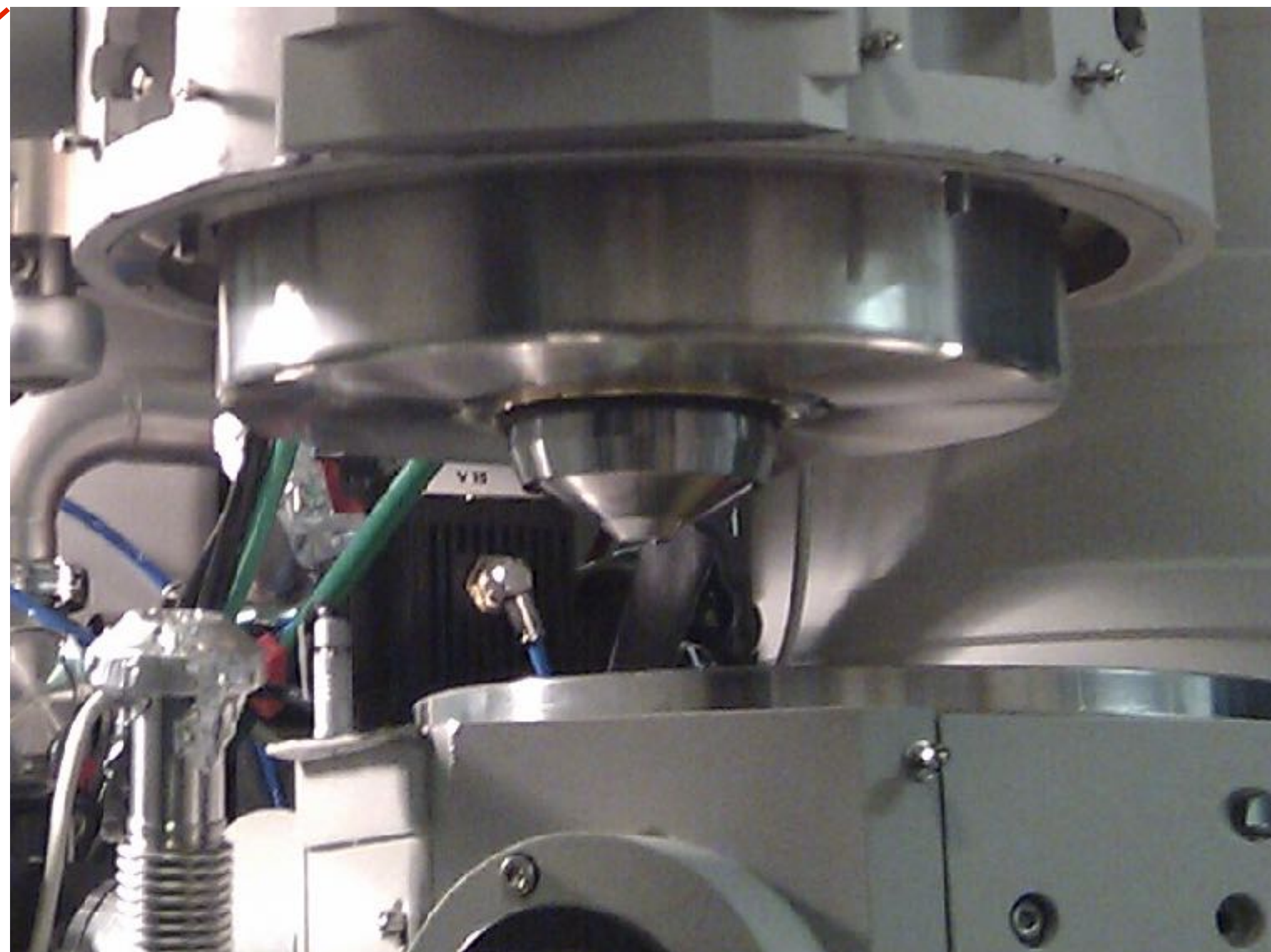
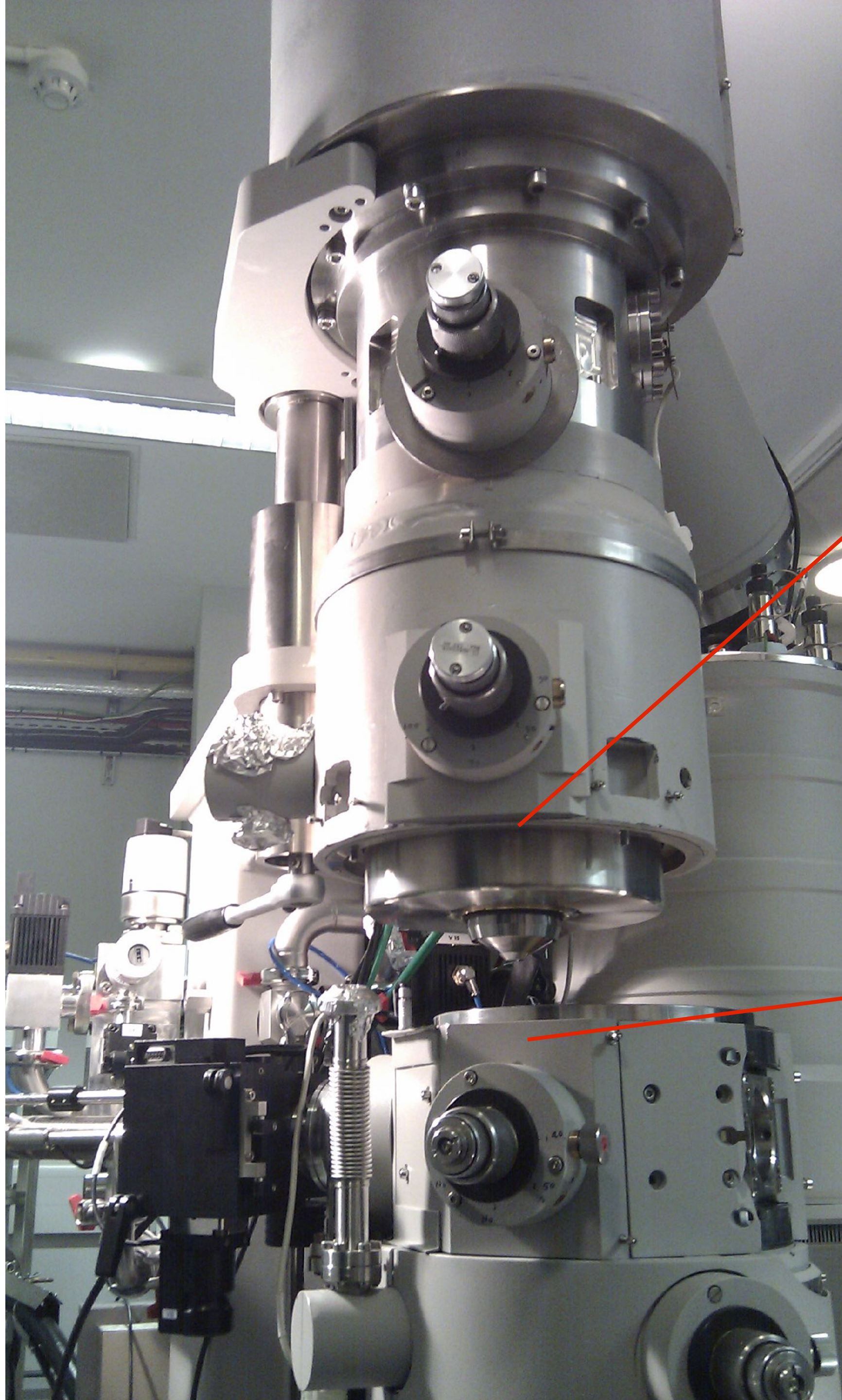
One of many types of TEMs



Example TEM schematic

One of many types of TEMs



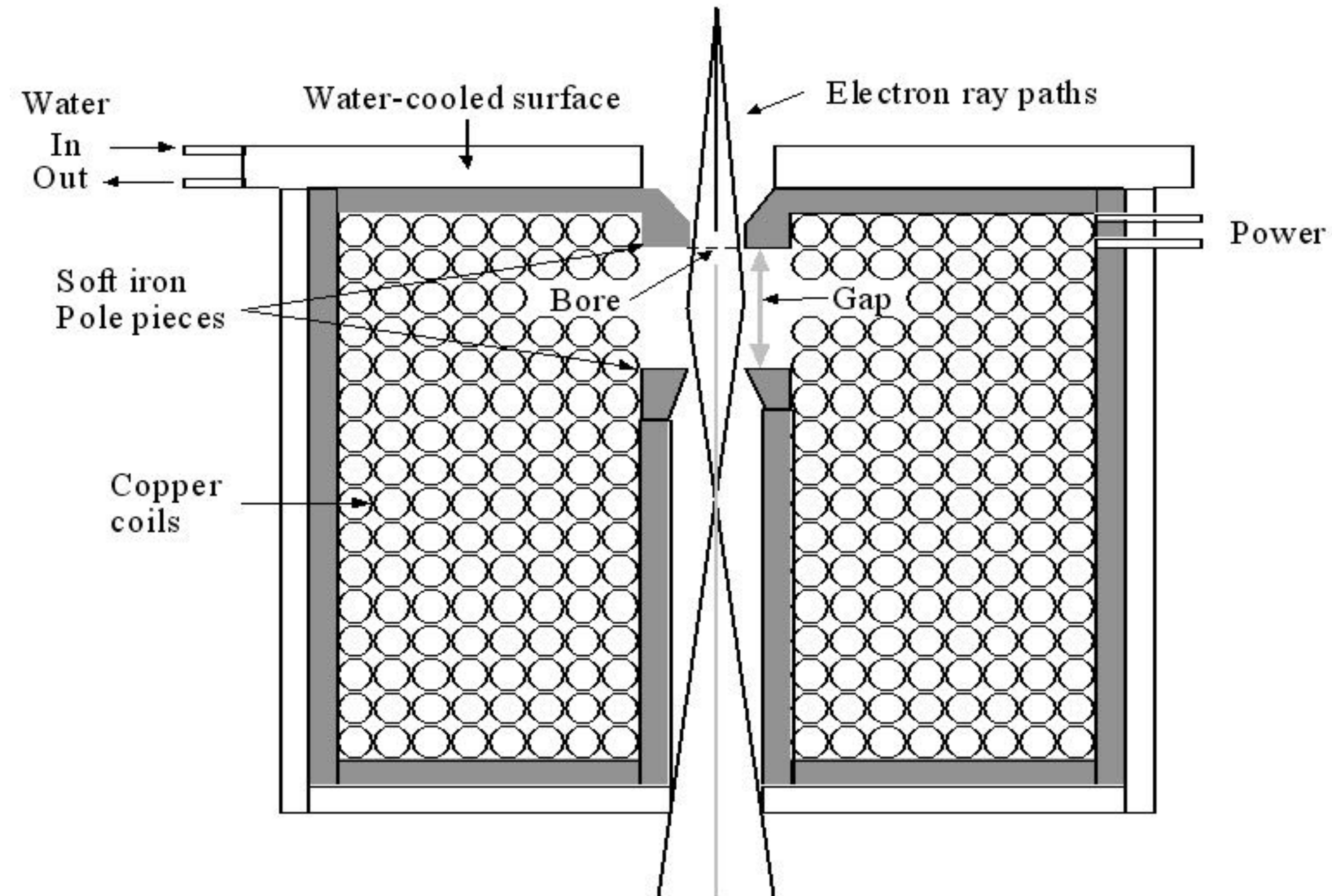


Magnetic Lens

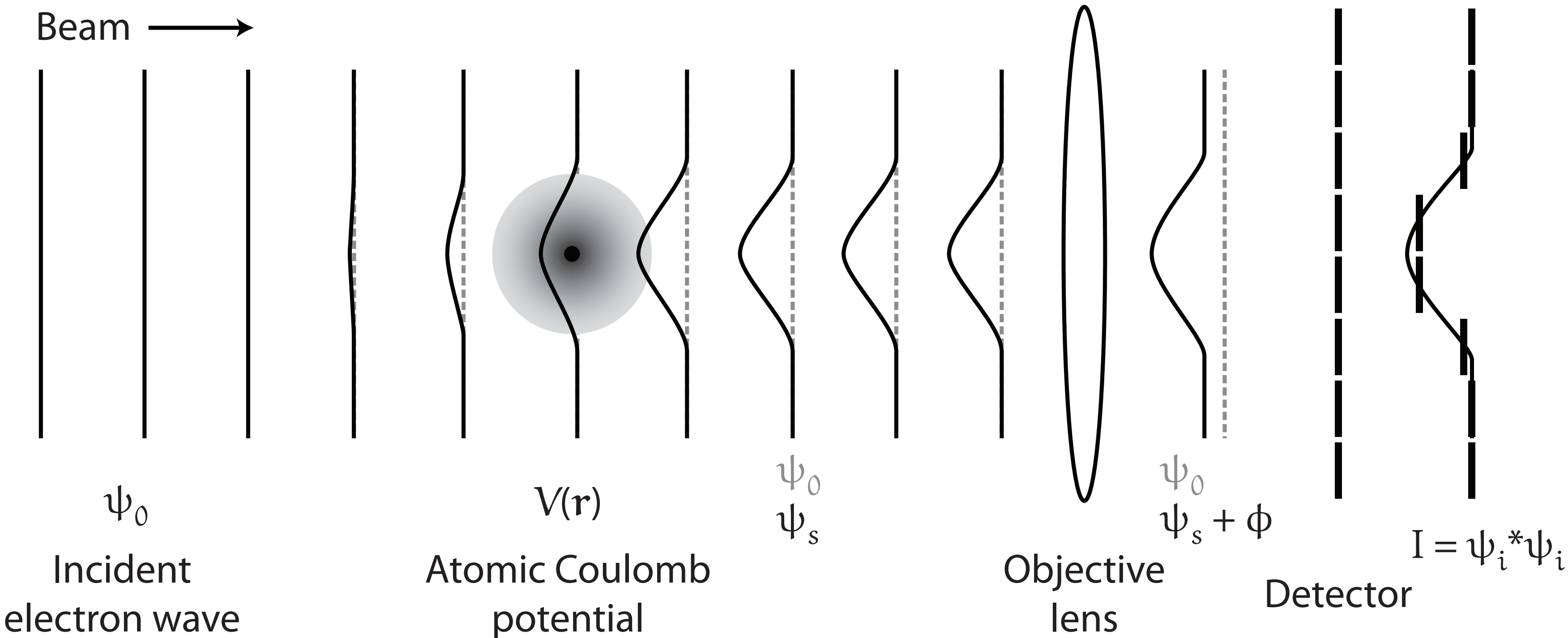
Concentrate flux

Field varies

Zero force on axial
electrons



Phase contrast and the perfect objective lens



The objective lens is *far* from perfect

How bad is the
objective lens?

Really bad



Electron lens aberrations

$$B(\mathbf{k}) = \exp \left[i \frac{2\pi}{\lambda} W(\mathbf{k}) \right]$$

2.2: Description of aberration constants to 6th order

A_0	Lateral image shift	$ \begin{aligned} W(\mathbf{k}) = & \Re \{ A_0 \lambda \mathbf{k}^* \\ & + \frac{1}{2} A_1 \lambda^2 \mathbf{k}^{*2} + \frac{1}{2} C_1 \lambda^2 \mathbf{k}^* \mathbf{k} \\ & + \frac{1}{3} A_2 \lambda^3 \mathbf{k}^{*3} + \frac{1}{3} B_2 \lambda^3 \mathbf{k}^{*2} \mathbf{k} \\ & + \frac{1}{4} A_3 \lambda^4 \mathbf{k}^{*4} + \frac{1}{4} S_3 \lambda^4 \mathbf{k}^{*3} \mathbf{k} + \frac{1}{4} C_3 \lambda^4 \mathbf{k}^{*2} \mathbf{k}^2 \\ & + \frac{1}{5} A_4 \lambda^5 \mathbf{k}^{*5} + \frac{1}{5} D_4 \lambda^5 \mathbf{k}^{*4} \mathbf{k} + \frac{1}{5} B_4 \lambda^5 \mathbf{k}^{*3} \mathbf{k}^2 \\ & + \frac{1}{6} A_5 \lambda^6 \mathbf{k}^{*6} + \frac{1}{6} S_5 \lambda^6 \mathbf{k}^{*4} \mathbf{k}^2 + \frac{1}{6} C_5 \lambda^6 \mathbf{k}^{*3} \mathbf{k}^3 + \frac{1}{6} R_5 \lambda^6 \mathbf{k}^{*5} \mathbf{k} + \dots \end{aligned} $
A_1	Two-fold astigmatism	
C_1	Defocus	
A_2	Three-fold astigmatism	
B_2	Axial coma	
A_3	Four-fold astigmatism	
S_3	Axial star aberration	
$C_3 = C_s$	Spherical aberration	
A_4	Five-fold astigmatism	
D_4	Three-lobe aberration	
B_4	Fourth-order axial coma	
A_5	Six-fold astigmatism	
S_5	Fifth-order star aberration	
C_5	Fifth-order spherical aberration	
R_5	Fifth-order rosette aberration	

Lens aberrations can also be visualized using Zernike polynomials

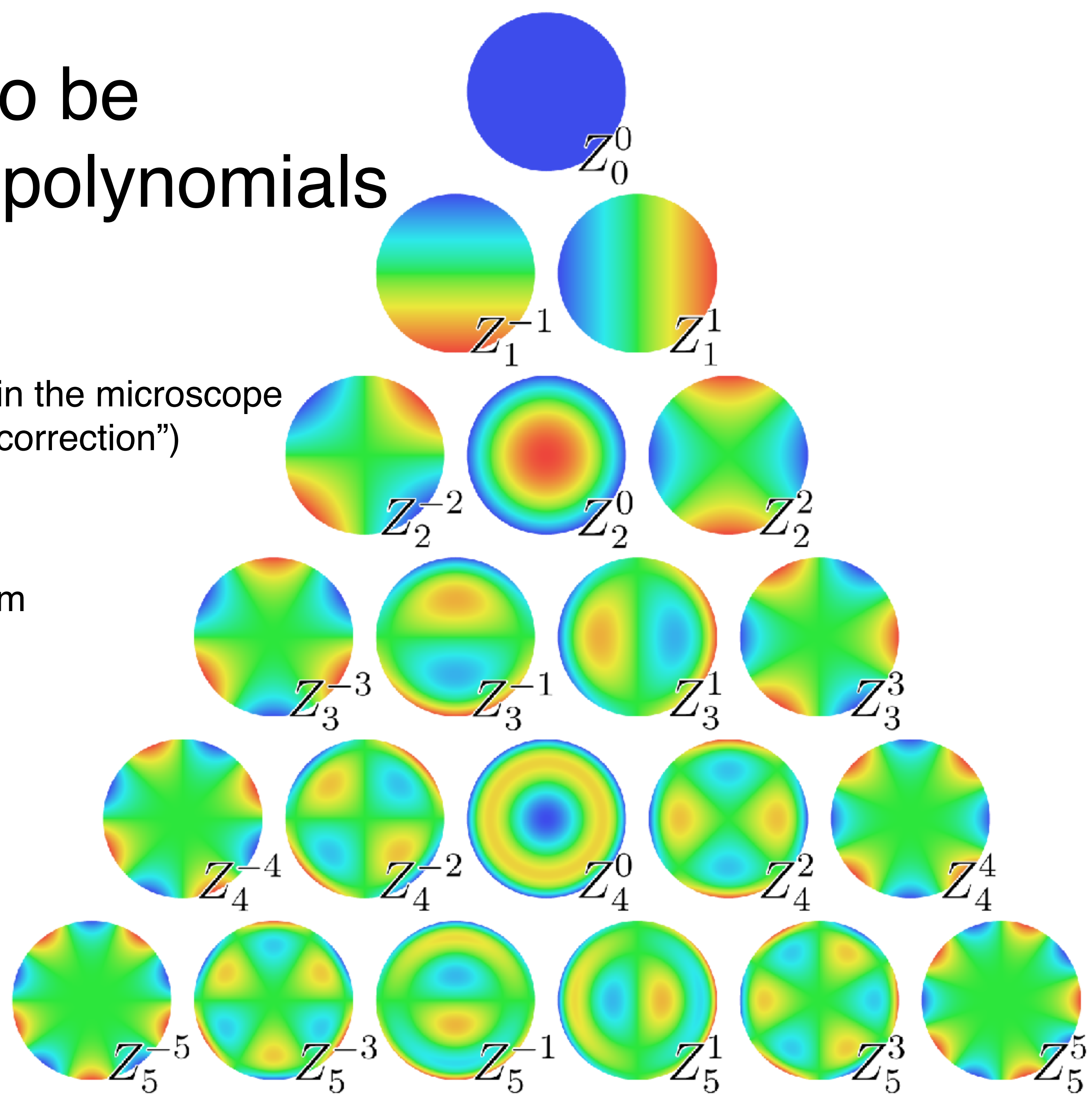
Aberrations are corrected with additional lenses in the microscope or in software after the image is collected (“CTF correction”)

Complete set of orthogonal functions

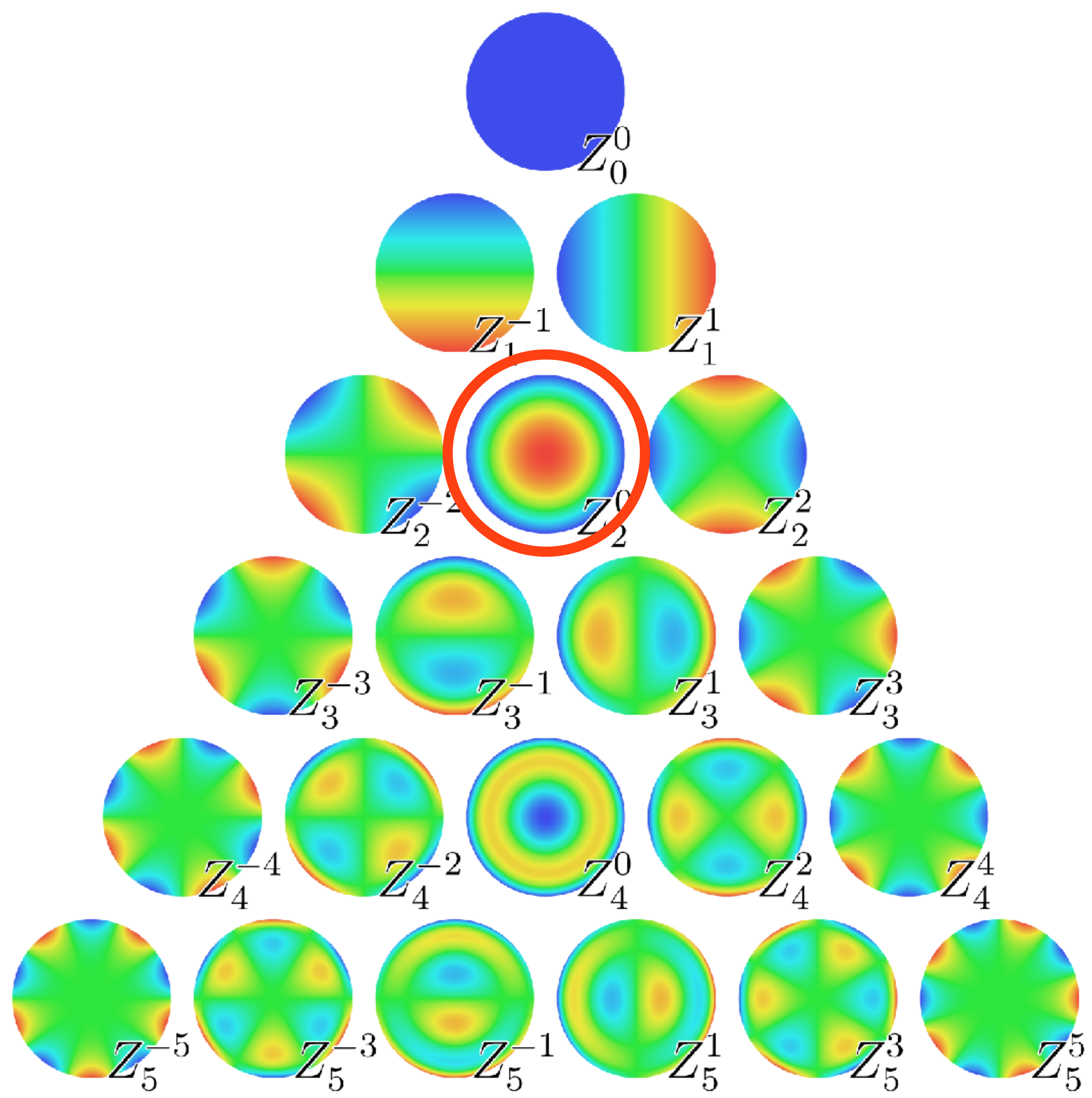
Zernike transform analogous to Fourier transform



Frits Zernike,
1953 Nobel Prize in Physics
inventor of phase contrast
microscopy



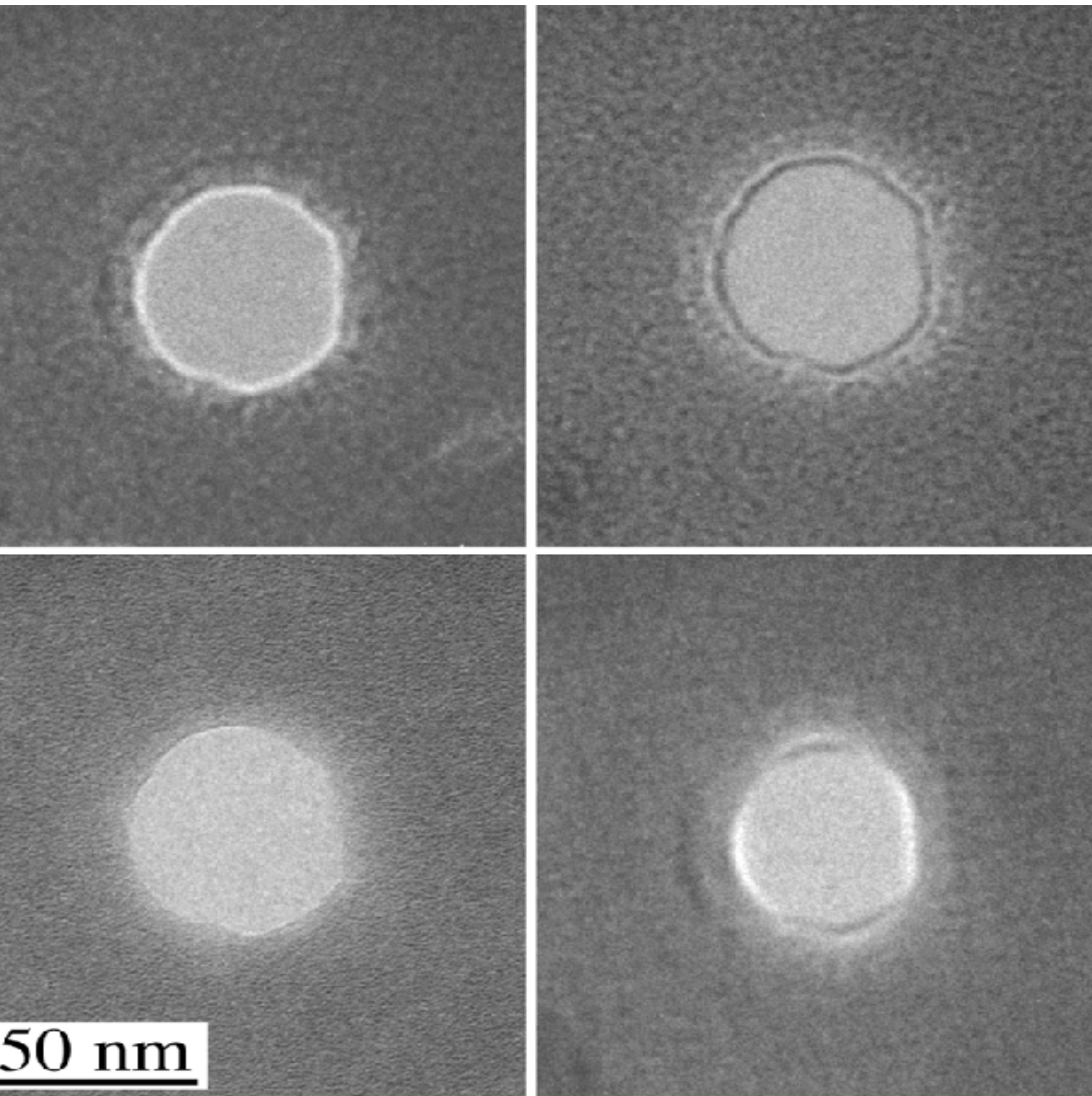
Defocus



Focus terminology

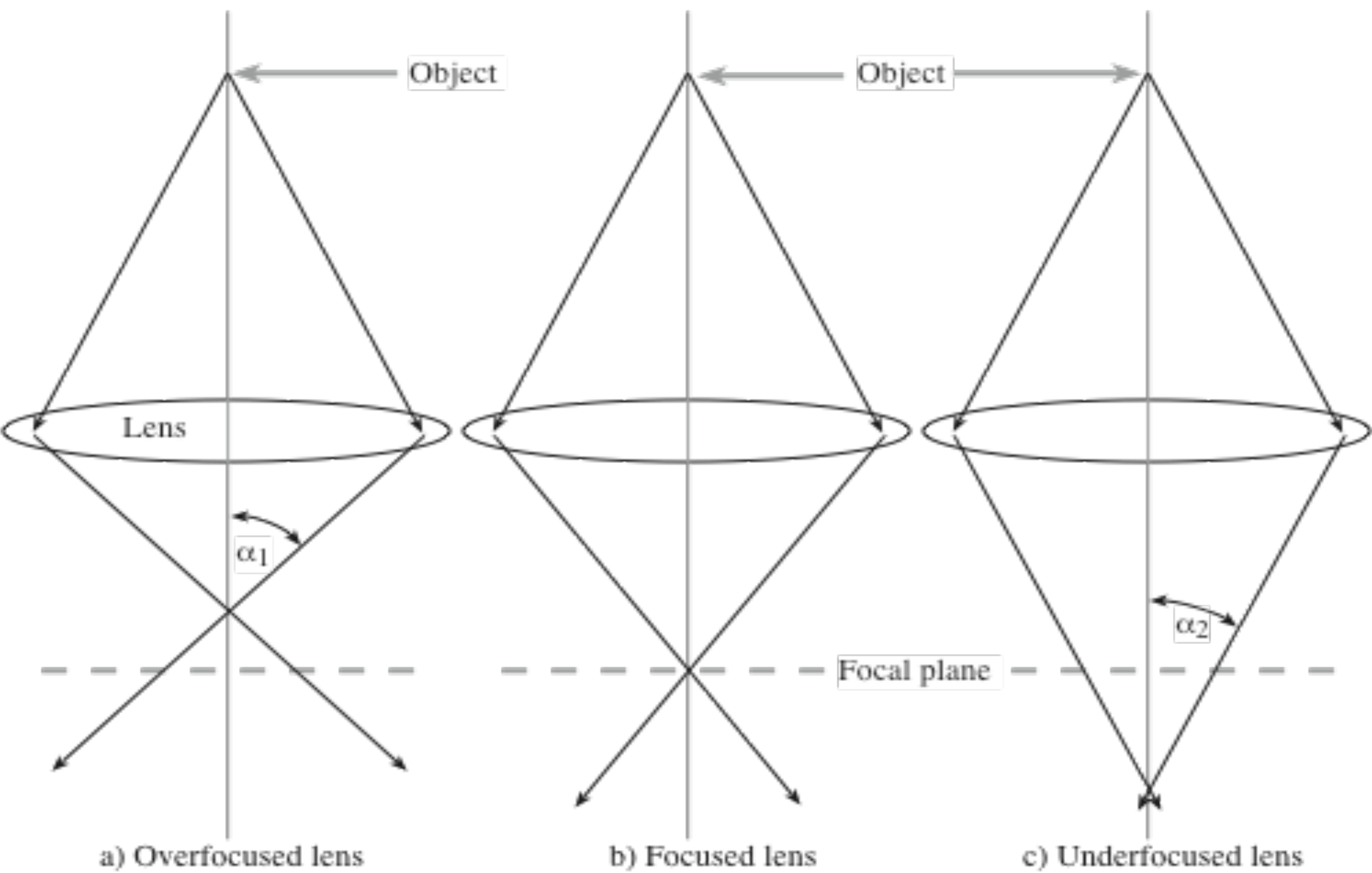
underfocus

overfocus



exact focus

astigmatism

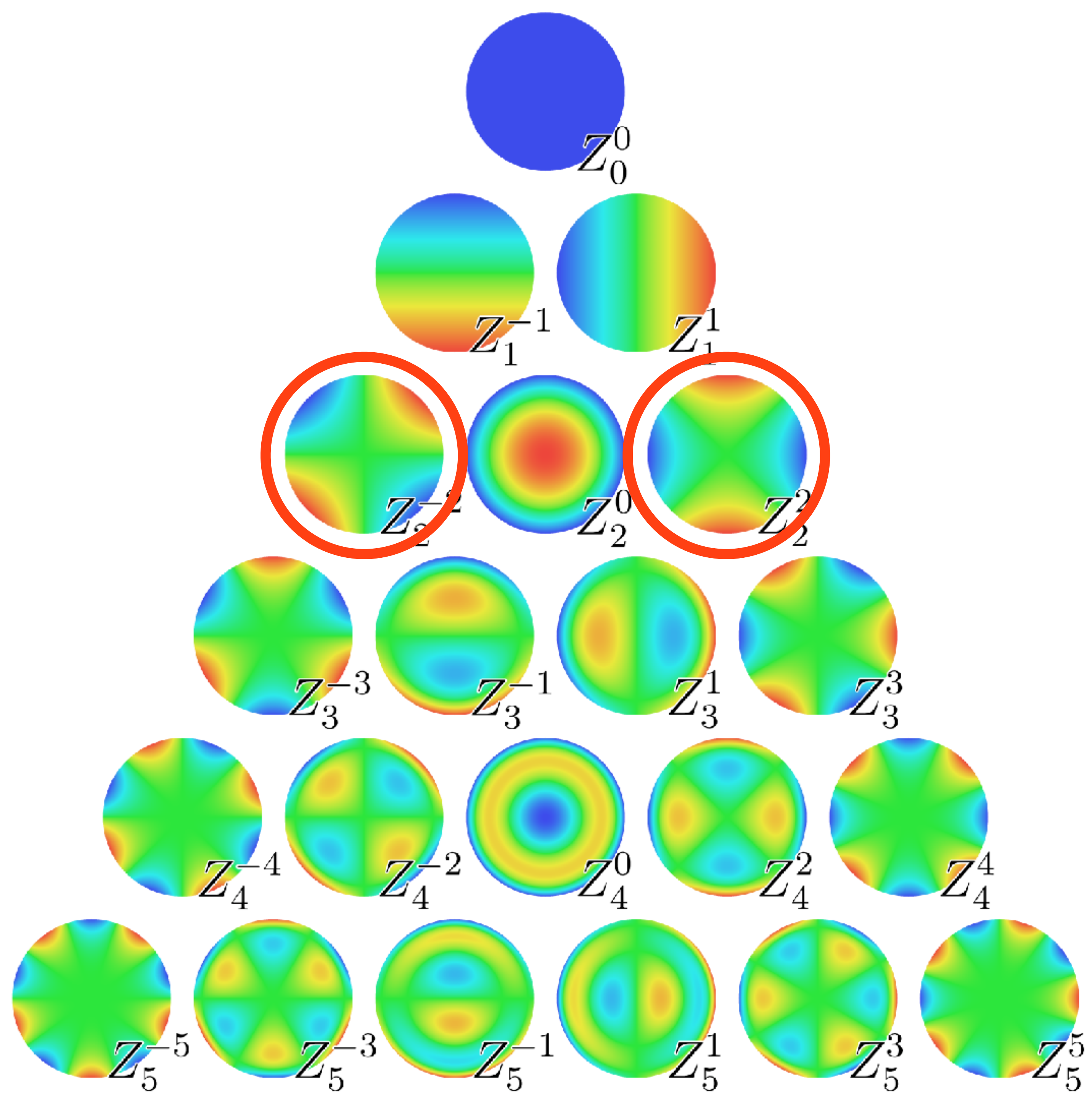


Too strong

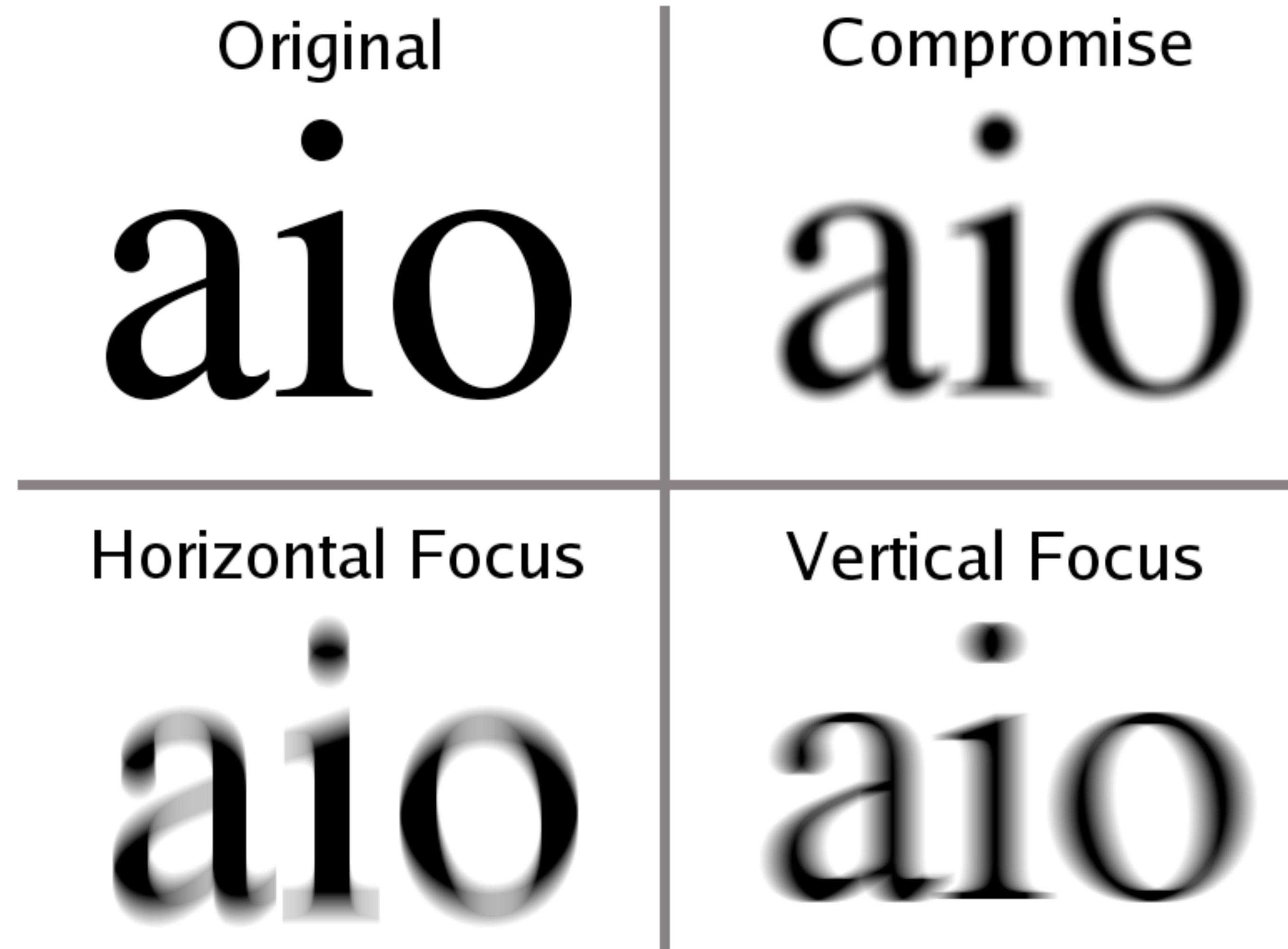
Just right

Too weak

Astigmatism



Astigmatism (example)



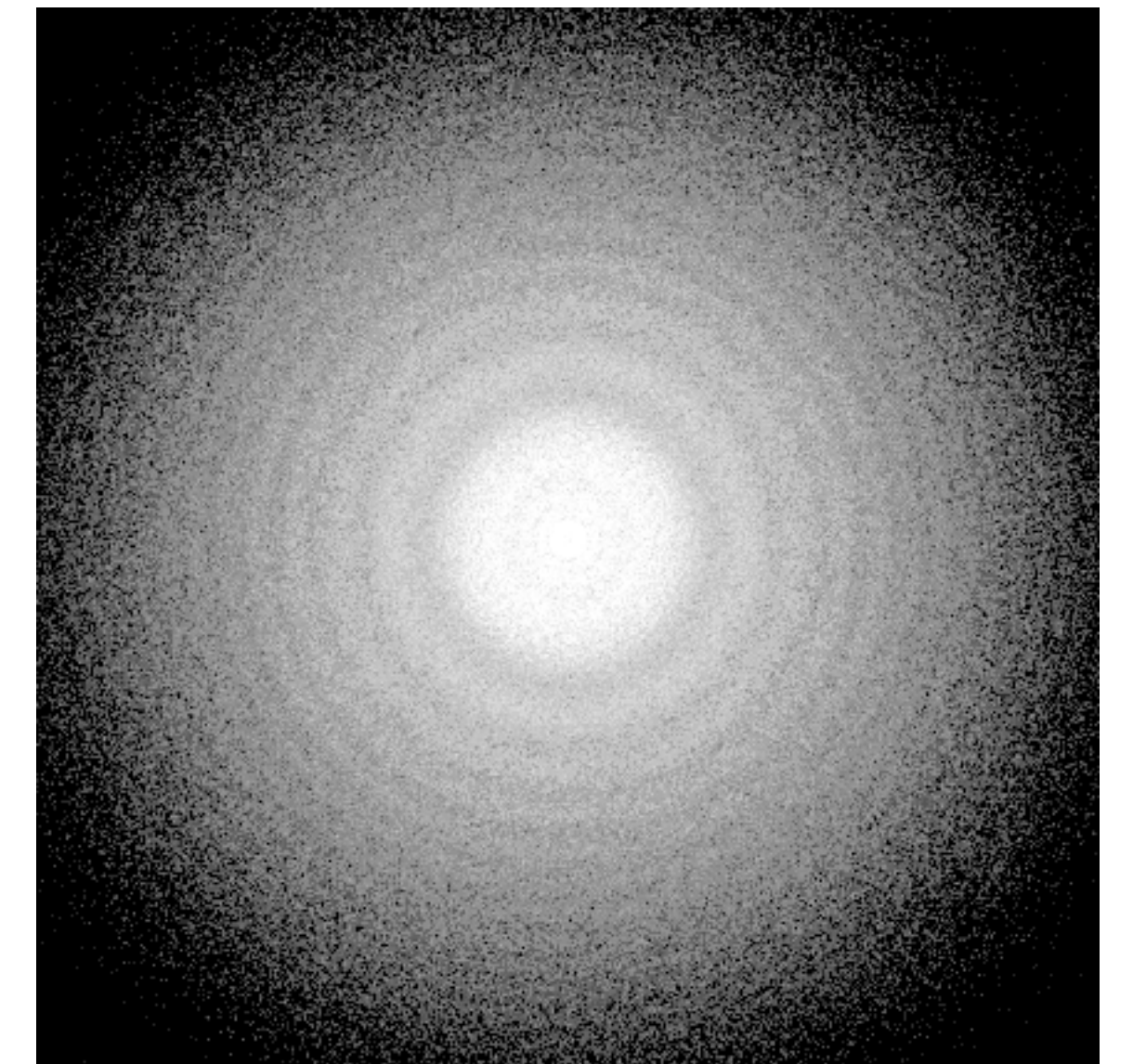
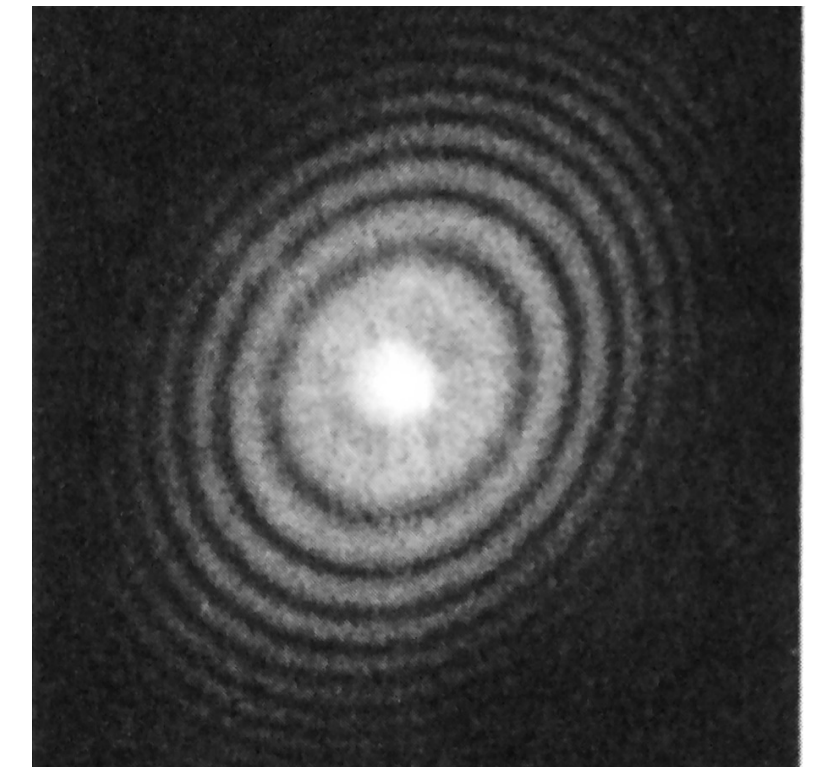
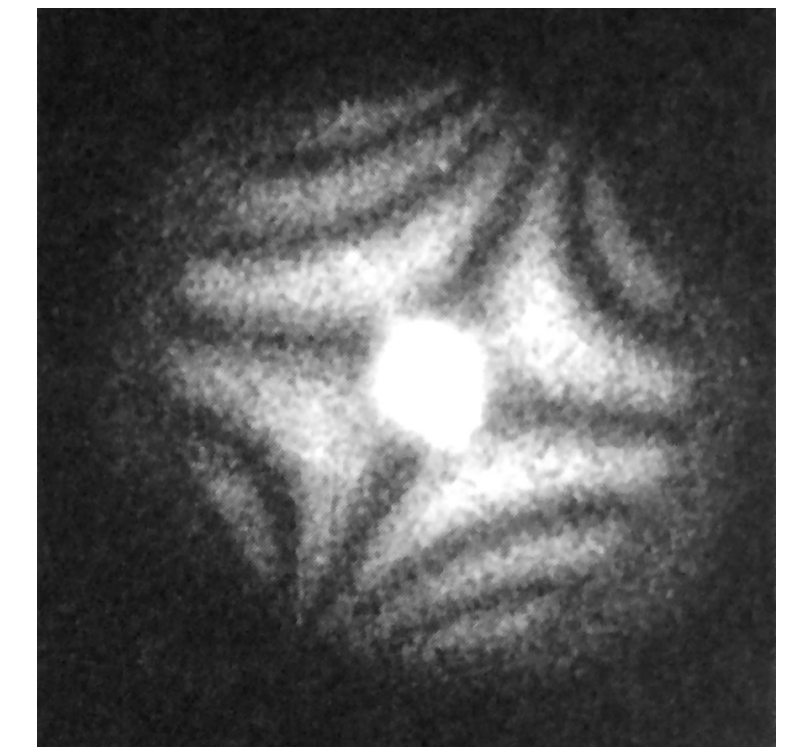
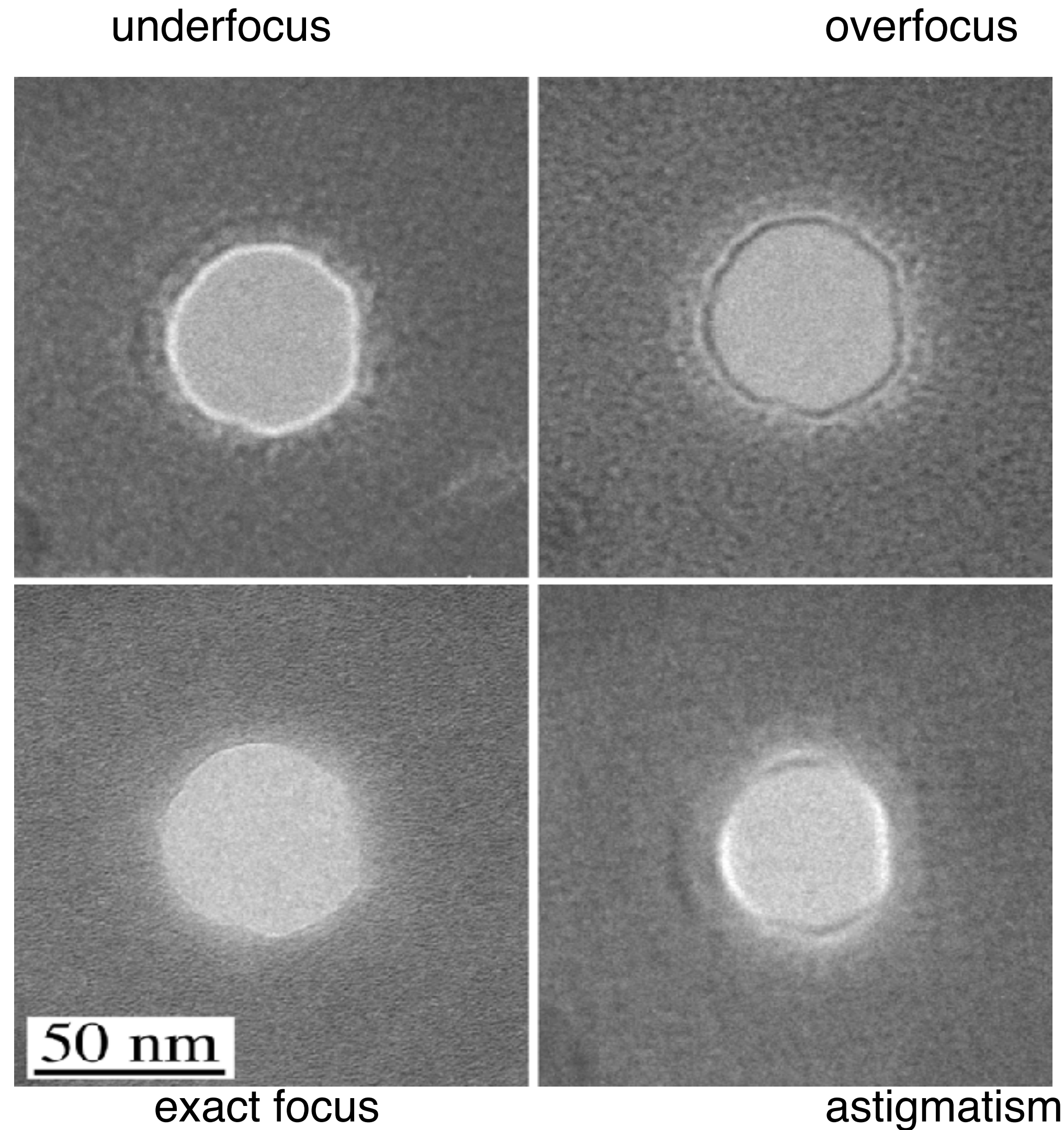
Astigmatism Correction

Correcting the
astigmatism
on the objective lens

Routine alignment using
Fresnel fringe

More accurate with FFT

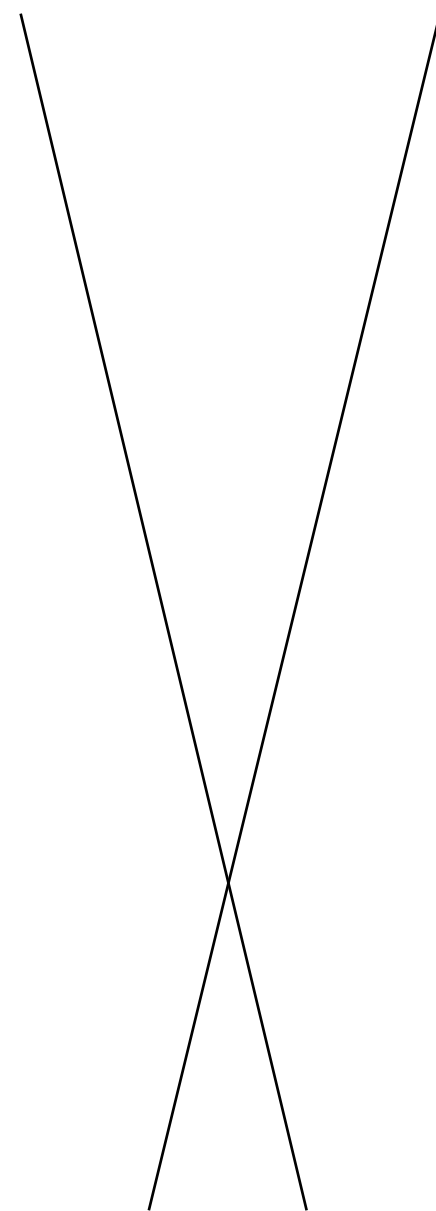
Remember to
correct the
condenser lens too



Beam Astigmatism Correction

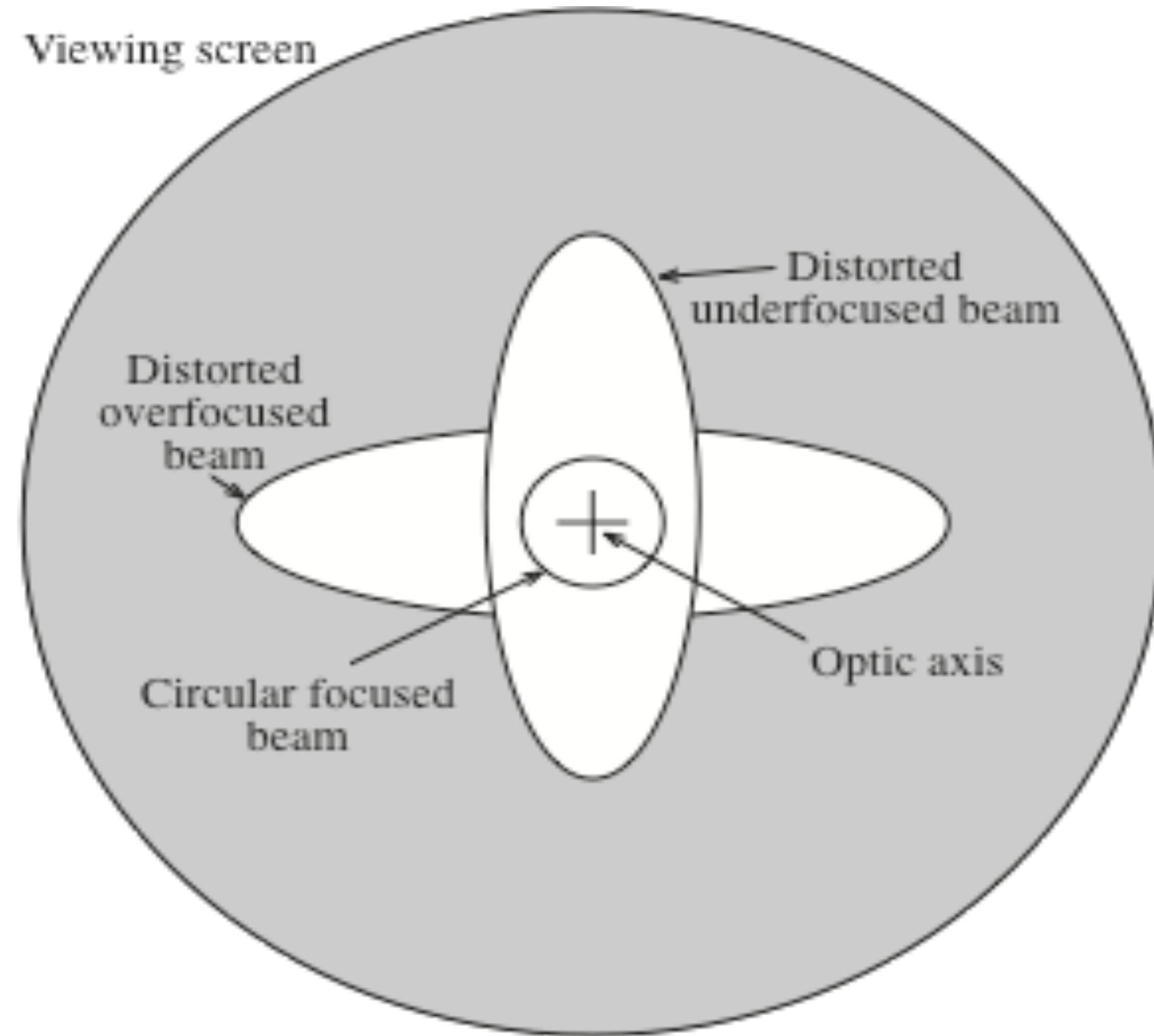
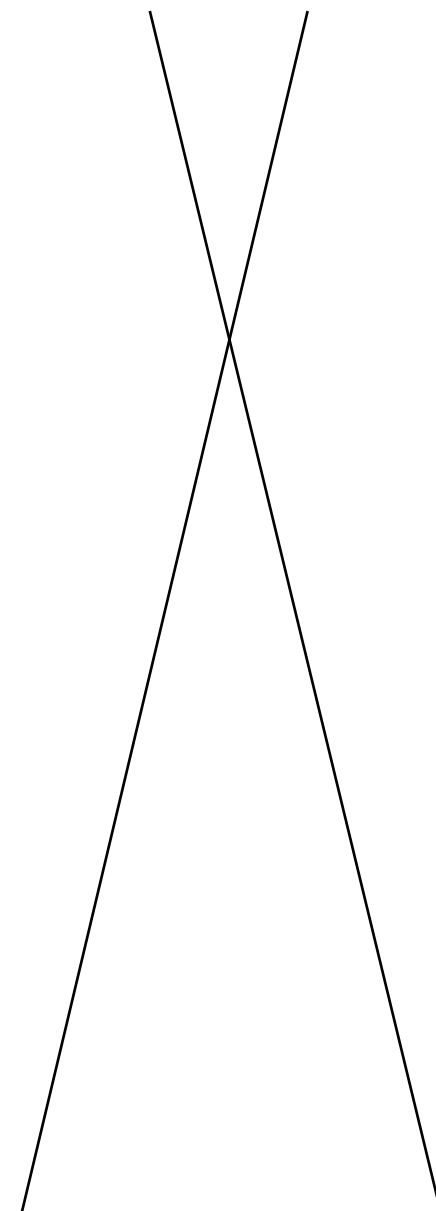
Just change focus

Underfocus

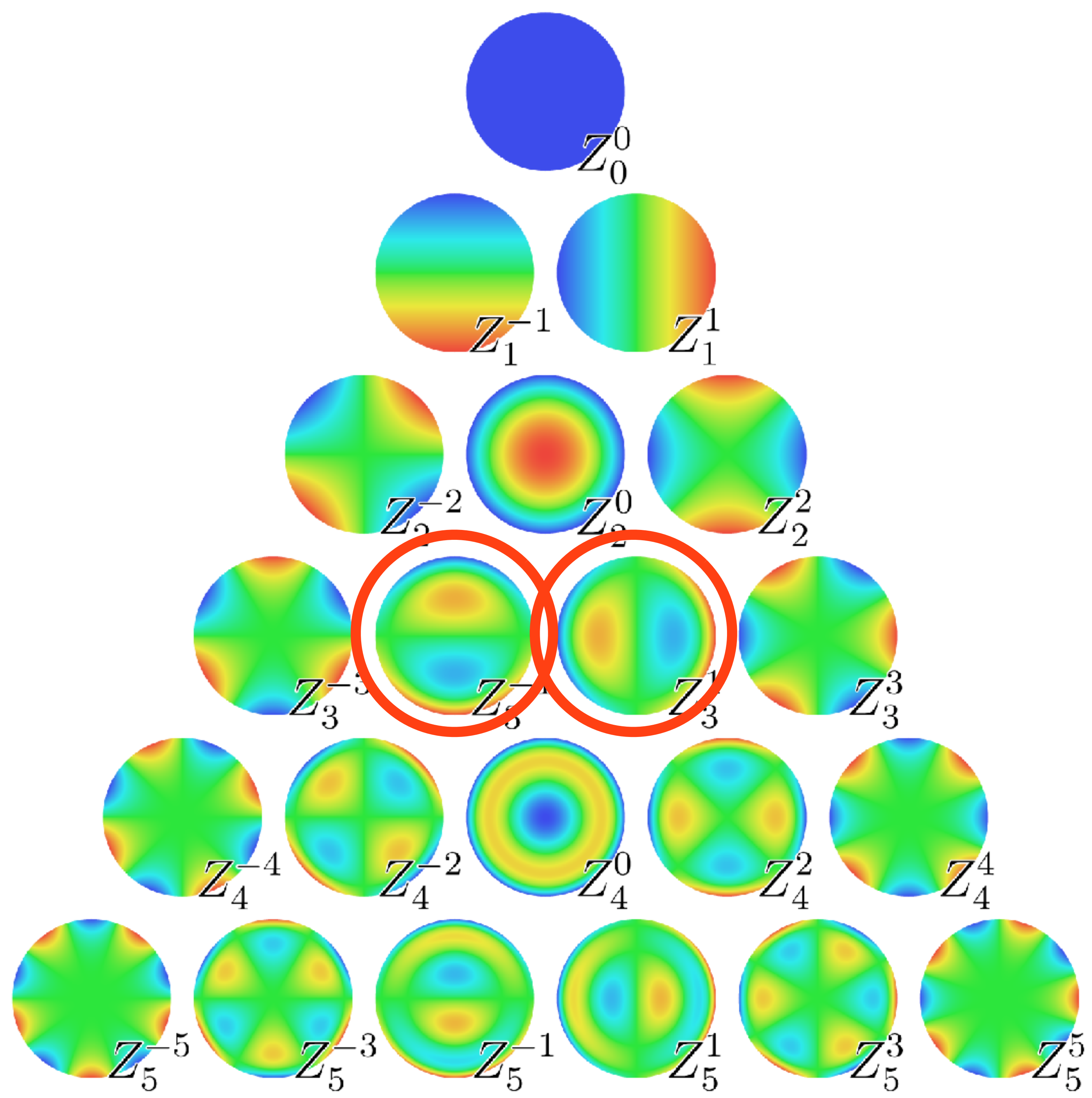


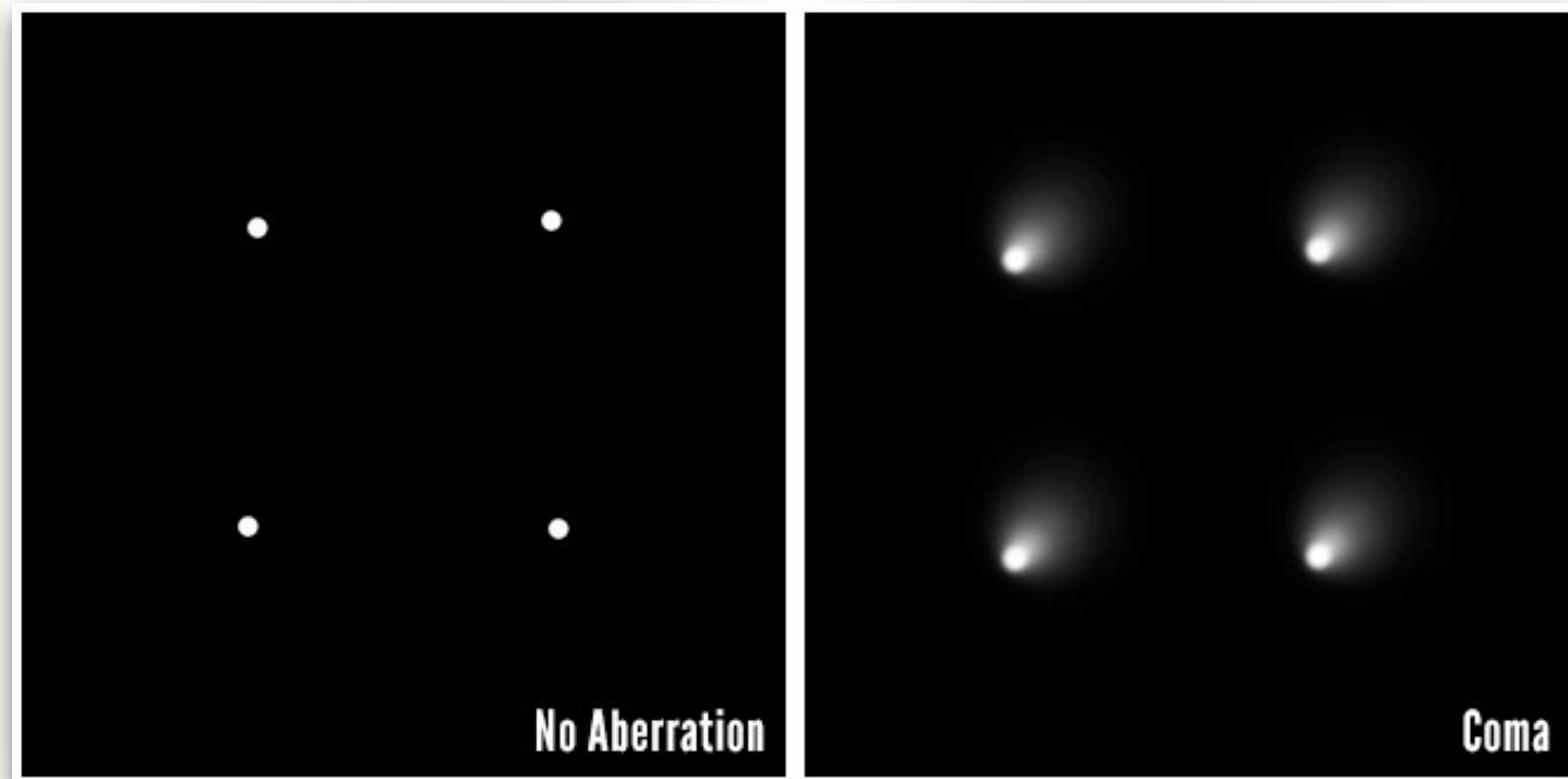
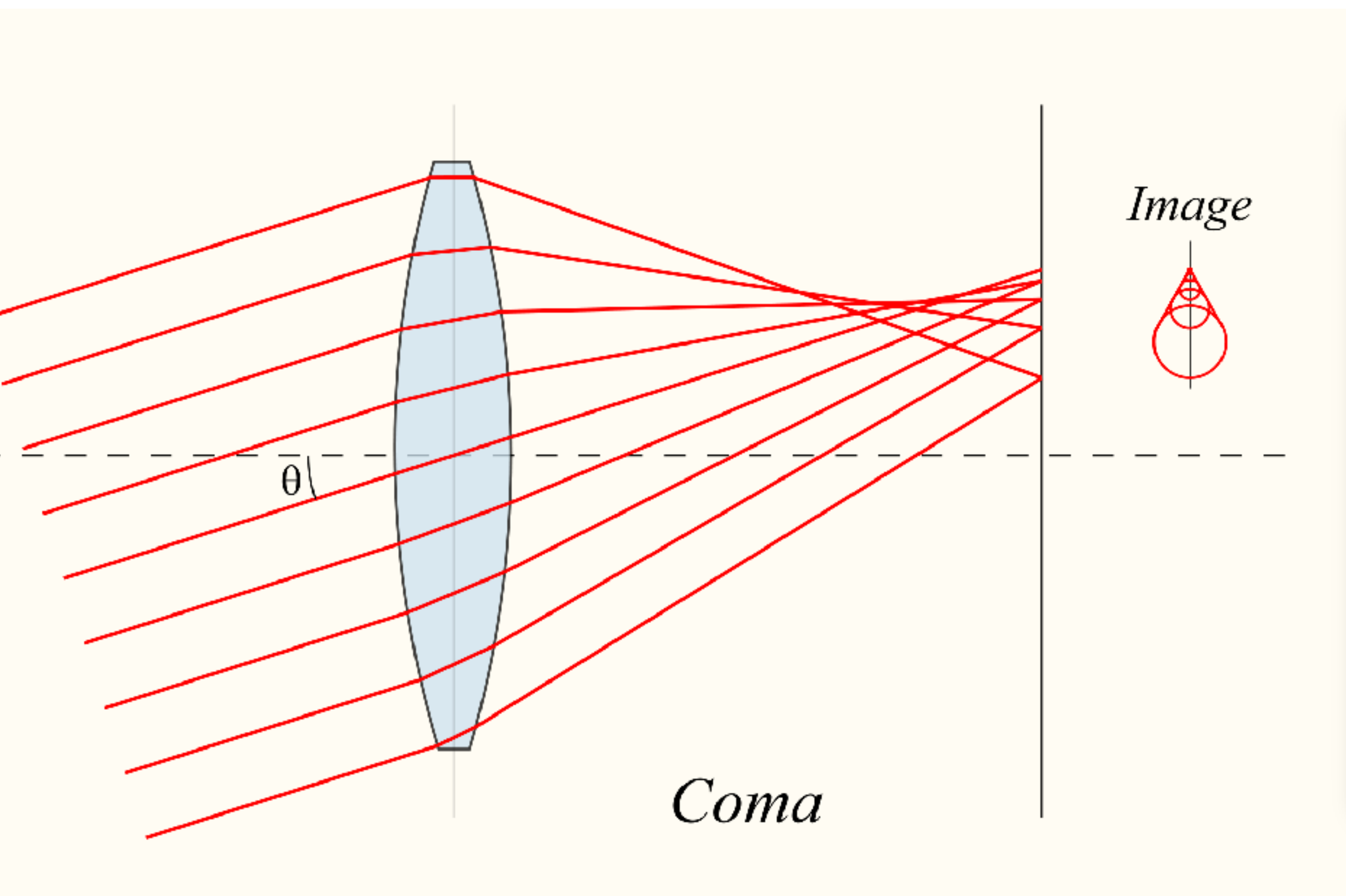
Overfocus

90°->



Coma

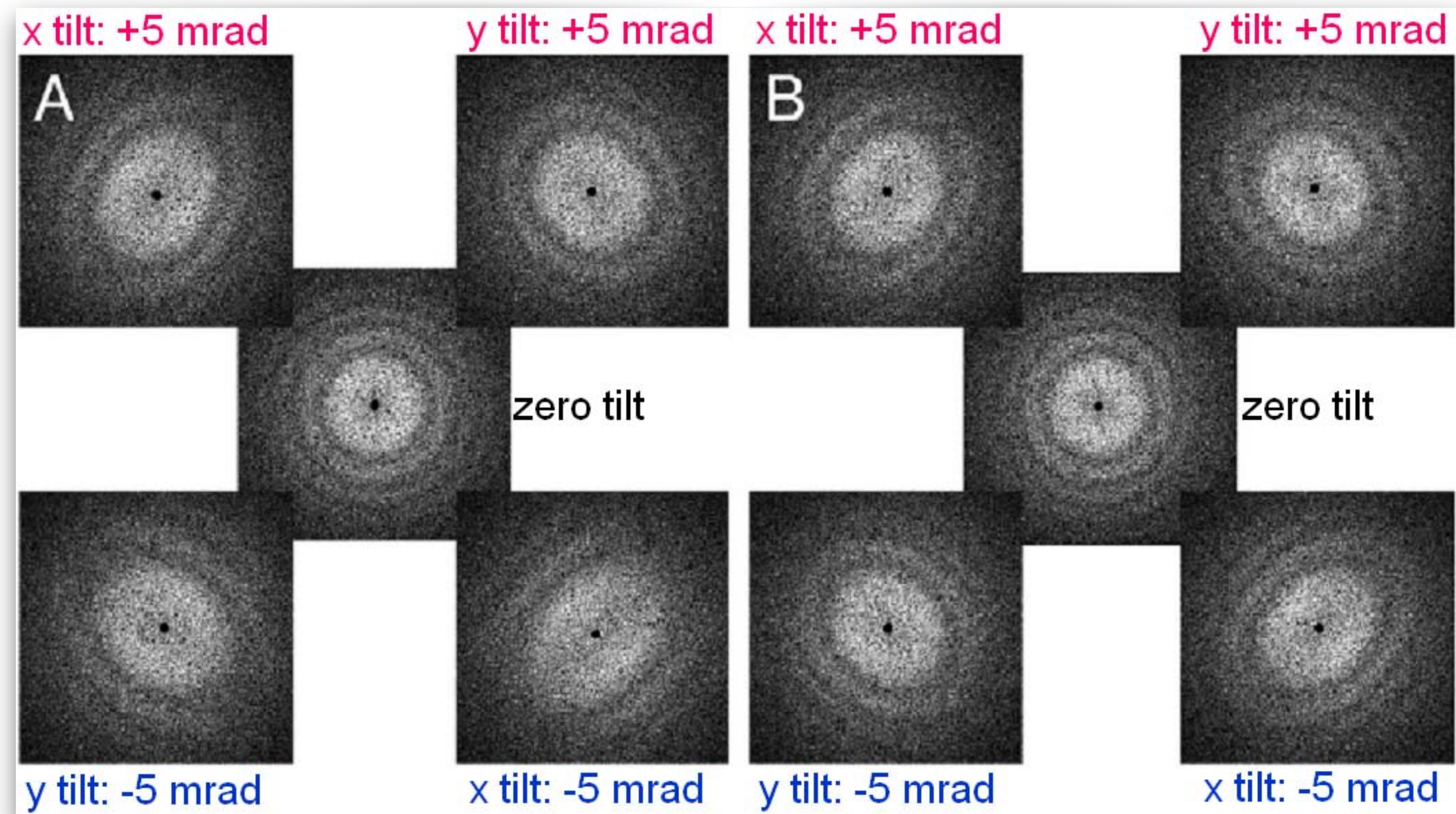




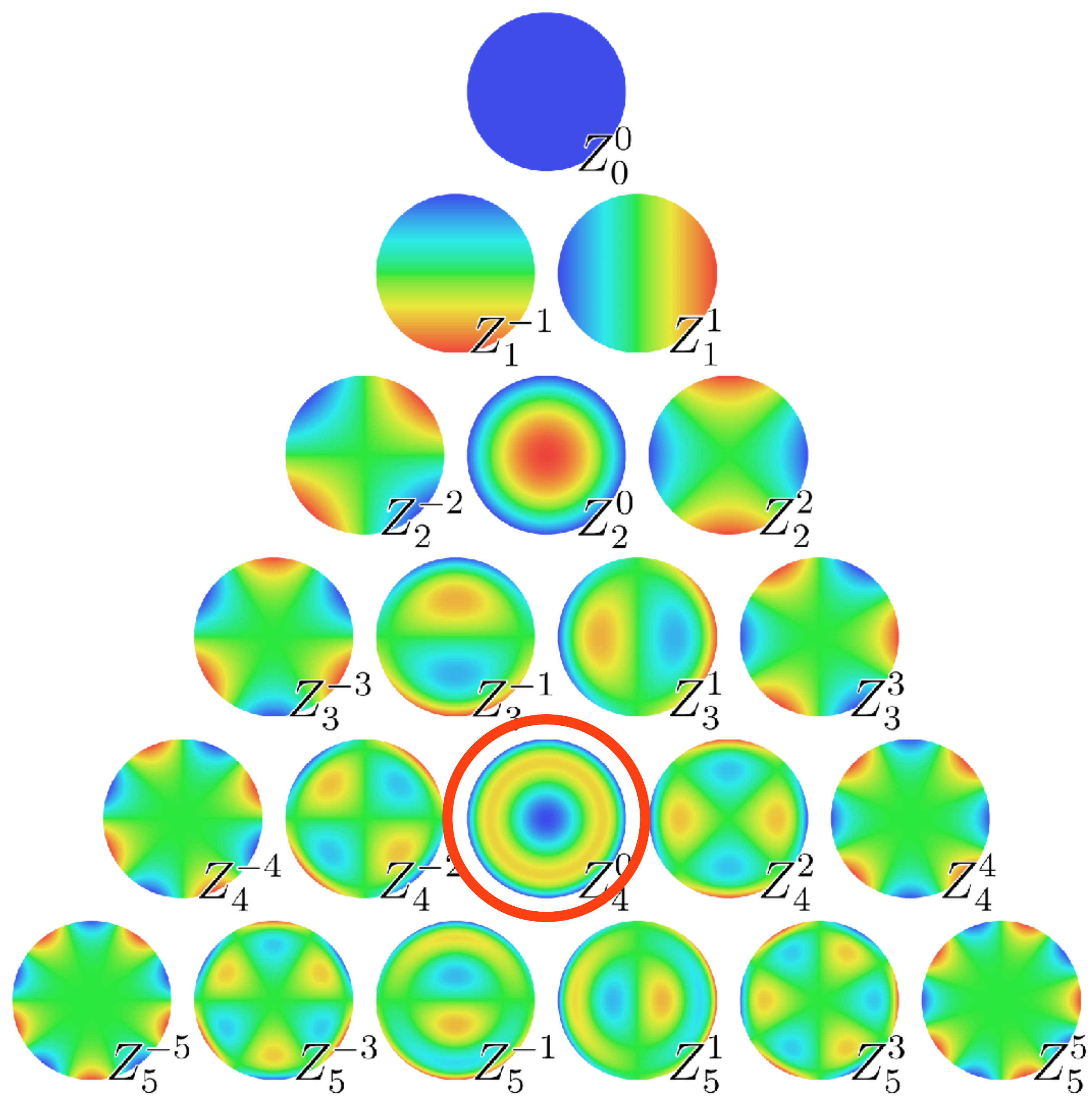
Example image from I. Norman

Reducing coma by minimising beam tilt

1. Voltage centring
2. Current centring
3. Zemlin Tableaux



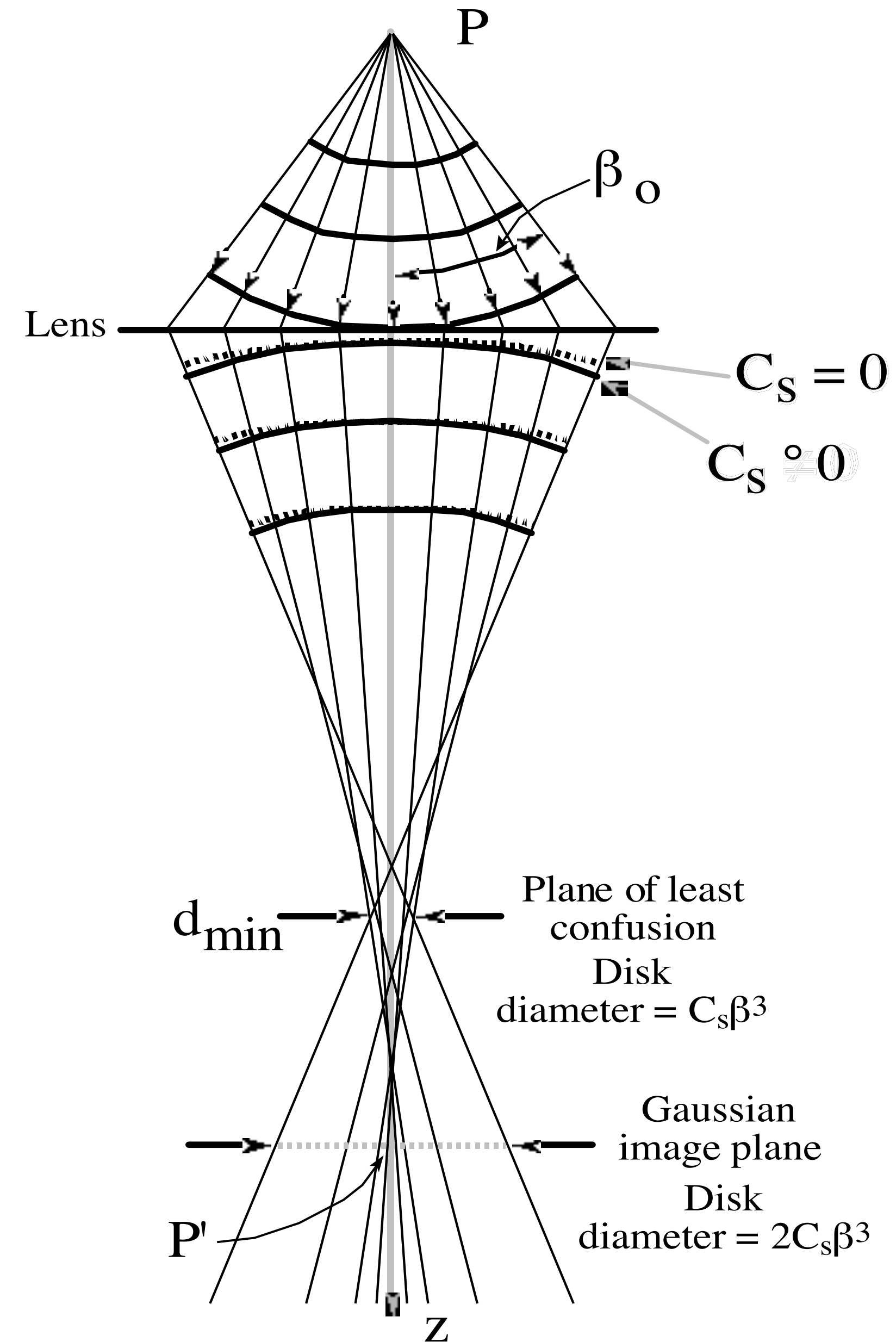
Spherical aberration



Spherical Aberration

Lens is stronger off axis

Plane of least confusion



CTF

Contrast
Transfer
Function

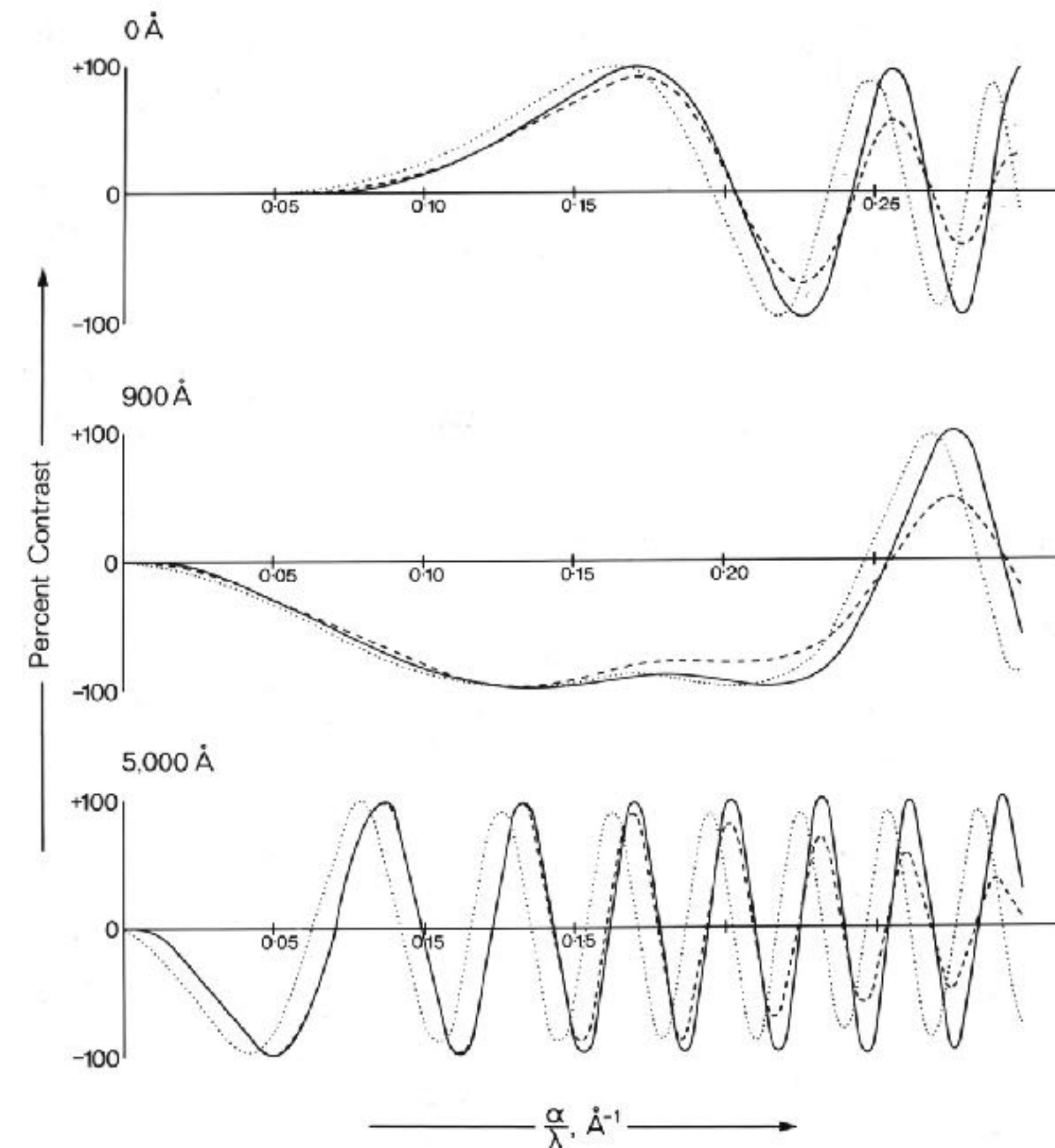
Phil. Trans. Roy. Soc. Lond. B. **261**, 105–118 (1971) [105]

Printed in Great Britain

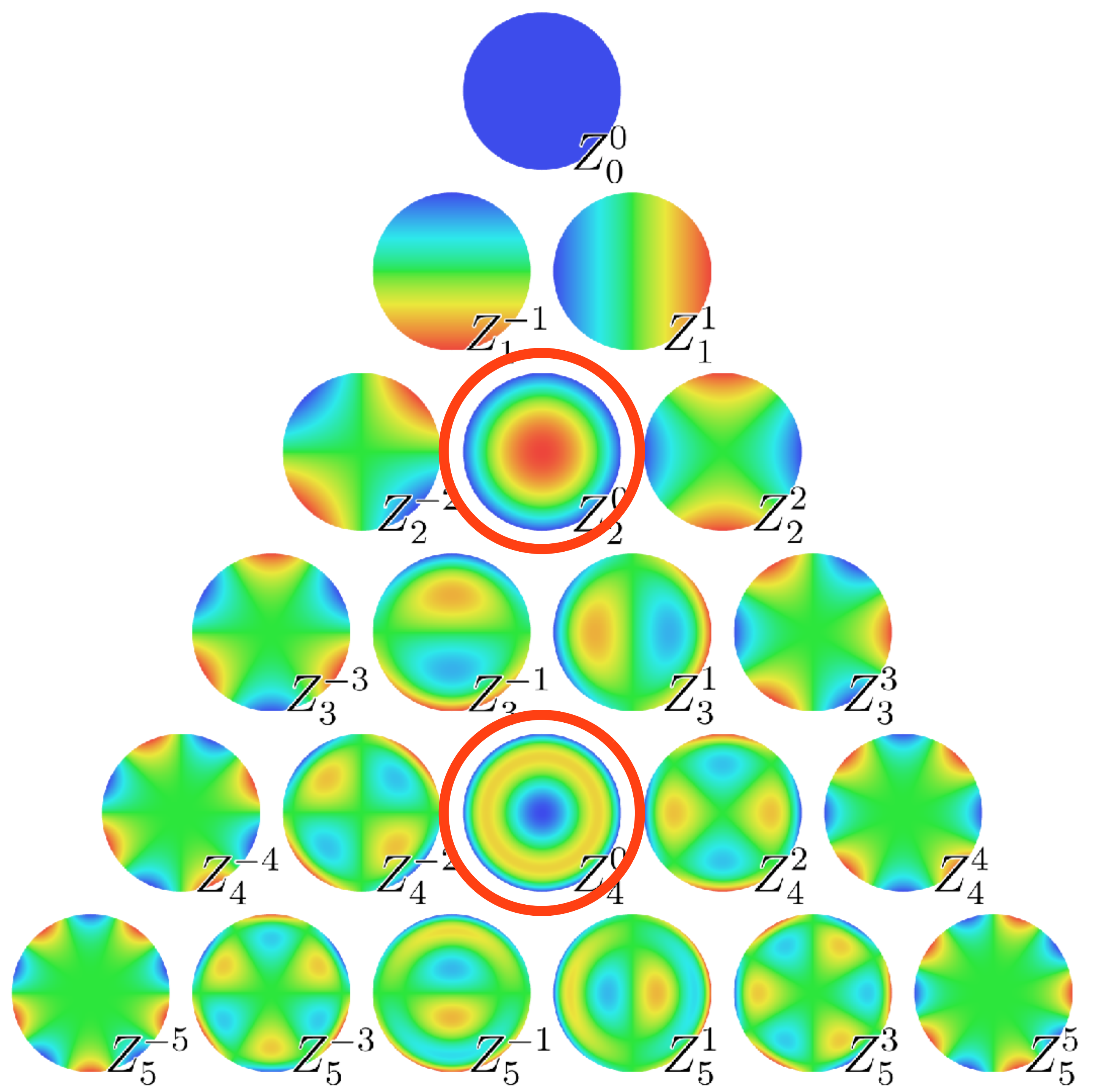
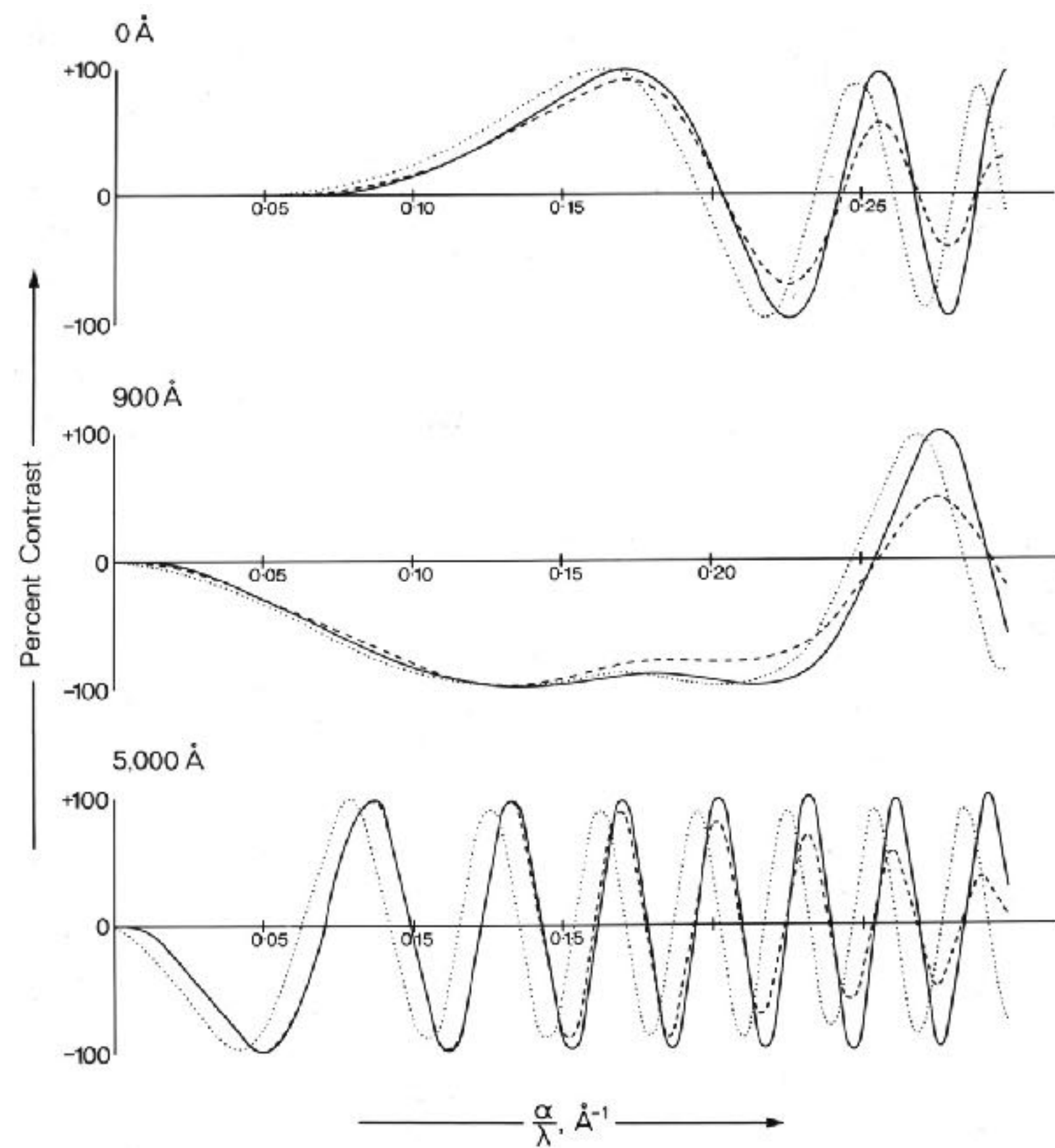
Measurement and compensation of defocusing and aberrations by Fourier processing of electron micrographs

BY H. P. ERICKSON AND A. KLUG, F.R.S.

Medical Research Council Laboratory of Molecular Biology, Cambridge



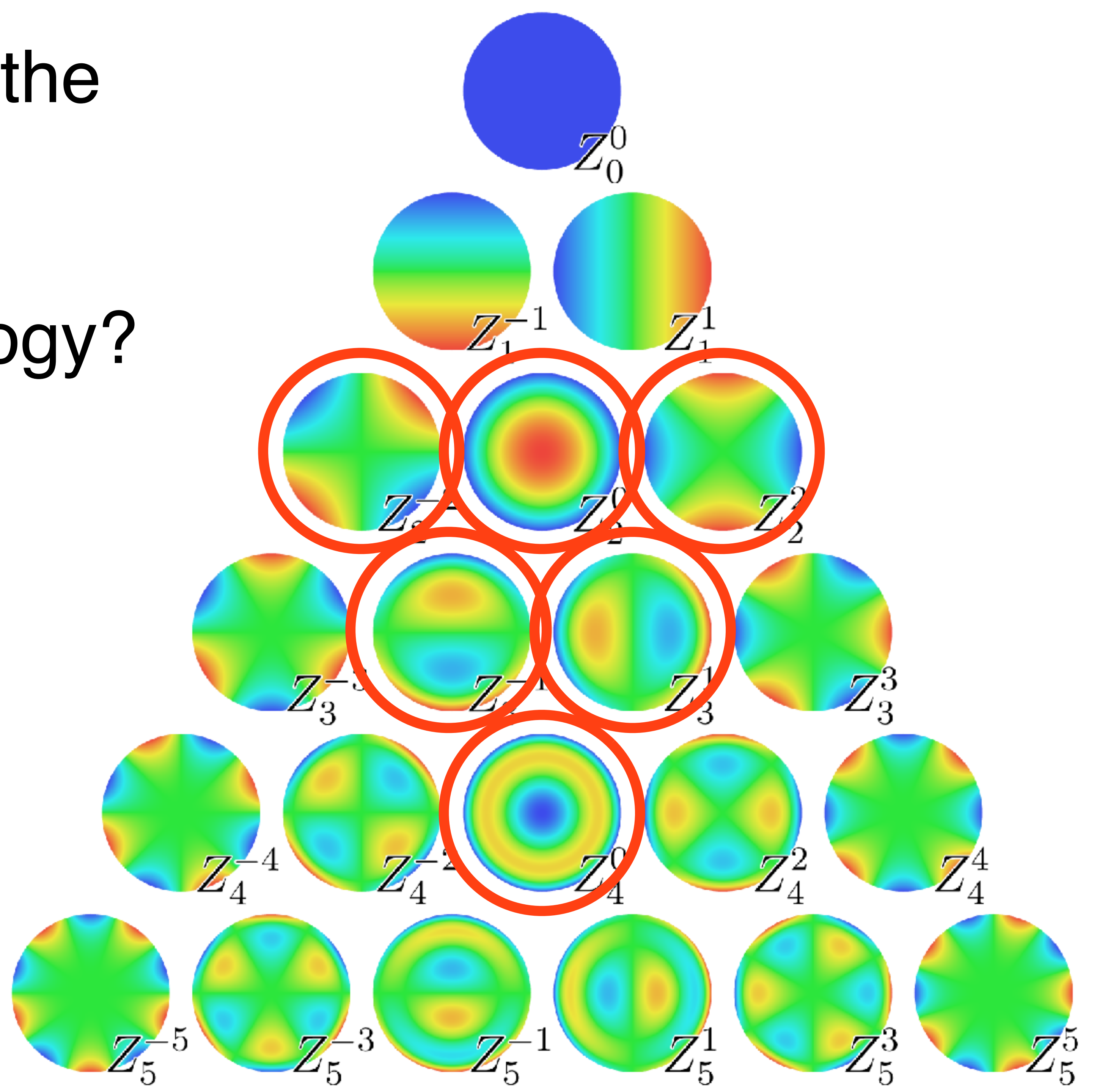
Correct with software instead:
CTFFIND, GCTF or similar



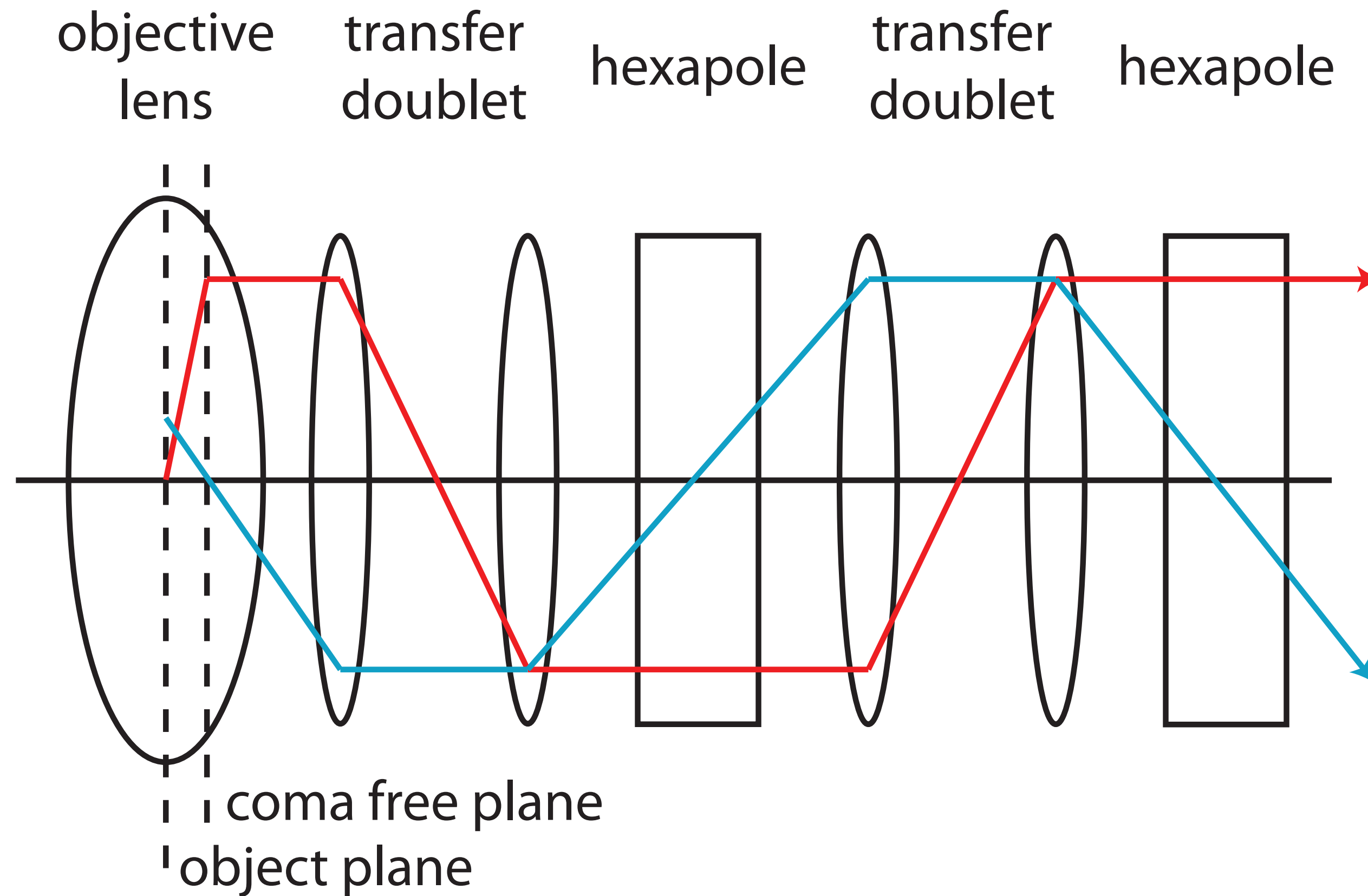
What about the rest of the
Lens aberrations?

Do they matter for biology?

not till $< 2 \text{ \AA}$



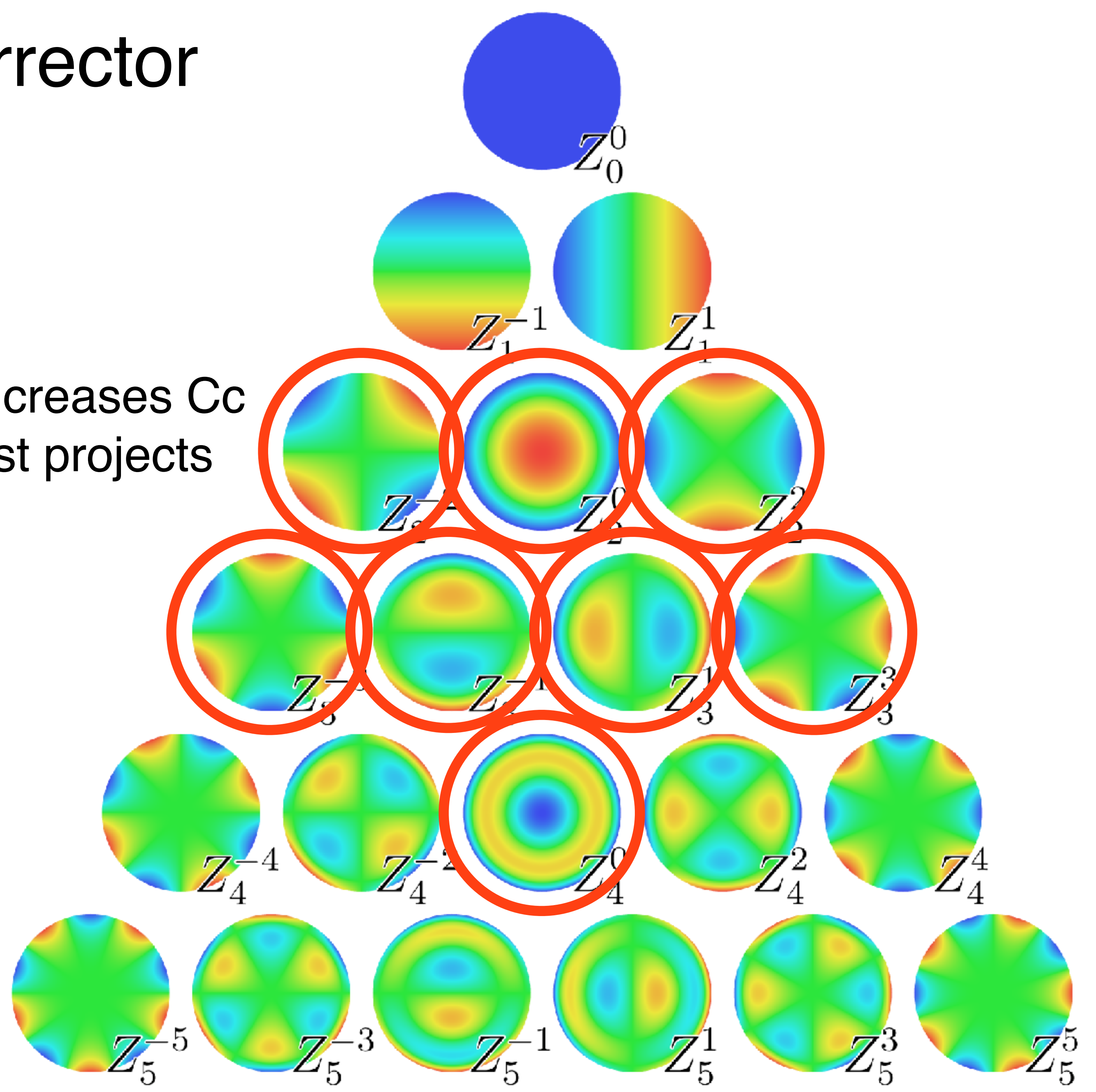
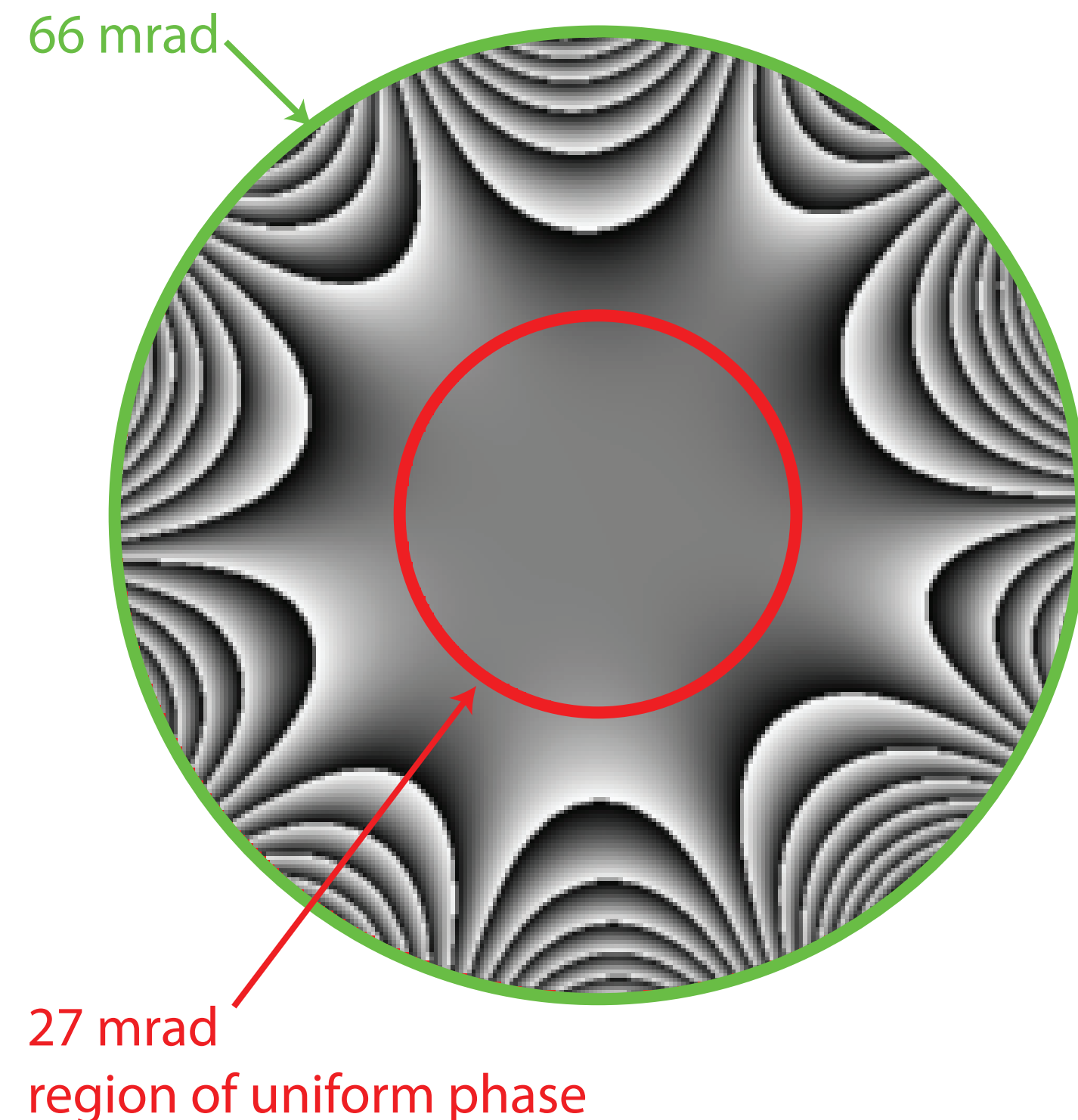
Aberration corrector



3rd order aberration corrector

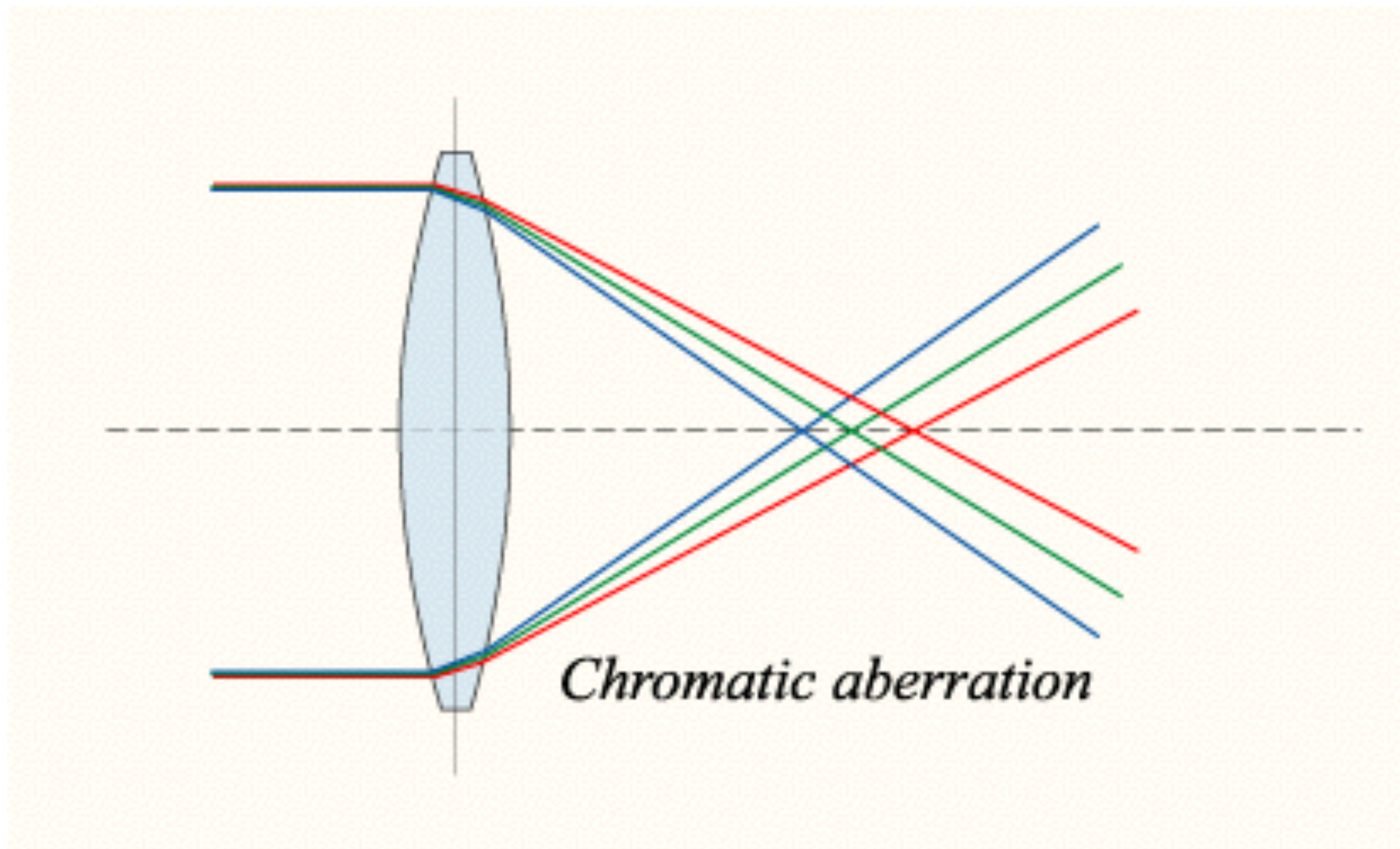
for going from 2 Å to 0.5 Å
or low energies (< 100 keV)

expensive, slows data collection, increases Cc
harder to use no advantage for most projects



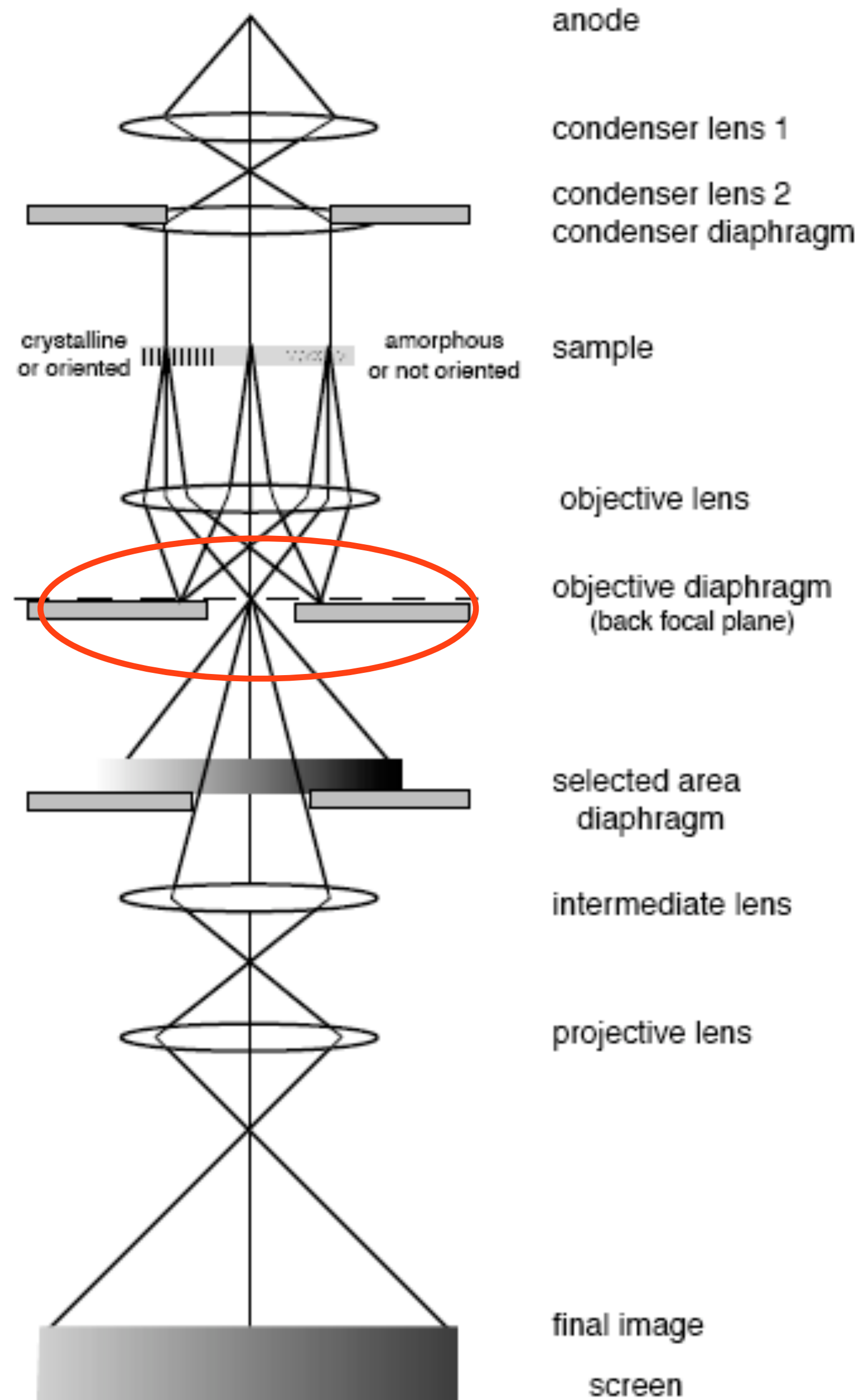
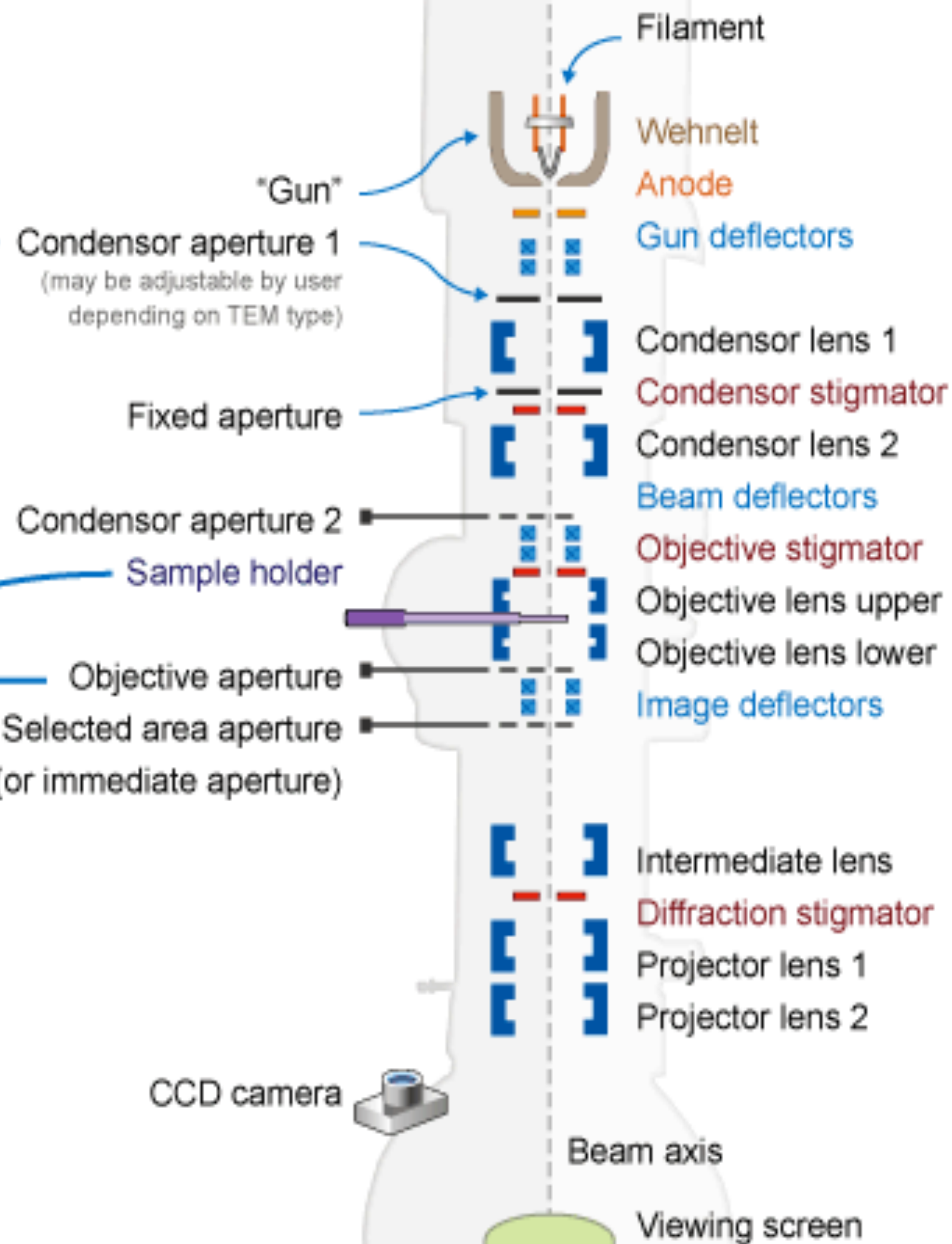
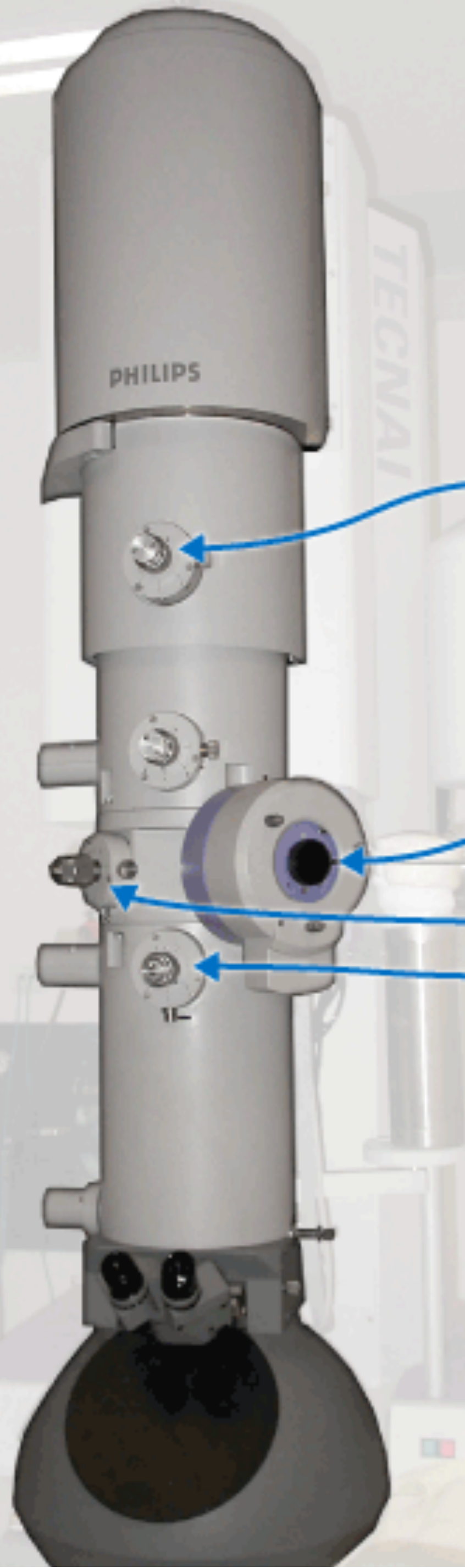
Chromatic Aberration

- Different wavelengths focus at different planes

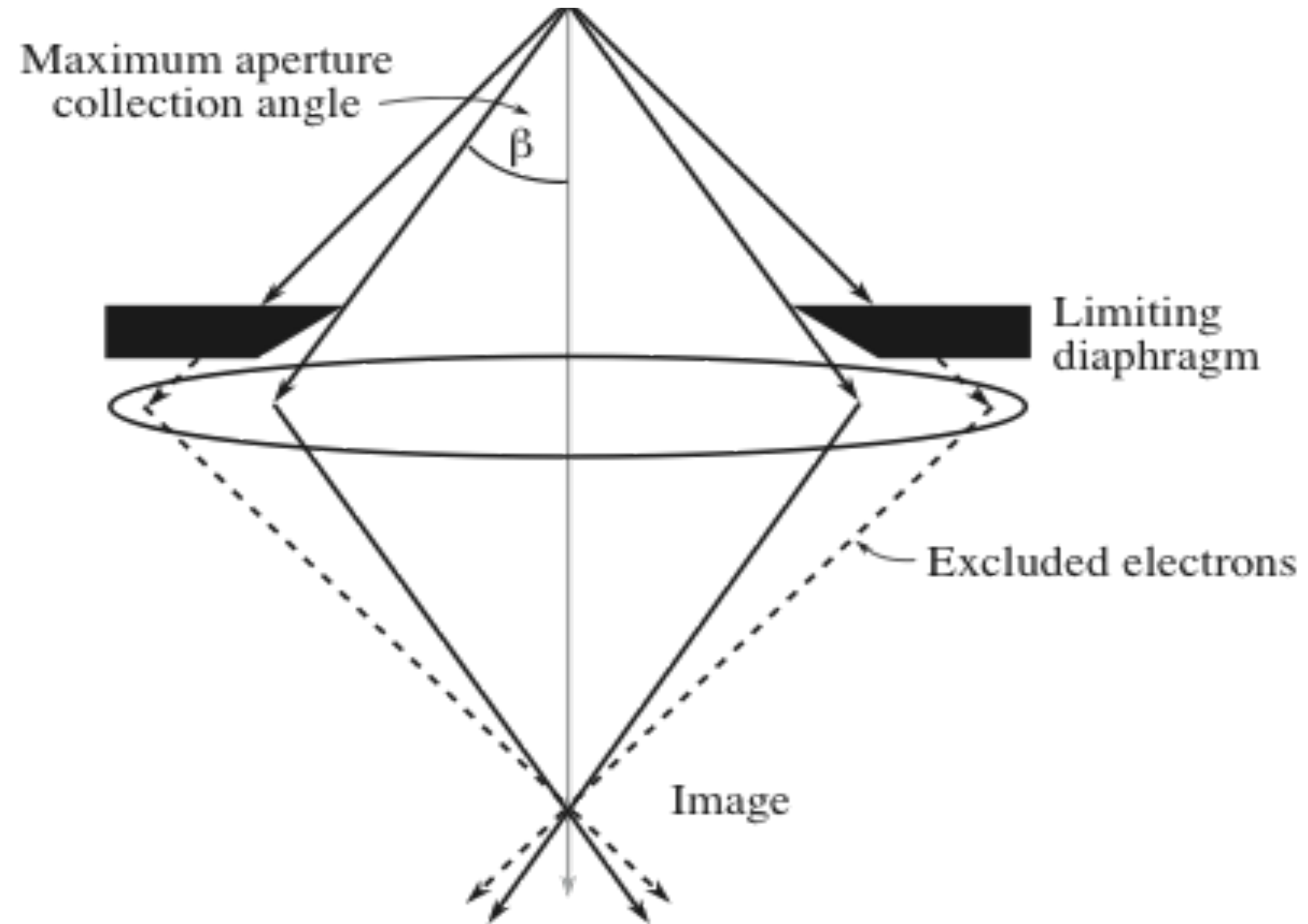


Example TEM schematic

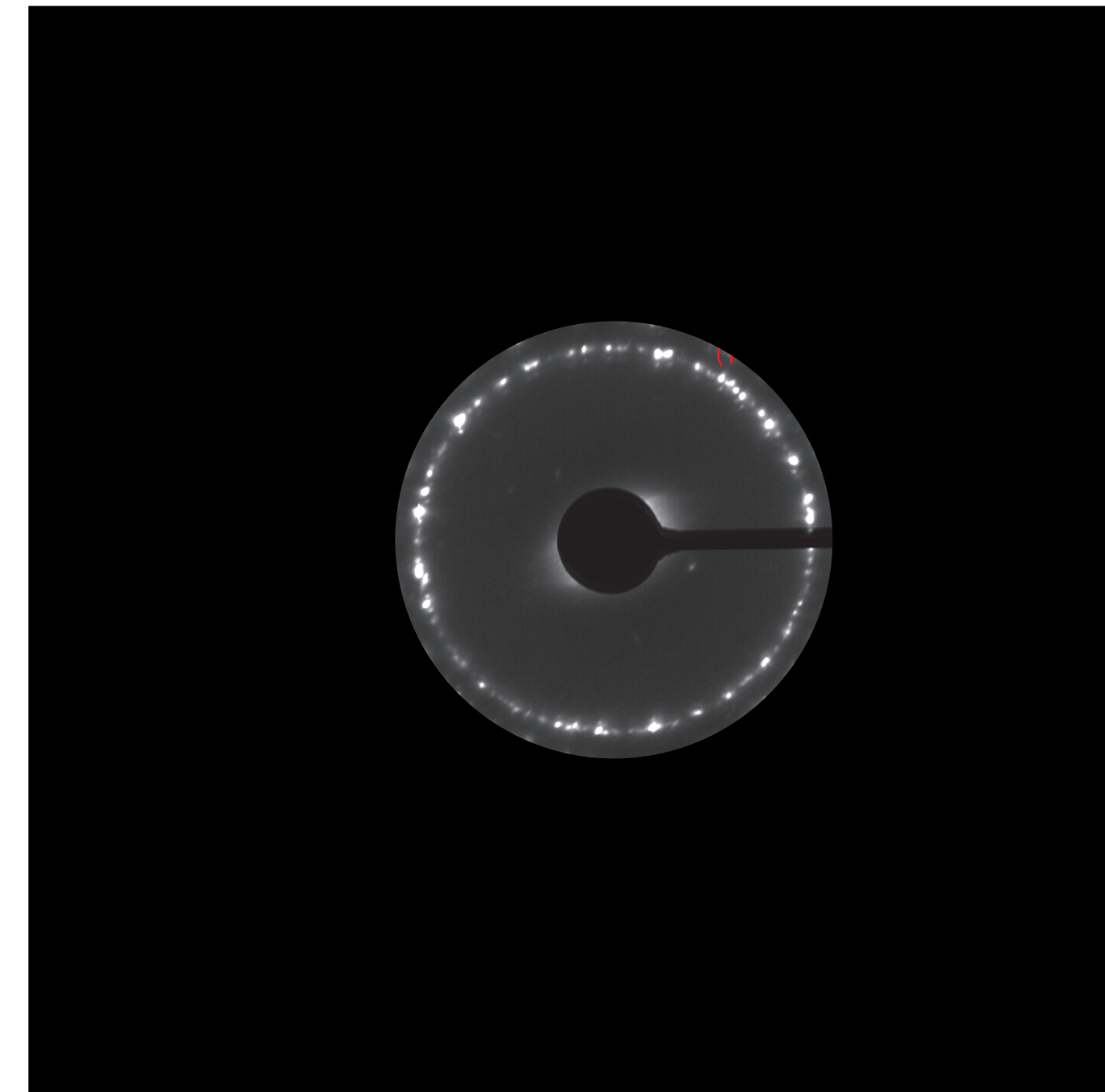
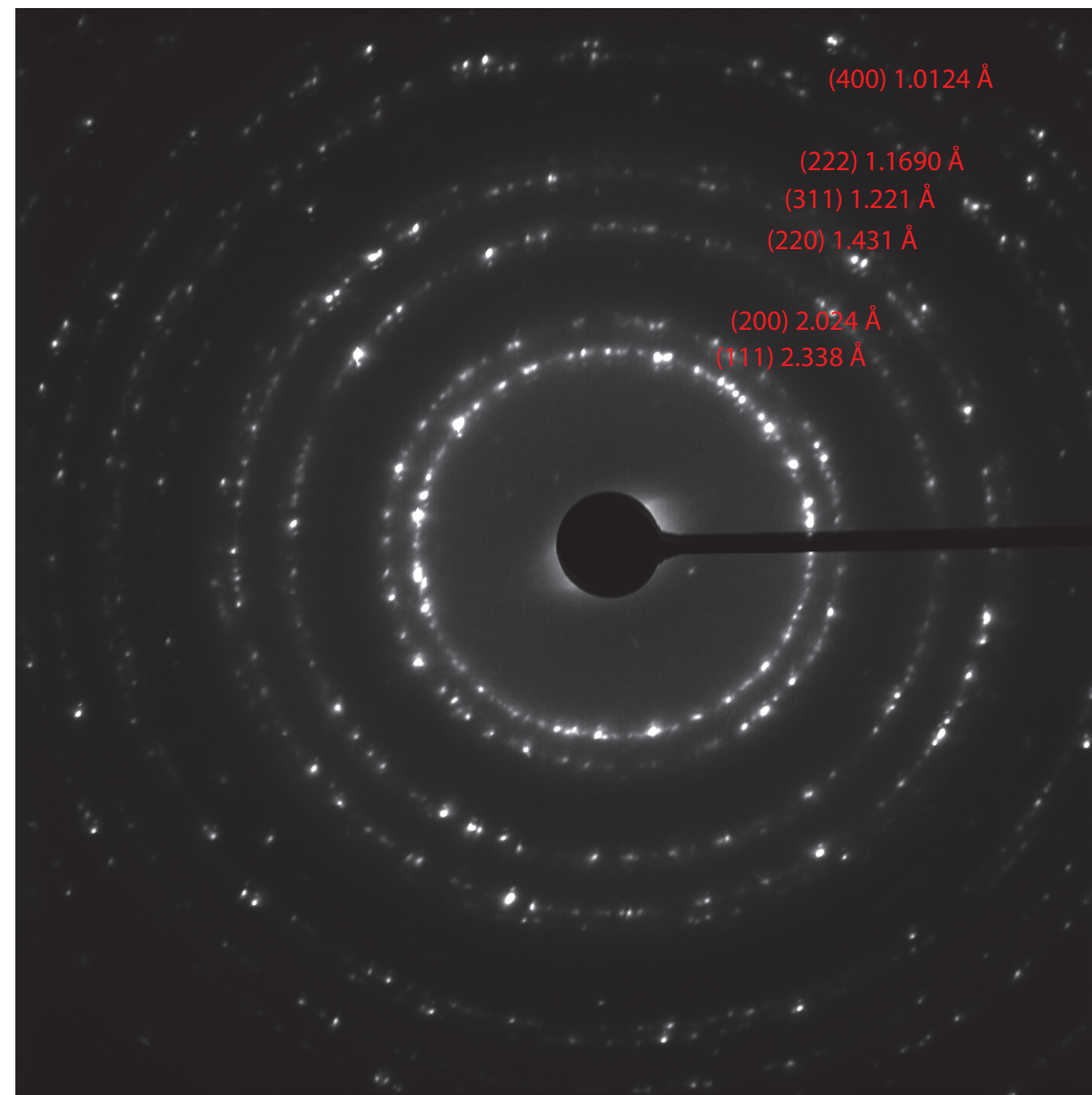
One of many types of TEMs



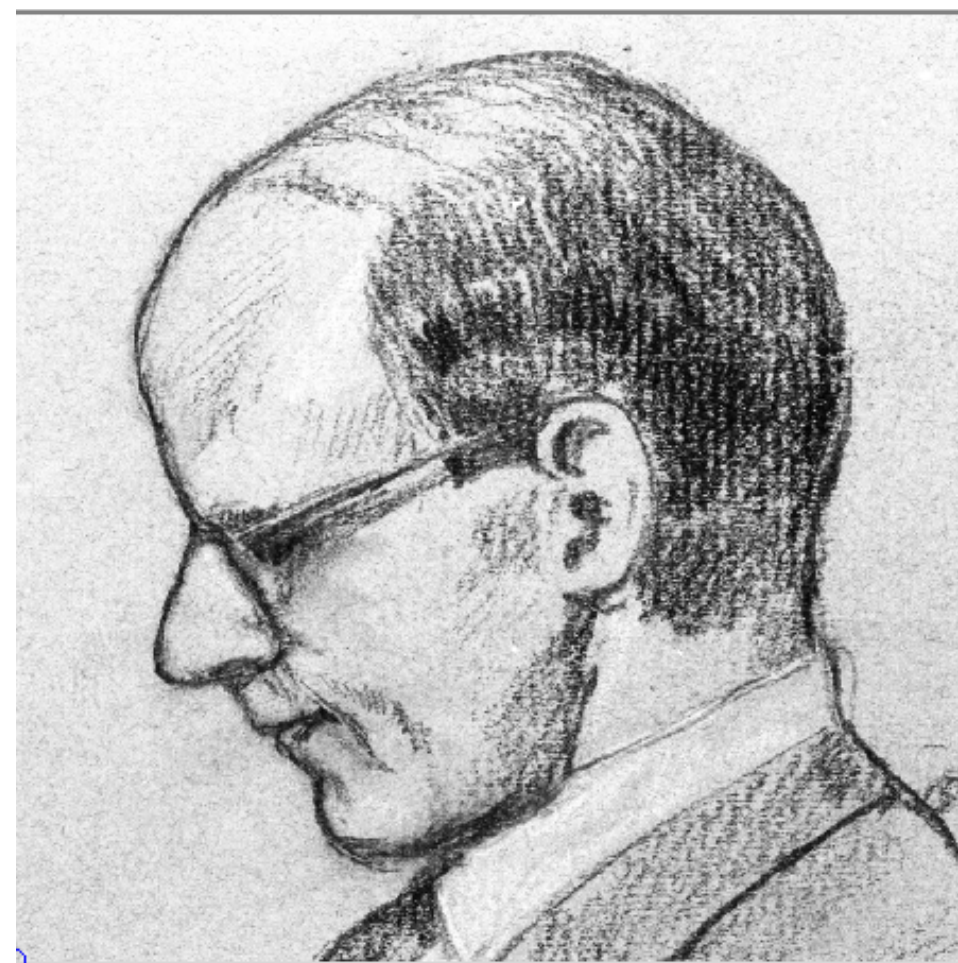
Objective aperture



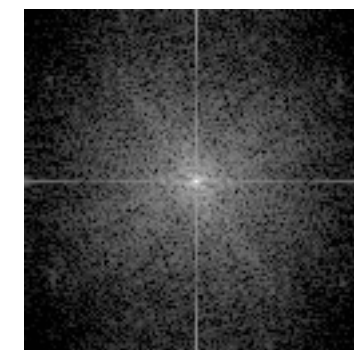
Objective aperture



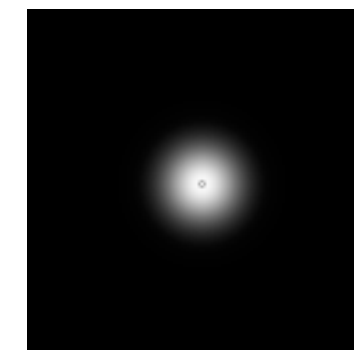
Beware...



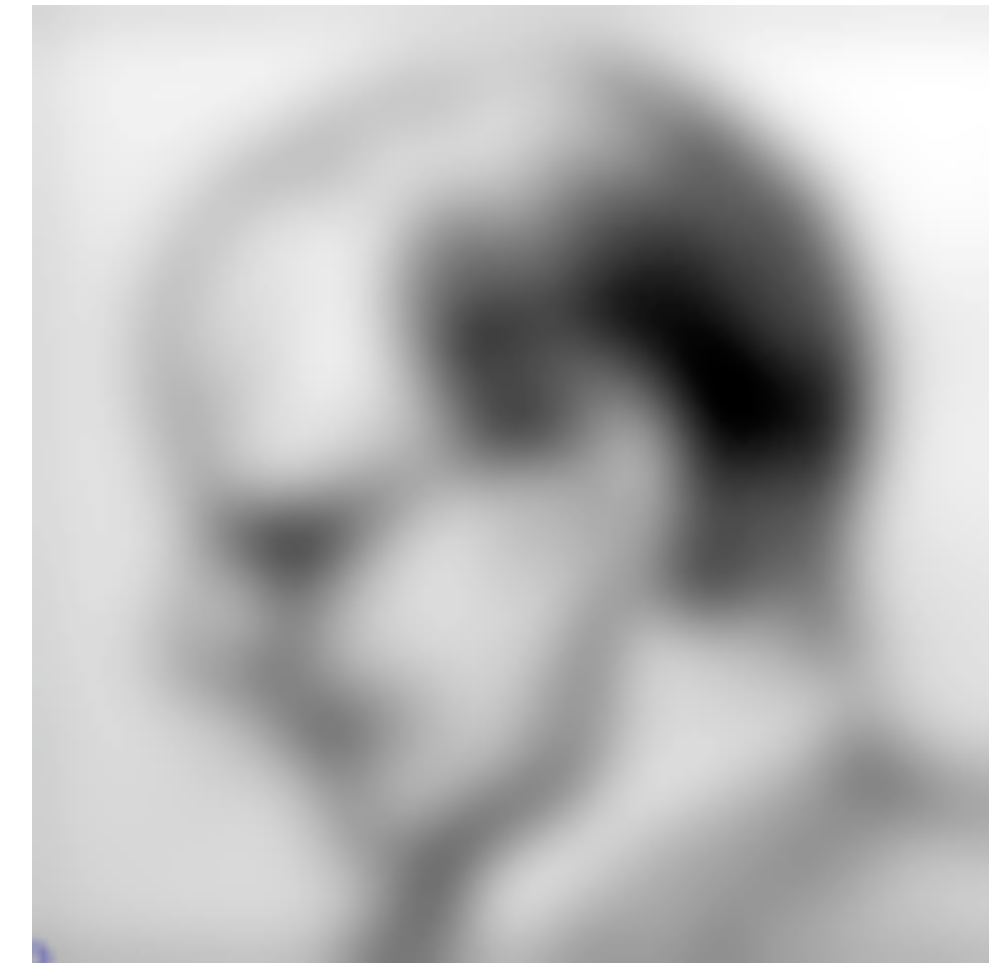
FT



x

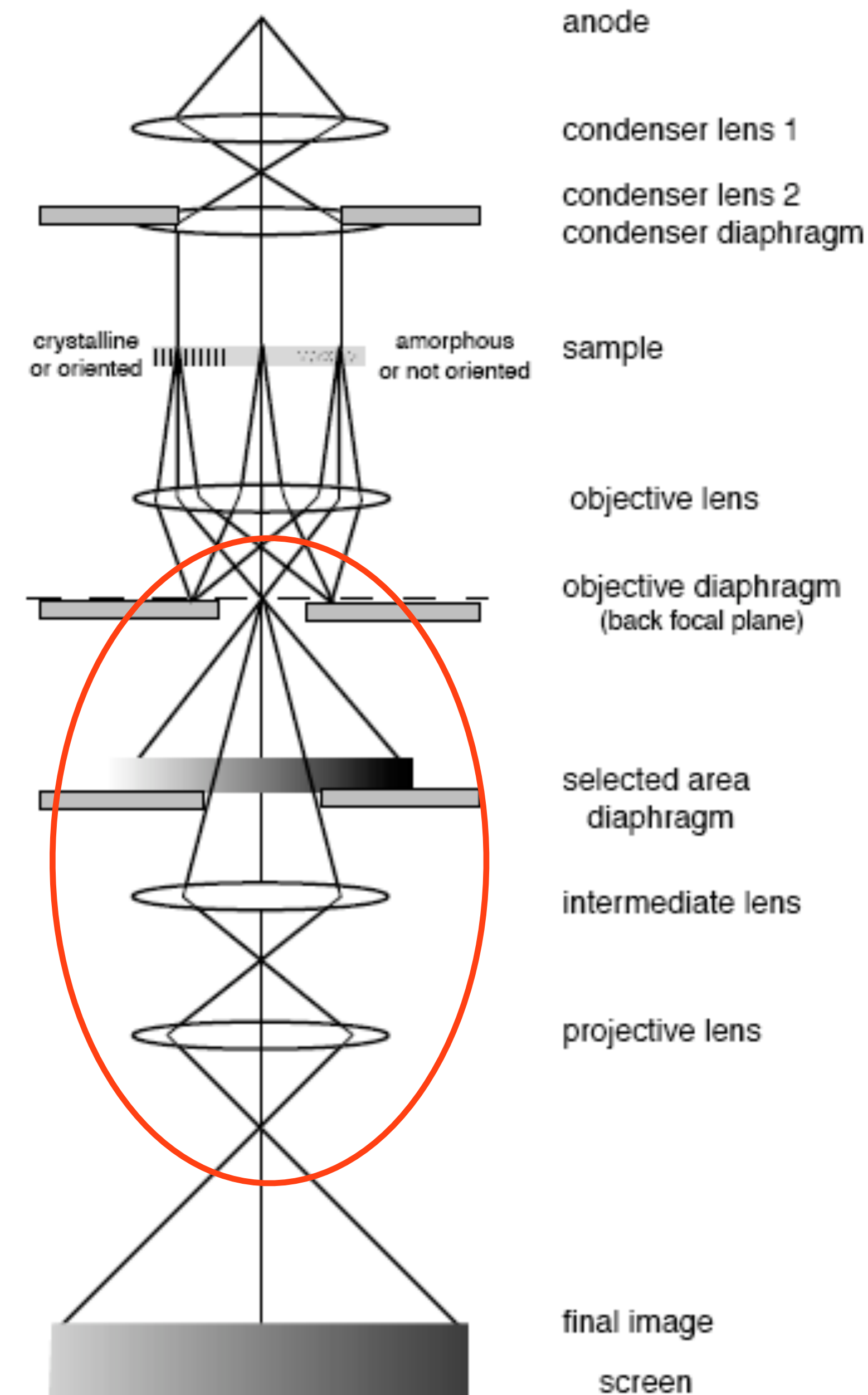
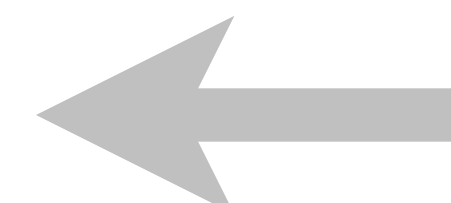
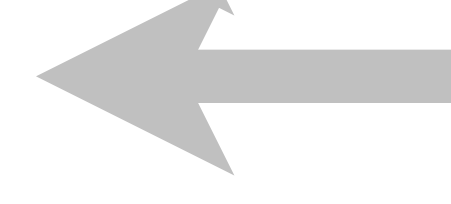
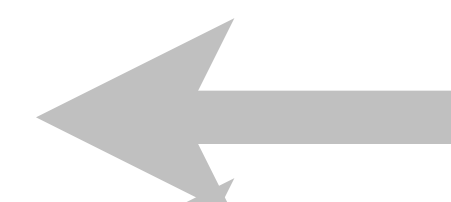
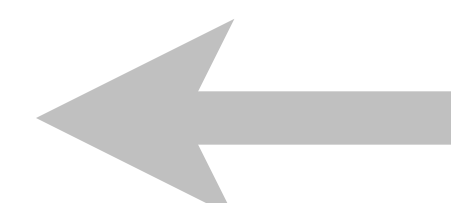
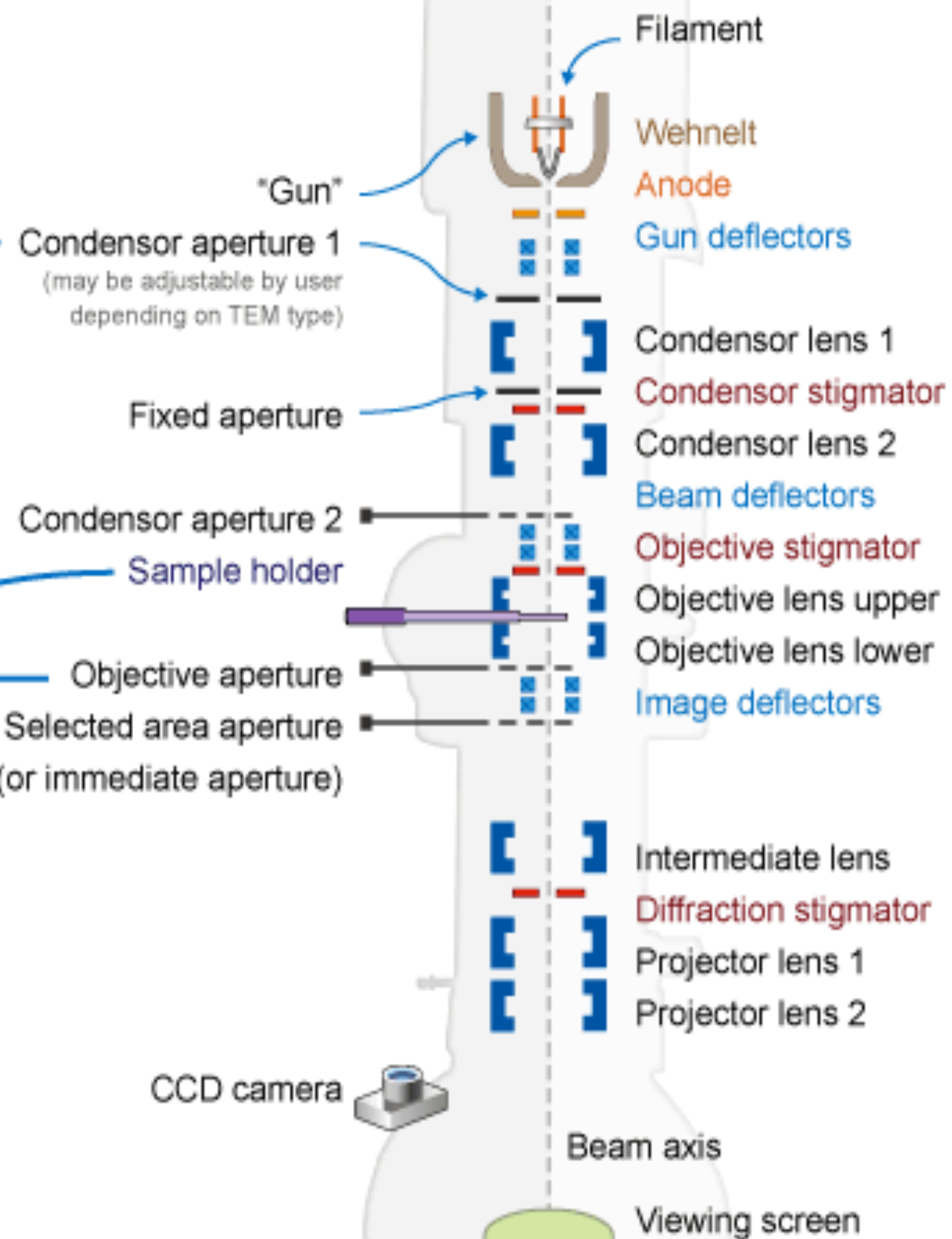
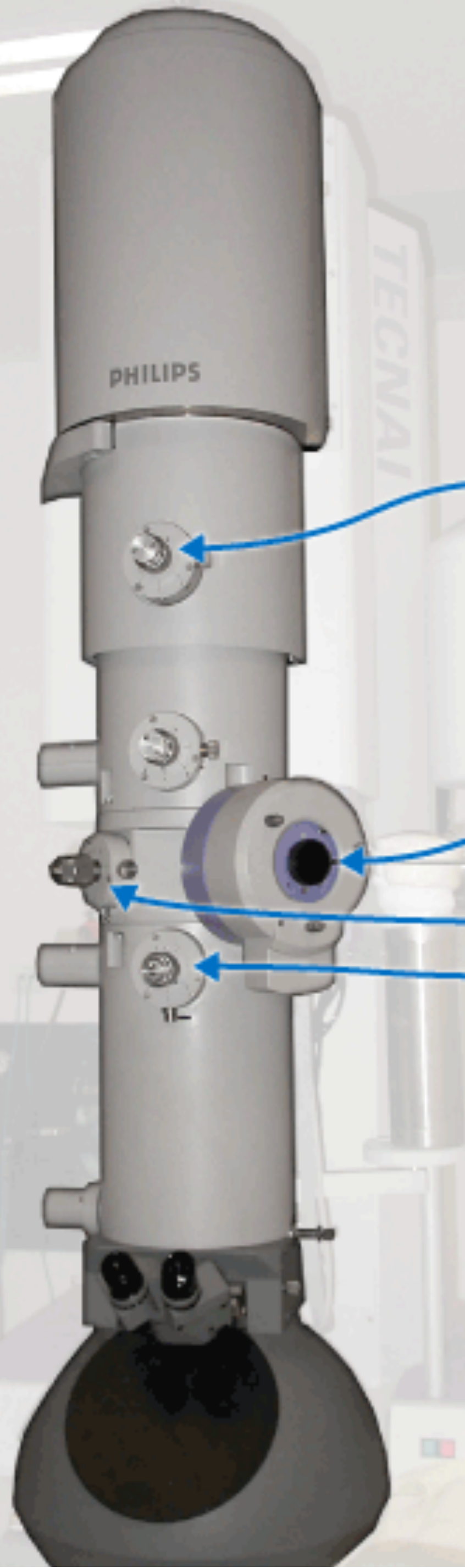


Low-pass filter



Example TEM schematic

One of many types of TEMs



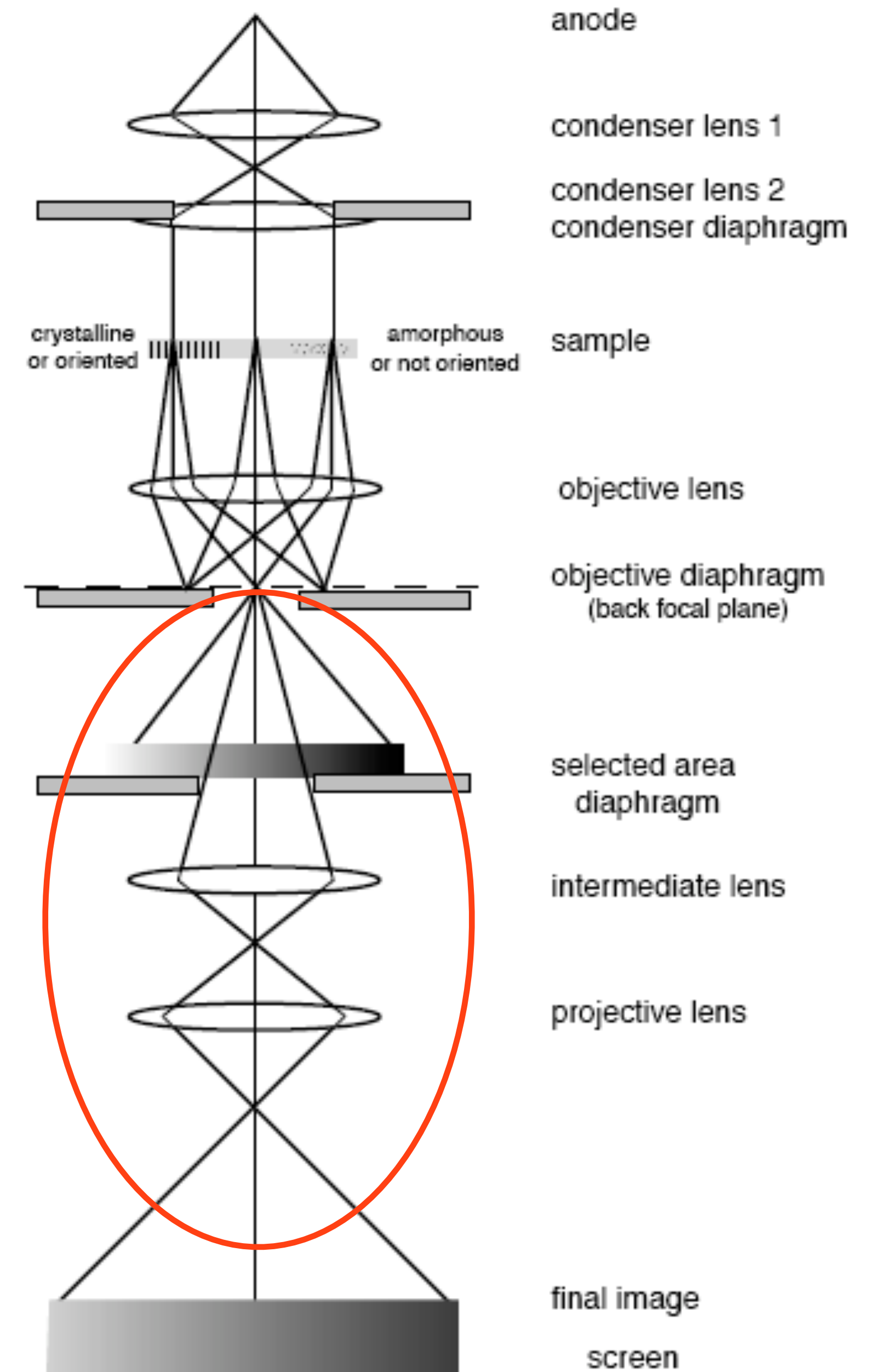
Magnify it!

Intermediate & projector lenses magnify the image created by the objective lens

Goal: take image created by the objective lens and match it to the detector with as little distortion as possible (don't forget Niquist...)

Nearly perfect lenses b/c very small angles used

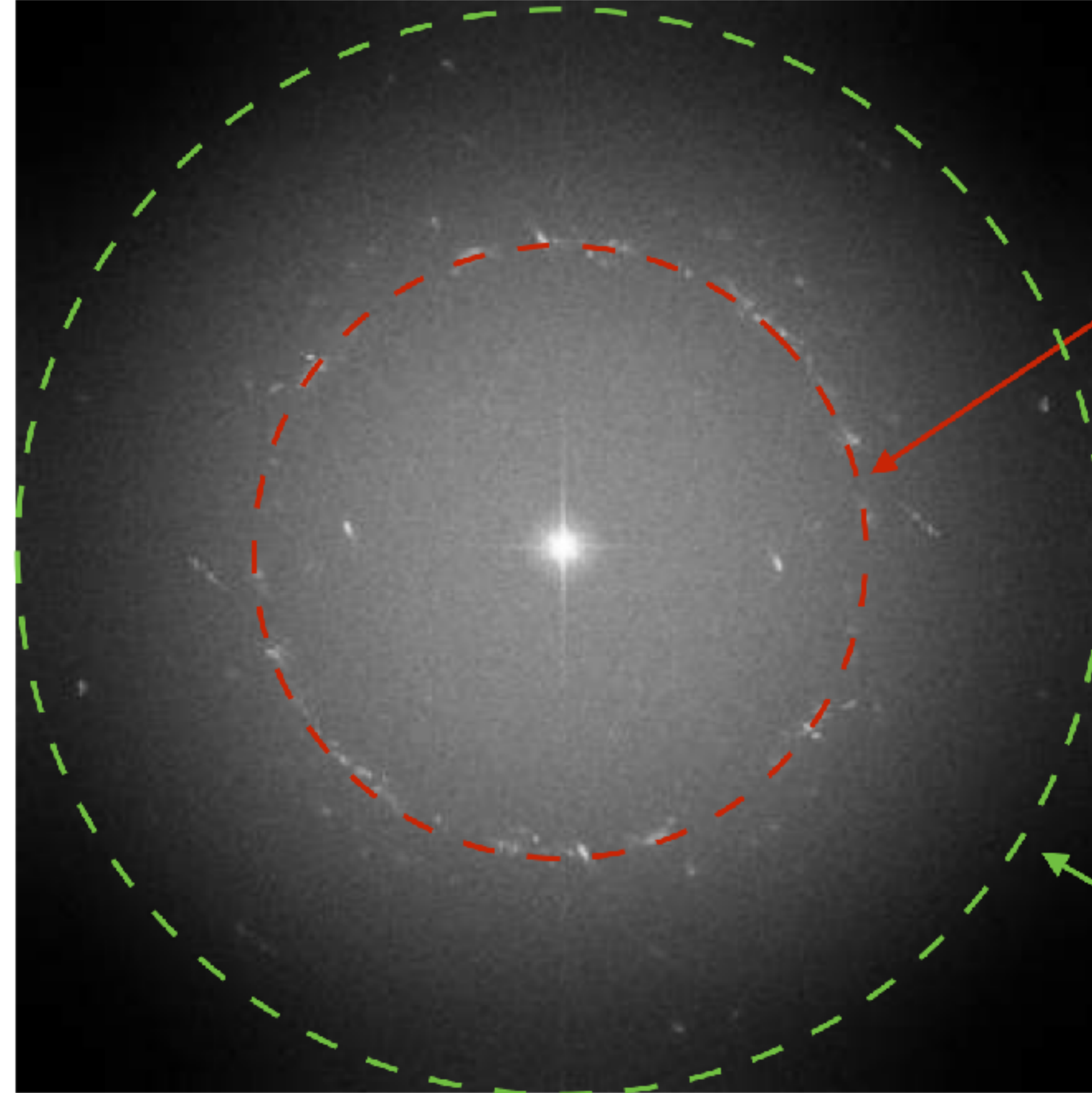
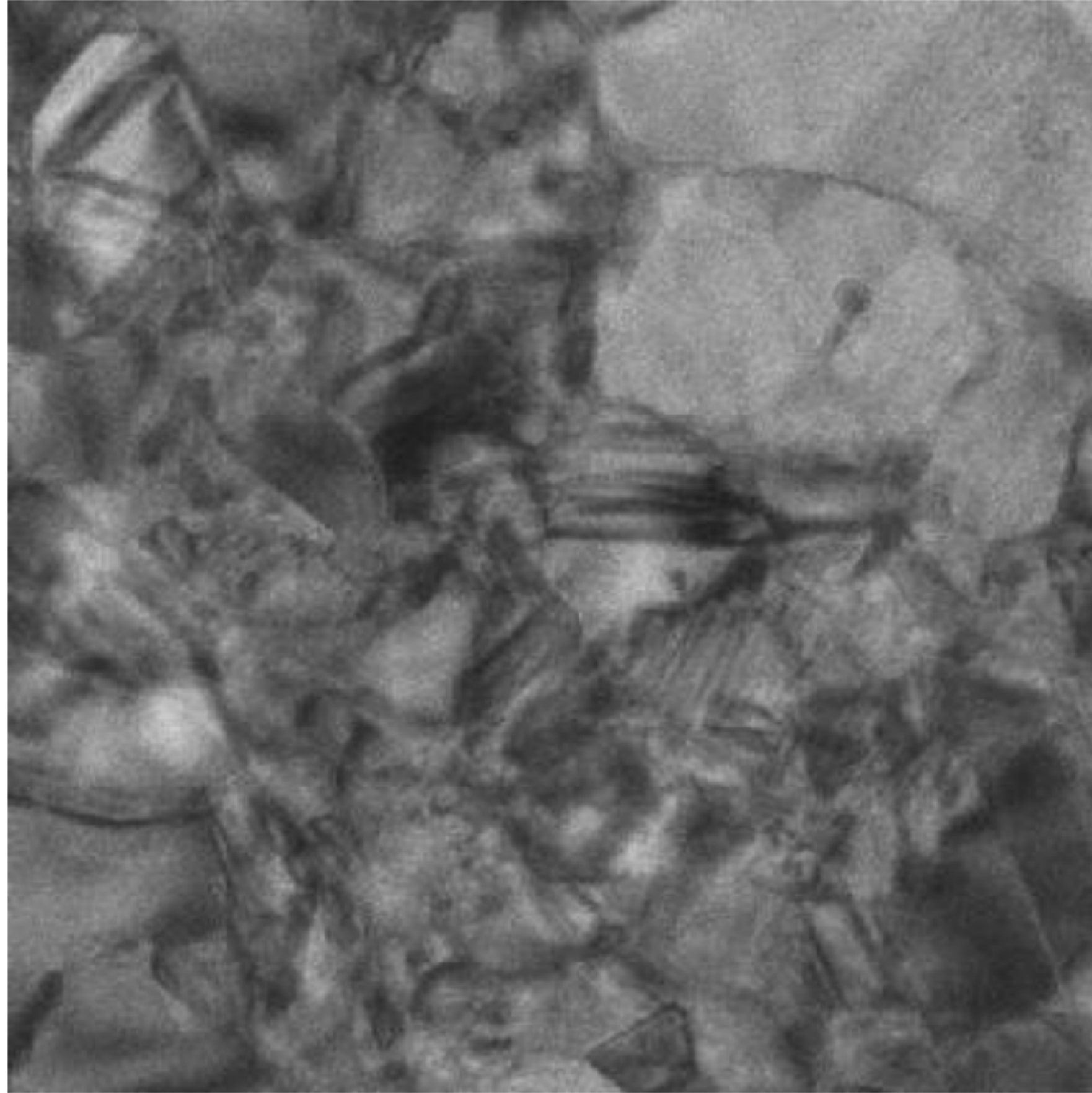
Beware: If not aligned properly, projector lenses can distort image causing differential magnification and other weird effects (barrel, etc.)



Magnification Calibration

- Pixel size is fixed - a property of the detector
- Magnification is variable from ~ 10 to 10^6 - must be calibrated
- Do it yourself for each dataset - it is easy
- Take an image of gold crystal or graphitised carbon (many other choices as well)
- Also helpful to check that the microscope is well aligned.

⇒ FT



Gold foil micrograph
(120 kX nominal)
4096 x 4096

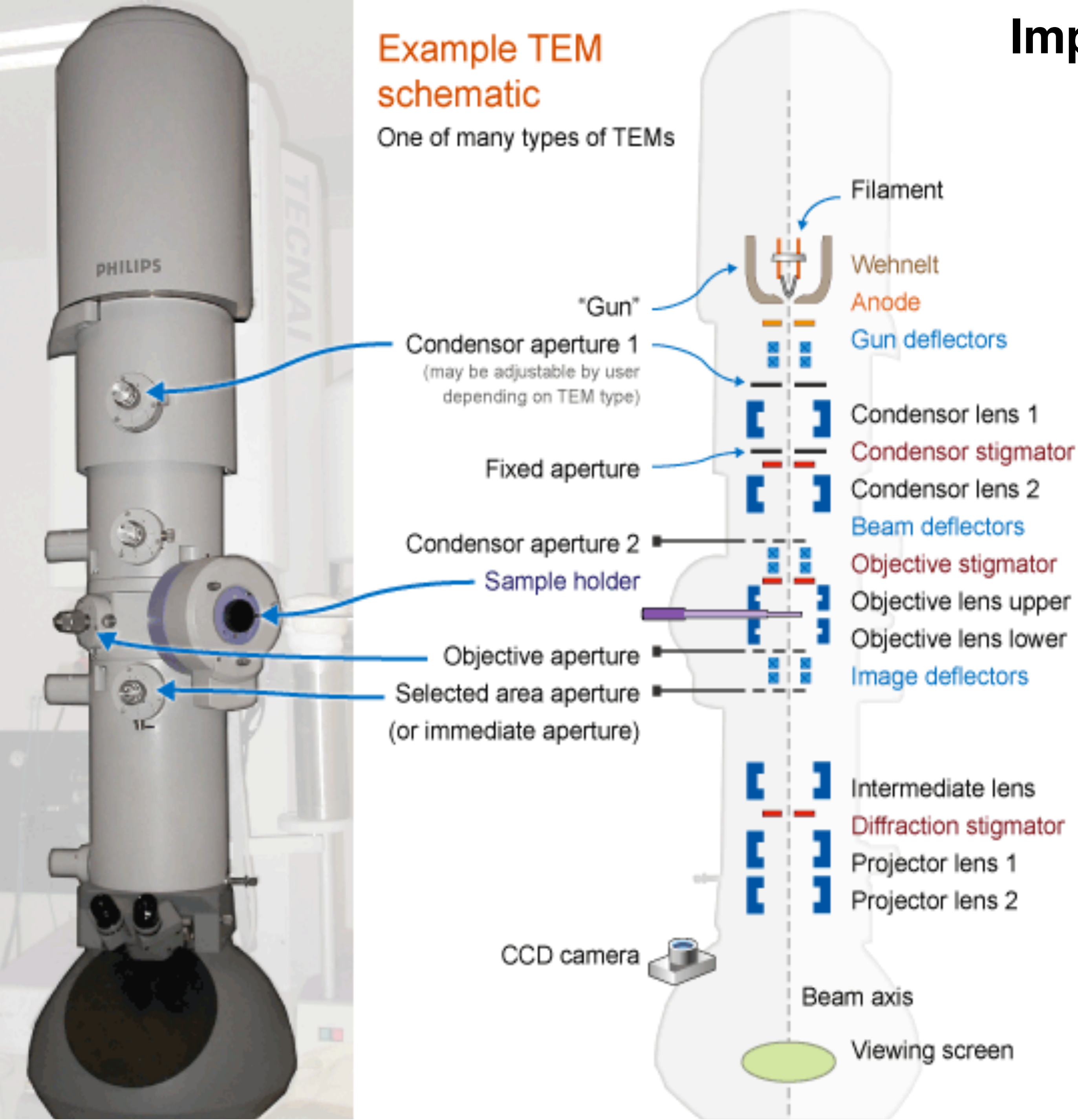
$$\frac{1155}{2048} = \frac{1/2.347 \text{ Å}}{2/\text{Pix.size}}$$

⇒ 0.662 Å/pix

Important hardware advances in CryoEM

Example TEM schematic

One of many types of TEMs

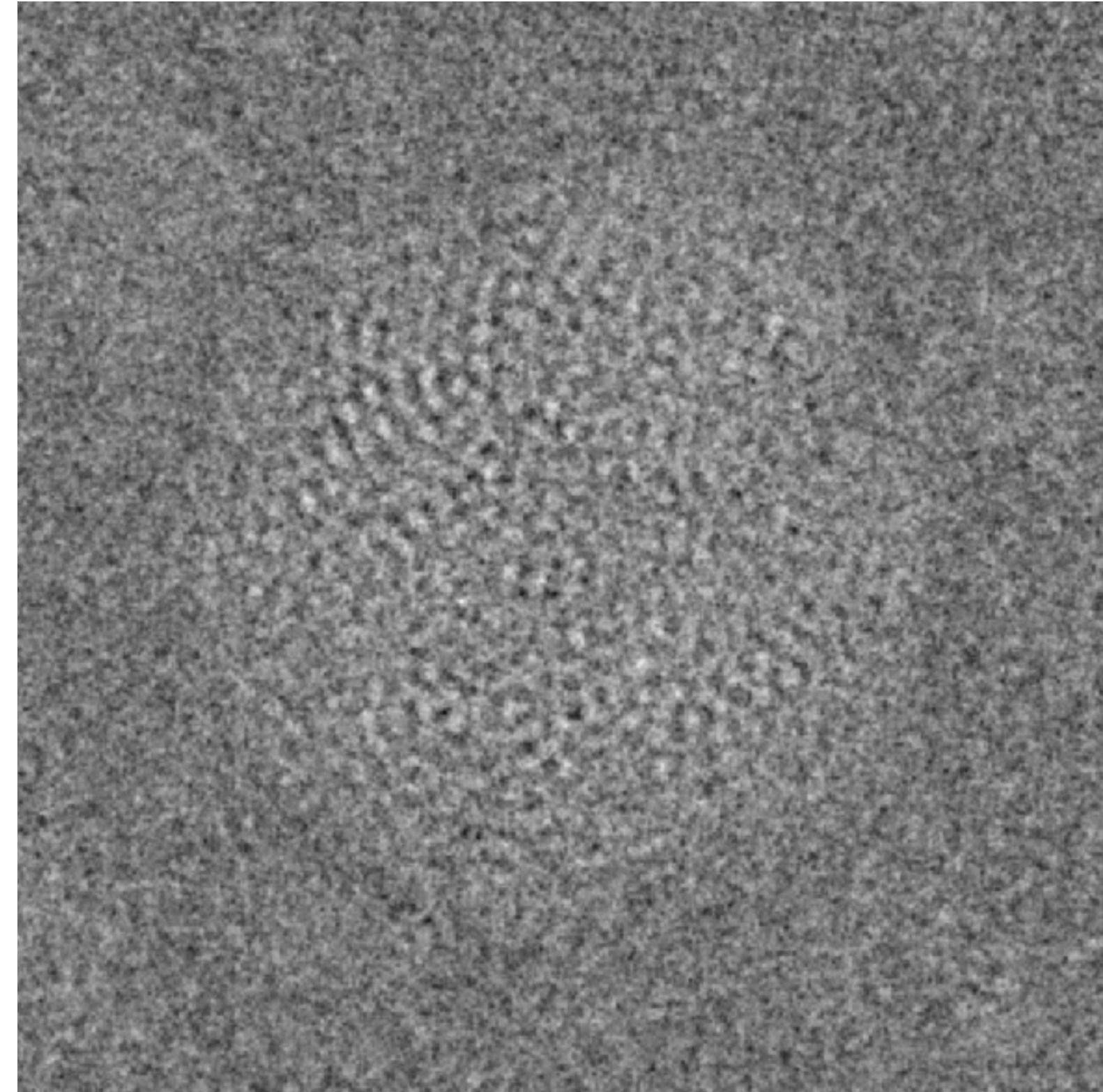
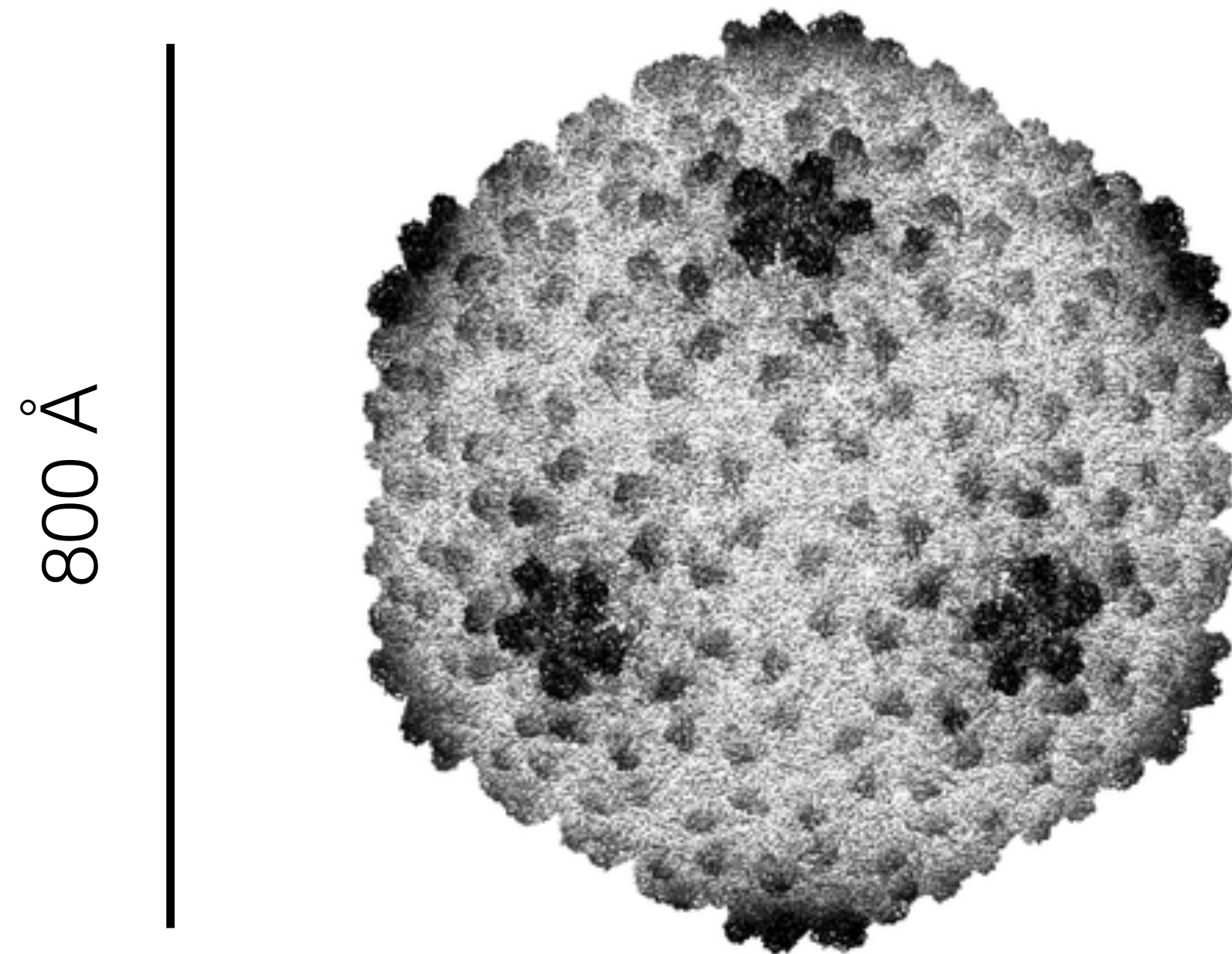


- Electron sources
- Stable lenses and power supplies
- Improved high vacuum systems w/ anti-contamination systems
- High-resolution objective lenses
- Low drift, low vibration, sample stages and cryo-specimen holders
- Stable specimen supports
- Computer control and automation of microscope lenses, stages and controls
- Methods for measuring and correcting lens aberrations
- Improved detectors

A brief aside

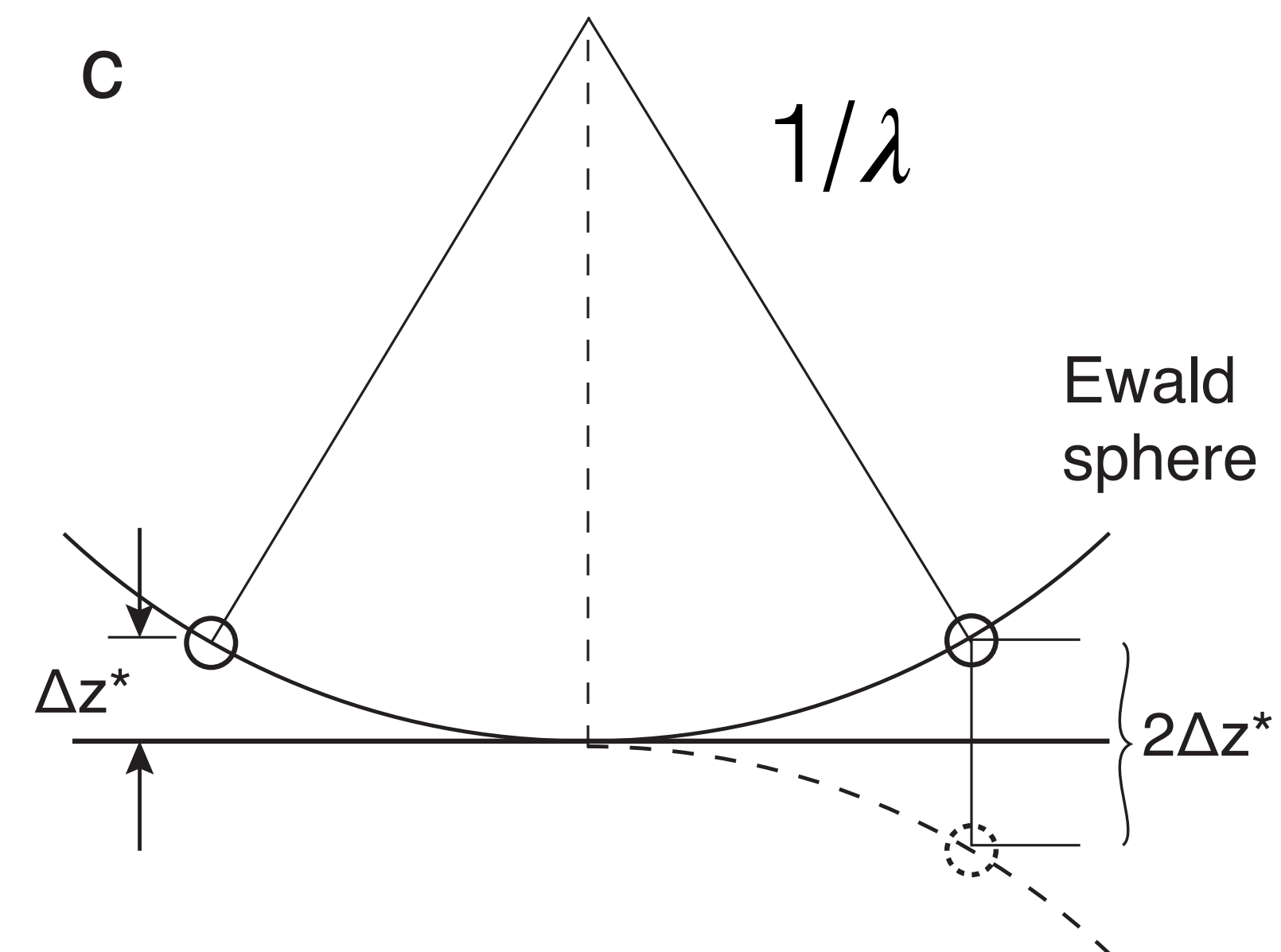
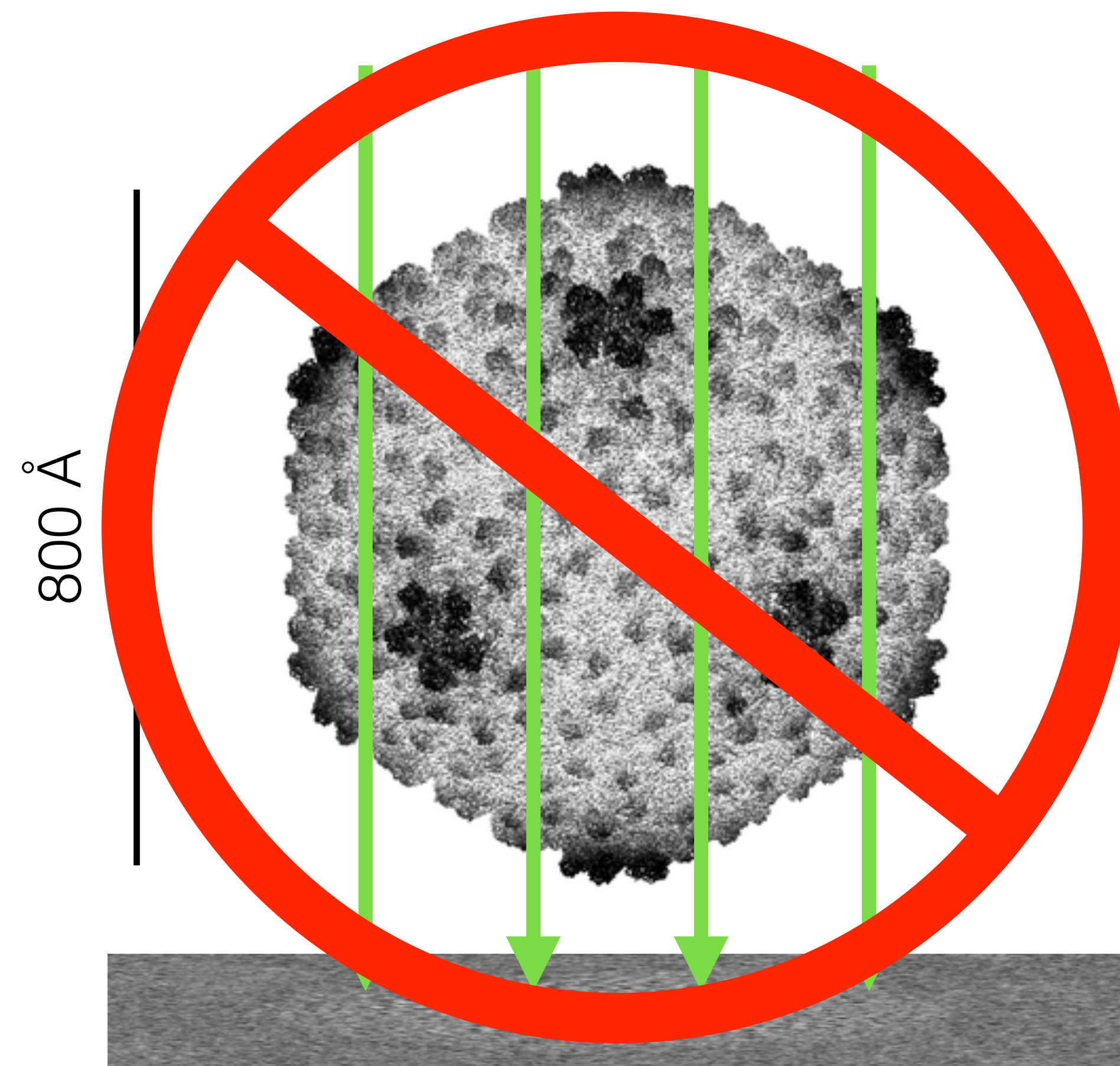
Ewald Sphere correction in EM

P22 virus structure
EMPIAR-10083



Chen et al. 2017

P22 virus structure
EMPIAR-10083



Some previous work on Ewald sphere correction

CONTRAST TRANSFER FOR FROZEN-HYDRATED SPECIMENS: DETERMINATION FROM PAIRS OF DEFOCUSED IMAGES

Chikaashi TOYOSHIMA *

Department of Cell Biology, Stanford University School of Medicine, Stanford, California 94305, USA

and

Nigel UNWIN

Medical Research Council Laboratory of Molecular Biology, Hills Road, Cambridge CB2 2QH, UK

Received 14 January 1988; received in revised form 30 March 1988

Electron imaging of frozen-hydrated biological molecules allows density maps to be obtained directly, without the need for fixation or stains. The appearance of such maps may, however, be strongly influenced by the contrast transfer properties, which have not previously been evaluated by quantitative experiments. Here we determine the contribution due to amplitude contrast in a typical (~ 300 Å thick) frozen specimen, consisting of arrays of acetycholine receptor, by comparing pairs of images recorded with different defocuses. We find that this specimen is imaged as a “weak-phase-weak-amplitude” object and that the contribution due to amplitude contrast is 7%.

1. Introduction

It is now well established that the linear theory of image formation provides a good approximation in accounting for the contrast present in electron micrographs of thin biological specimens (see ref. [1], for a recent review). In this approximation, the phase contrast produced by defocusing modulates components of the object having different spacings as $\sin \chi(v)$ (χ is the phase shift of the scattered wave and v is the spatial frequency; see section 2) causing them to be recorded with different weights [2]. Thus there is a direct relation between the object and the image, and it is possible to compensate computationally for the variation in $\sin \chi(v)$ (i.e. the phase contrast transfer function) to derive a more accurate representation of the densities composing the specimen [3,4].

* Present address: Medical Research Council Laboratory of Molecular Biology, Hills Road, Cambridge CB2 2QH, UK.
0304-3991/88/030350 © Elsevier Science Publishers B.V. (North-Holland Physics Publishing Division)

Compensation for the effect of the contrast transfer function (CTF) is not usually needed in the analysis of images of negatively stained molecules, where amplitude contrast, which modulates as $\cos \chi(v)$, largely makes up for the reduction in phase contrast that occurs at low resolution [4]. However, with unstained, ice-embedded specimens [5–7] the amplitude contrast, in the absence of heavy metal salts, has a weaker effect and compensation is more likely to be necessary [8]. In addition, specimens preserved by freezing may contain more precise information about the structure, making the accuracy of the compensation – and hence the exact proportion of the amplitude contrast – more critical. The corrections are most important with small crystalline arrays and isolated particles, where electron diffraction cannot be used to obtain a measure of the unmodulated strengths of different spatial components [9], yet quantitative measurements of the influence of amplitude contrast in such cases have not so far been made.



Correction of high-resolution data for curvature of the Ewald sphere

David J. DeRosier*

W.M. Keck Institute for Cellular Visualization, Rosenthal Basic Medical Sciences Research Center, Brandeis University,
MS029, 415 South Street, Waltham, MA 02454, USA

Received 6 April 1999; received in revised form 25 August 1999

Abstract

At sufficiently high resolution, which depends on the wavelength of the electrons, the thickness of the sample exceeds the depth of field of the microscope. At this resolution, pairs of beams scattered at symmetric angles about the incident beam are no longer related by Friedel's law; that is, the Fourier coefficients that describe their amplitudes and phases are no longer complex conjugates of each other. Under these conditions, the Fourier coefficients extracted from the image are linear combinations of independent (as opposed to Friedel related) Fourier coefficients corresponding to the three-dimensional (3-D) structure. In order to regenerate the 3-D scattering density, the Fourier coefficients corresponding to the structure have to be recovered from the Fourier coefficients of each image. The requirement for different views of the structure in order to collect a full 3-D data set remains. Computer simulations are used to determine at what resolution, voltage and specimen thickness the extracted coefficients differ significantly from the Fourier coefficients needed for the 3-D structure. This paper presents the theory that describes this situation. It reminds us that the problem can be treated by considering the curvature of the Ewald sphere or equivalently by considering that different layers within the structure are imaged with different amounts of defocus. The paper presents several methods to extract the Fourier coefficients needed for a 3-D reconstruction. The simplest of the methods is to take images with different amounts of defocus. For helical structures, however, only one image is needed. © 2000 Elsevier Science B.V. All rights reserved.

Keywords: Electron microscopy; Depth of field

1. Introduction

The assumption in three-dimensional (3-D) image reconstruction is that the image is a projection of the 3-D structure [1]. This assumption breaks down if the object does not obey the weak phase object approximation or if size of the specimen exceeds the depth of field of the microscope. This paper considers the latter problem only. The assumption that the image is a projection breaks down at sufficiently high resolution [2] at which resolution the thickness of the specimen exceeds the depth of field of the microscope.

* Tel.: +1 781 7362494; fax: +1 781 7362419.
E-mail address: derosier@brandeis.edu (D.J. DeRosier).



Ewald sphere correction for single-particle electron microscopy

Matthias Wolf^a, David J. DeRosier^a, Nikolaus Grigorieff^{a,b,*}

^a Rosenthal Basic Medical Sciences Research Center, Brandeis University, 415 South Street, Waltham, MA 02454, USA

^b Harvard Hughes Medical Institute, Brandeis University, 415 South Street, Waltham, MA 02454, USA

Received 19 August 2005; received in revised form 9 November 2005; accepted 11 November 2005

Abstract

Most algorithms for three-dimensional (3D) reconstruction from electron micrographs assume that images correspond to projections of the 3D structure. This approximation limits the attainable resolution of the reconstruction when the dimensions of the structure exceed the depth of field of the microscope. We have developed two methods to calculate a reconstruction that corrects for the depth of field. Either method applied to synthetic data representing a large virus yields a higher resolution reconstruction than a method lacking this correction.

© 2005 Elsevier B.V. All rights reserved.

Keywords: 87.64.Bb; 87.64.Dz

Keywords: Three-dimensional reconstruction; Resolution; Depth of field; FREALIGN

1. Introduction

The three-dimensional (3D) reconstruction of a biological molecule or complex from images of single, isolated particles is an important step in electron microscopy (EM) of macromolecules. The reconstruction algorithms commonly used assume that the images are projections of the three-dimensional (3D) object. Although this assumption is a valid approximation for many situations, it breaks down when the size of the object and the desired resolution exceed the depth of field of the microscope [1]. The present work describes two methods to accommodate the depth of field in the reconstruction and alignment of single particles without the use of tilt or defocus pairs. We demonstrate the validity of the approach using simulations.

2. Theory

2.1. Ewald construction

A 3D reconstruction algorithm can be understood most easily by considering its action in reciprocal space. The Fourier transform of the data from each image does not correspond to a plane through the origin (central section) but rather to the surface of the Ewald sphere (EWS, [2]) that passes through the origin of the 3D Fourier transform. The construction in Fig. 1 shows that the deviation, Δz , between the sphere and a plane increases with increasing resolution (determined by the length of the vector g). The value of the Fourier transform of the object differs between the two points B, where the transform is sampled, and B', where the data corresponding to a projection lies; the larger the difference, the greater the deviation of the image from a projection. The magnitude of the difference depends on the dimensions of the object and is larger for objects having a longer dimension along the beam direction.

The error made in the reconstruction when using the planar approximation depends, therefore, on the resolution, the size of the object, and the radius of the EWS (the wavelength of the radiation). DeRosier [1] performed an analysis of the expected phase error between B and B' and showed that a phase error of 60° for the planar approximation of a spherical shell, such as a virus, occurs at a resolution $R = \sqrt{2 \times 0.7 / (D)} \approx 0.7$ is a dimensionless empirical factor for a spherical shell, object diameter D and wavelength λ are given in units of Å [1]. For example, for a virus of 500 Å diameter and a wavelength of 0.025 Å

0304-3991/\$ - see front matter © 2005 Elsevier B.V. All rights reserved.
doi:10.1016/j.ultramic.2005.11.001

* Corresponding author. Tel.: +1 781 7362444; fax: +1 781 7362419.
E-mail address: ngrigorieff@brandeis.edu (N. Grigorieff).

Estimating the effect of finite depth of field in single-particle cryo-EM

Kenneth H. Downing, Robert M. Glaeser

Lawrence Berkeley National Laboratory, University of California, Berkeley CA 94720, USA

ARTICLE INFO

Article history:
Received 13 April 2017
Revised 3 August 2017
Accepted 15 August 2017
Available online 19 August 2017

ABSTRACT

The extent to which the resolution varies within a three-dimensional (3-D) reconstruction, when the diameter of an object is large, is investigated computationally. Numerical simulation is used to model ideal three-dimensional point-spread functions at different radial positions within an object. It is shown that reconstructed density maps are affected less than might have been expected when particles are larger than the depth of field. This favorable outcome is attributed mainly to the fact that a point which lies outside the depth of field relative to the center, for some orientations of the object, will also lie within the depth of field for other orientations. We find, as a result, that the diameter of a particle can be as much as four times the depth of field (as defined by a 30° phase-error criterion) before curvature of the Ewald sphere becomes a limiting factor in determining the resolution that can be achieved.

© 2017 Elsevier B.V. All rights reserved.

1. Introduction

High-resolution electron microscopy of unstained biological macromolecules (single-particle cryo-EM for short) has recently made significant advances [1–3]. Three-dimensional density maps of large macromolecules are now being obtained with a resolution in the range from 3 to 4 Å, and in a few cases the resolution has already exceeded 2.5 Å [1,4,11]. A fundamental approximation used in this method is that the image intensity is linear in the projected Coulomb potential of the specimen – see, for example, Chapter 4 of [1]. Equivalently, when referring to Fourier space rather than real space, the corresponding approximation is that curvature of the Ewald sphere [1] can be neglected.

Validity of the assumed “projection” approximation requires, among other things, that all portions of the specimen are imaged with the same amount of defocus. This only happens, of course, if the size of the object (i.e. its thickness) is much less than the optical depth of field. As a result, the fundamental approximation, i.e. that the image is a projection of the object, is not expected to be useful if the size of the object is similar to, or much greater than, the depth of field.

This issue has been raised in the past, both in the context of very large virus particles [10,17] and in the context of smaller particles that are randomly distributed within a certain range of z -heights, which is determined by the overall ice thickness [8]. It seemed to be paradoxical, for example, that high-resolution, three-dimensional reconstructions were obtained from images of icosahedral virus particles whose diameters are larger than the corresponding depth of field [13,12,16]. An often-mentioned resolution of this paradox is that a large number of (symmetry-related) subunits are located at the same z -height as is the middle of the virus particle. At the same time, it is suggested – reasonably so – that estimation of the defocus value for the image of a virus particle is biased towards the middle, i.e. its center of mass. Thus, if the contrast-transfer-function (CTF) correction for the region near to the middle of a large virus particle is done correctly, a significant amount of signal may be produced from the many subunits whose images have been properly corrected. The suggestion is that this signal can overwhelm the (high-resolution) “noise” contributed by other subunits that lie at z -heights that are outside the depth of field. Because of this argument, it seemed plausible that the depth of field might be a greater limitation for asymmetric particles than it is for icosahedral virus particles; it thus remains inconclusive that no improvement in the quality of density maps was obtained when computational algorithms were used to compensate for violation of the projection approximation for images of large, icosahedral virus particles [11,15].

We now repeat the question by using computational simulations to better understand what limitations to expect when the size of a particle approaches, and even exceeds, the depth of field for a given resolution. The approach that we have taken is to first calculate noise-free, three-dimensional (3-D) reconstructions of “single points” that are located at different distances from the center of an object. The resulting 3-D point-spread functions are then convoluted with high-resolution density maps for atomic models of two peptide structures found in tubulin, the sizes of which are both much smaller than the depth of field for 300 keV

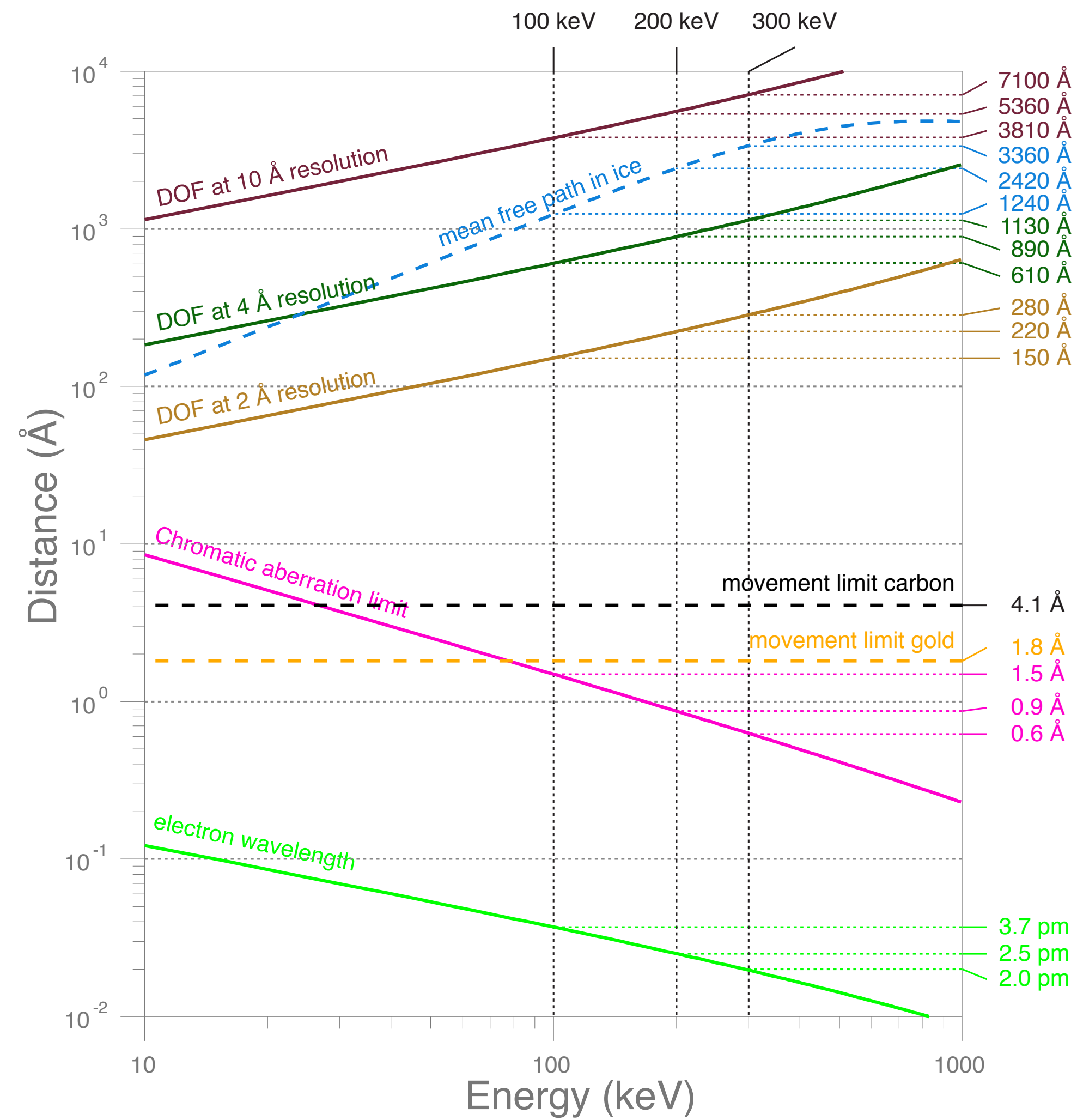
* Corresponding author.
E-mail address: rmglaeser@lbl.gov (R.M. Glaeser).
http://dx.doi.org/10.1016/j.ultramic.2017.08.007
0304-3991/© 2017 Elsevier B.V. All rights reserved.

Toyoshima & Unwin 1988

DeRosier 2000

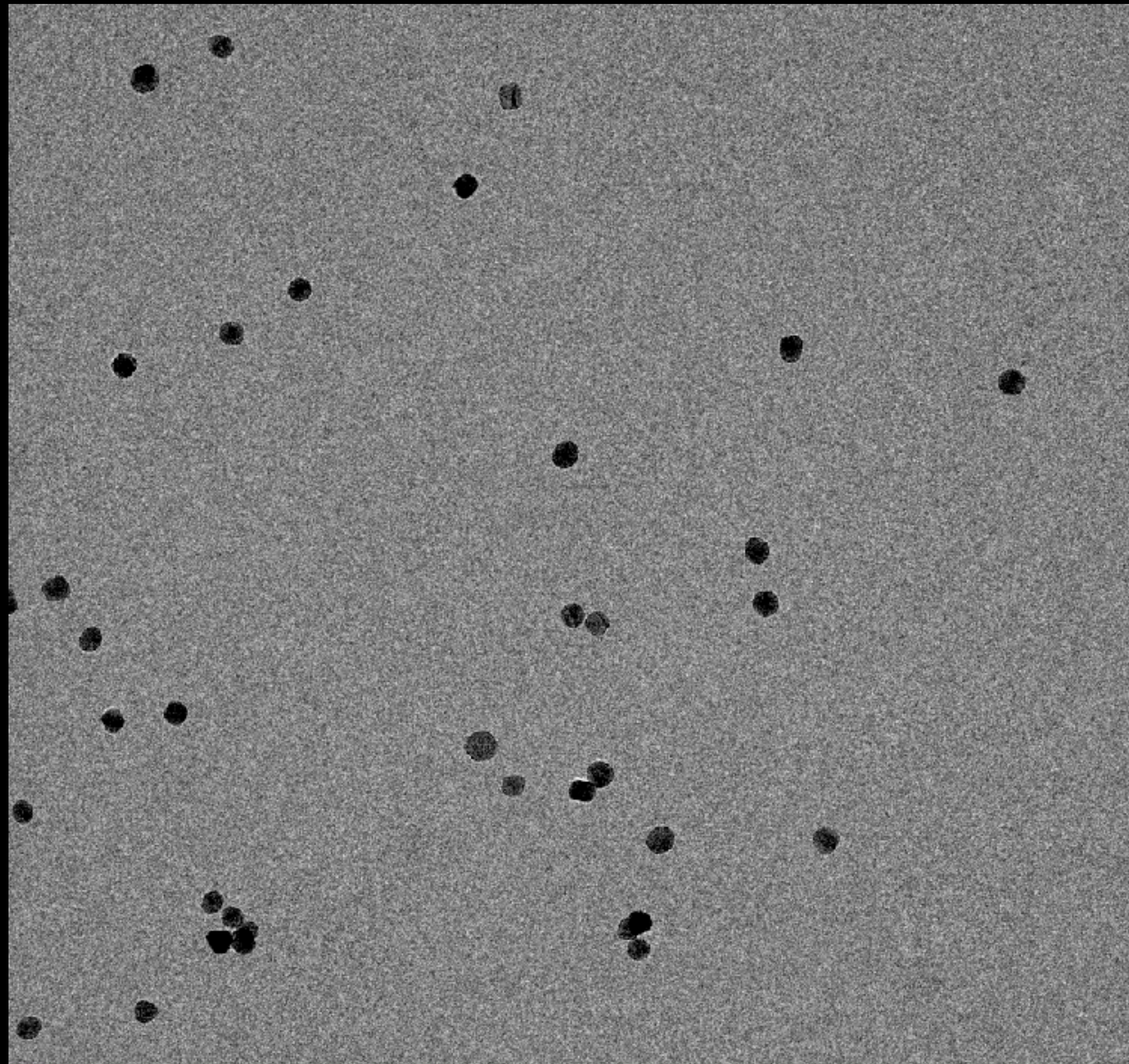
Wolf et al. 2006

Downing & Glaeser 2017



Electron energy scaling limits relevant to cryo-EM

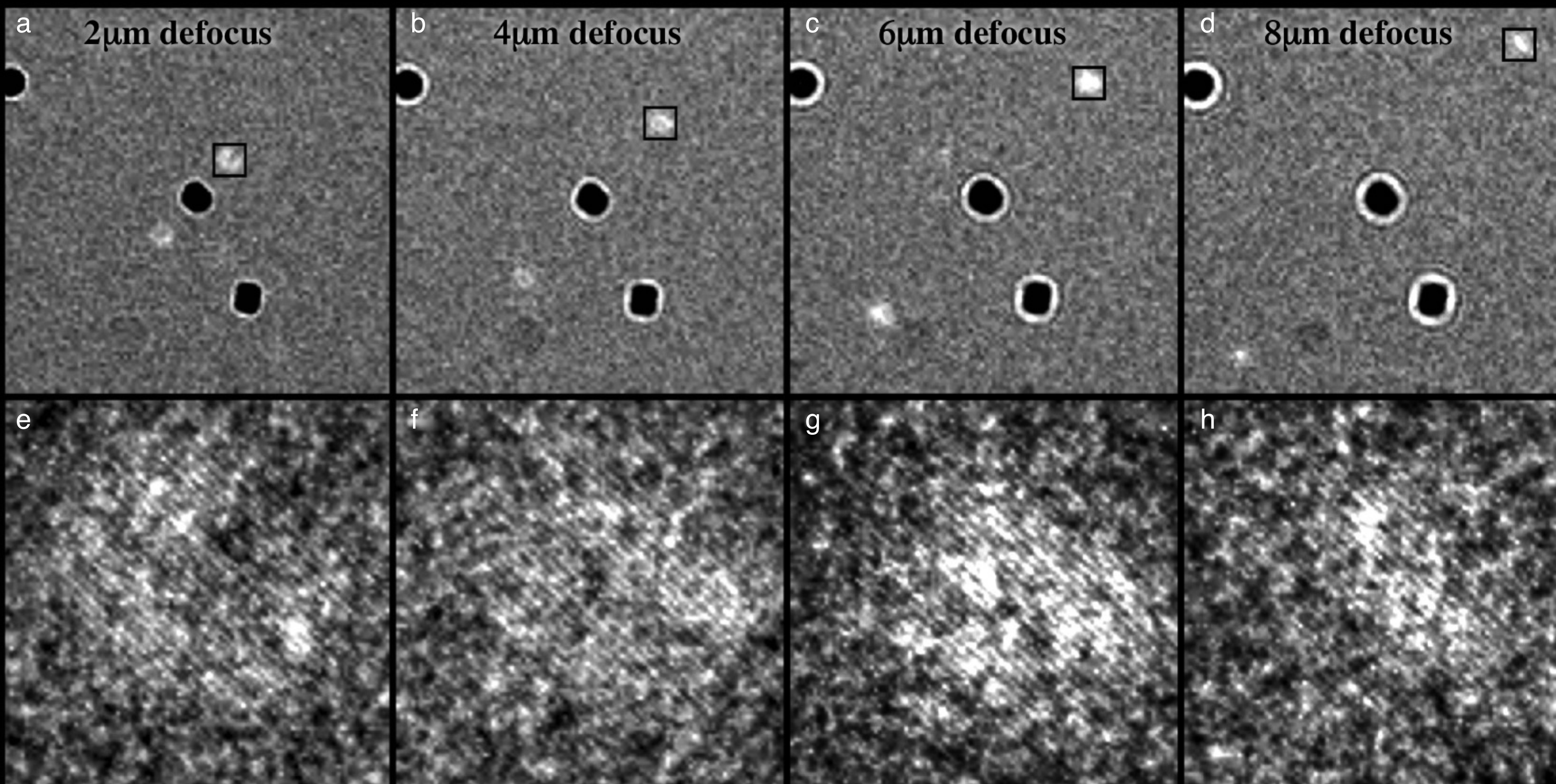
- Wavelength
- Optics
- Depth of field (DOF)
- Mean free path (inelastic)
- Particle movement



10 nm gold
particles in
amorphous ice
defocus series
from 0 to $-10\ \mu\text{m}$

300 keV
80 K

Russo & Henderson 2018b



Measurement and compensation of defocusing and aberrations by Fourier processing of electron micrographs

By H. P. ERICKSON AND A. KLUG, F.R.S.
Medical Research Council Laboratory of Molecular Biology, Cambridge

[Plates 17 and 18]

The effects of defocusing and spherical aberration in the electron microscope image are most simply and directly displayed in the Fourier transform of the image. We have investigated the process of image formation by determining the changes in the transform of the image of a thin crystal of catalase, which has discrete diffraction maxima in the resolution range of 10 to 2.5 nm, as a function of defocusing. The changes in amplitude and phase of these diffraction maxima have been measured and compared with the predictions of a first-order theory of image formation. The theory is generally confirmed, and the transfer function of the microscope is completely determined by finding the relative contributions from phase and amplitude contrast. A 'true' maximum contrast image of the catalase crystal, compensated for the effects of defocusing, is reconstructed from the set of micrographs in the focal series. The relation of this compensated image to individual underfocused micrographs, and the use of underfocus contrast enhancement in conventional electron microscopy, are discussed.

This approach and the experimental methods can be extended to high resolution in order to compensate for spherical aberration as well as defocusing. In as much as spherical aberration is the factor presently limiting the resolution of electron lenses, this could provide a considerable extension of the resolution of the electron microscope.

INTRODUCTION

In the analysis of structure from electron micrographs it is important to know how contrast enhancement and artefacts from defocusing and aberrations affect the image in the electron microscope. These effects are displayed much more simply and directly in the Fourier transform of the image than in the image itself, and are best analysed in terms of the transform. The analysis of these effects through the image transform is of particular interest because of the involvement of the transform in systems for the analysis of periodic structures in electron micrographs, and in the system used for three-dimensional reconstruction by electron microscopy (De Rosier & Klug 1968).

Conventional microscopy today is largely concerned with the imaging of details from 10 or 20 nm down to 2 nm resolution. Especially with the microscopy of biological specimens there is generally little preservation of meaningful structural details beyond 2 nm resolution. As modern electron lenses are essentially perfect to this resolution, the only electron optical factor affecting the image is defocusing. This is important in practical microscopy since micrographs are normally taken somewhat under focus, both because it is technically more difficult to obtain a perfectly in-focus image, and because the defocusing produces a useful enhancement of image contrast. We have analysed the effects of defocusing theoretically and experimentally, and in terms of the results of the investigation can specify conditions for the proper use of underfocus contrast enhancement and the nature of artefacts that will occur with excessive defocusing.

At higher resolution the spherical aberration of the electron lens affects the image in a manner very similar to defocusing. Under optimum conditions modern microscopes can record image details at a point to point resolution of about 0.2 nm. As discussed below, however, the

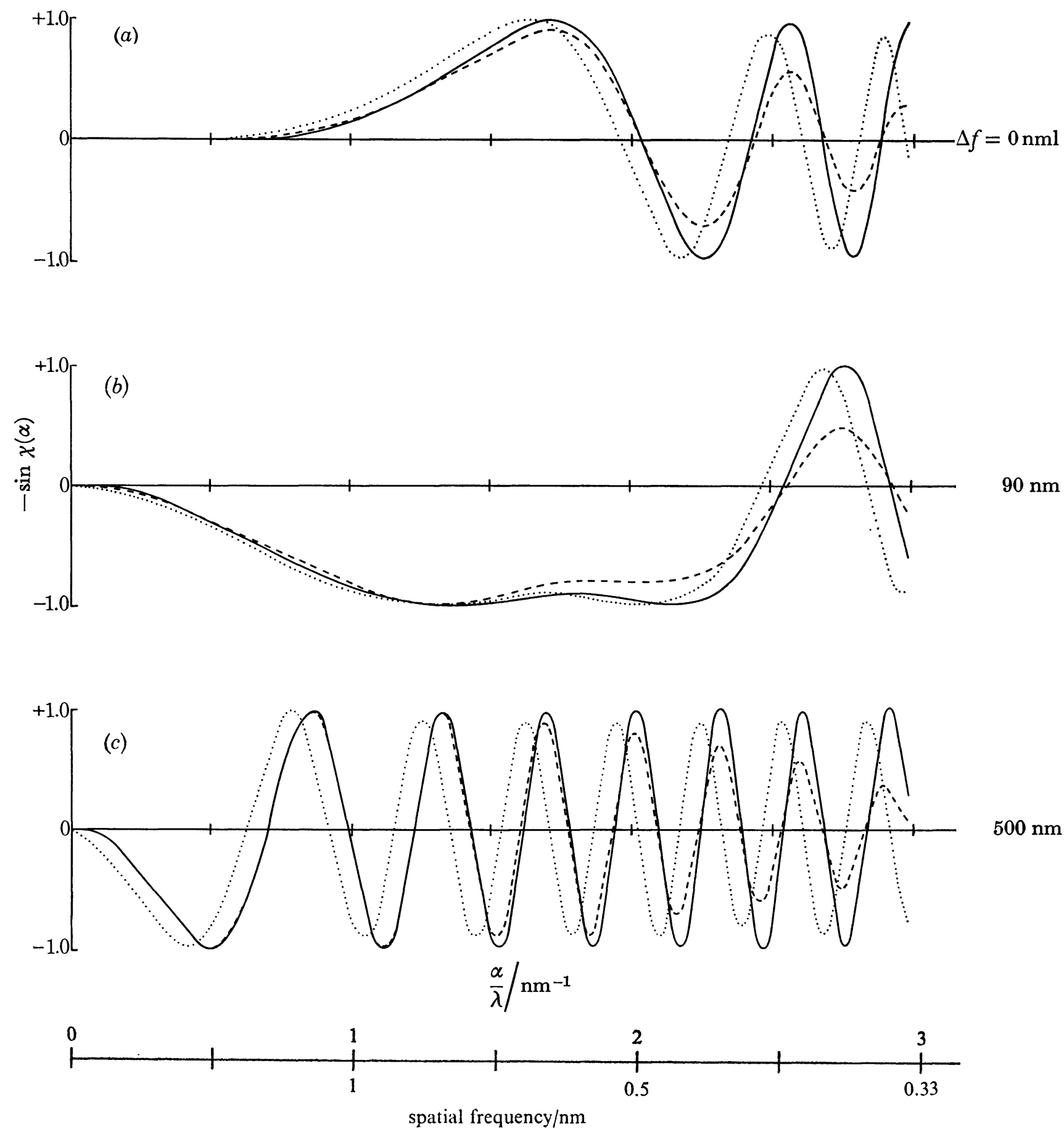
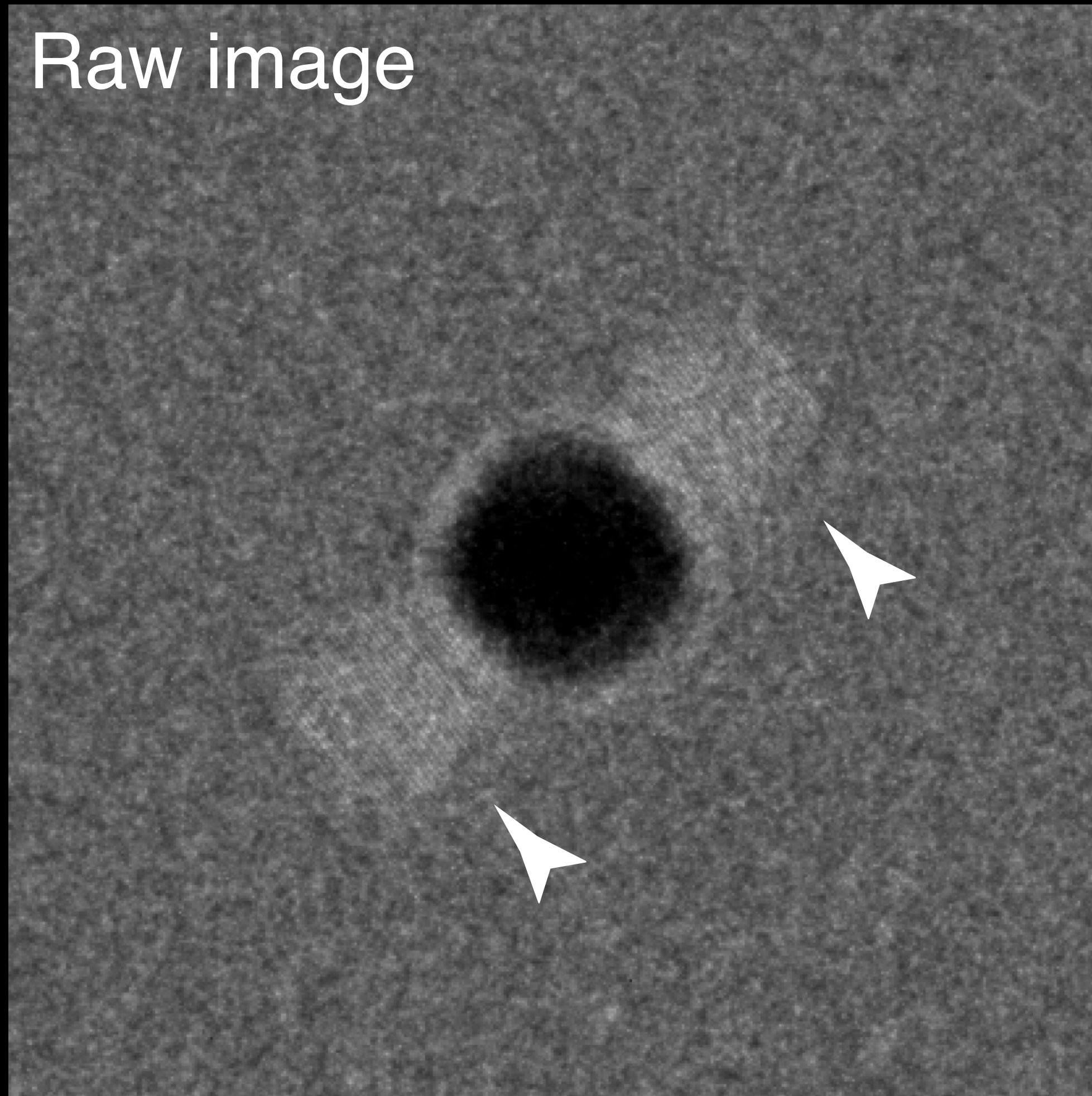
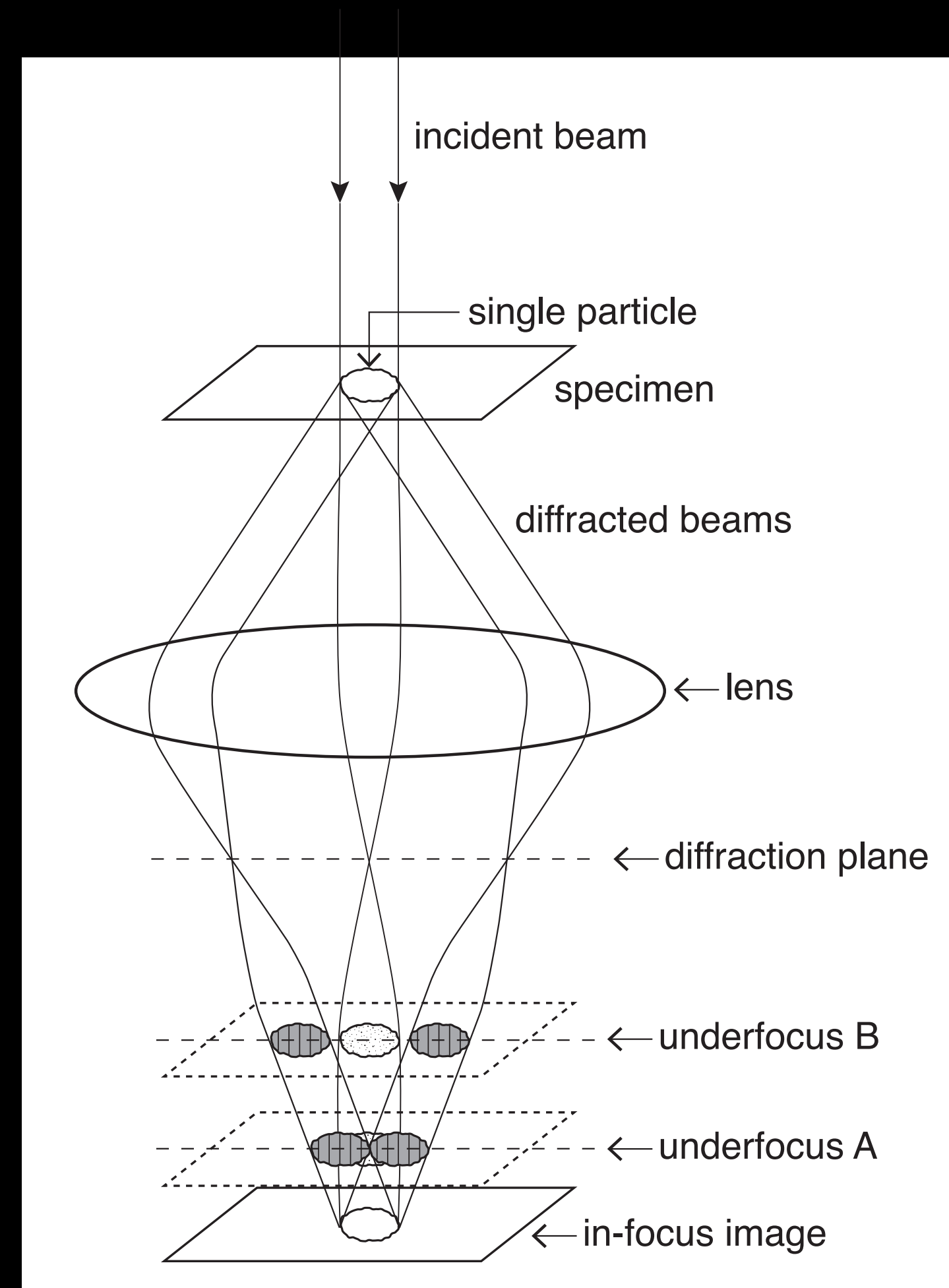


FIGURE 1. The phase-contrast transfer function, $-\sin \chi(\alpha)$, plotted as a function of α/λ , in nm^{-1} , for $\lambda = 0.0042 \text{ nm}$,

Raw image

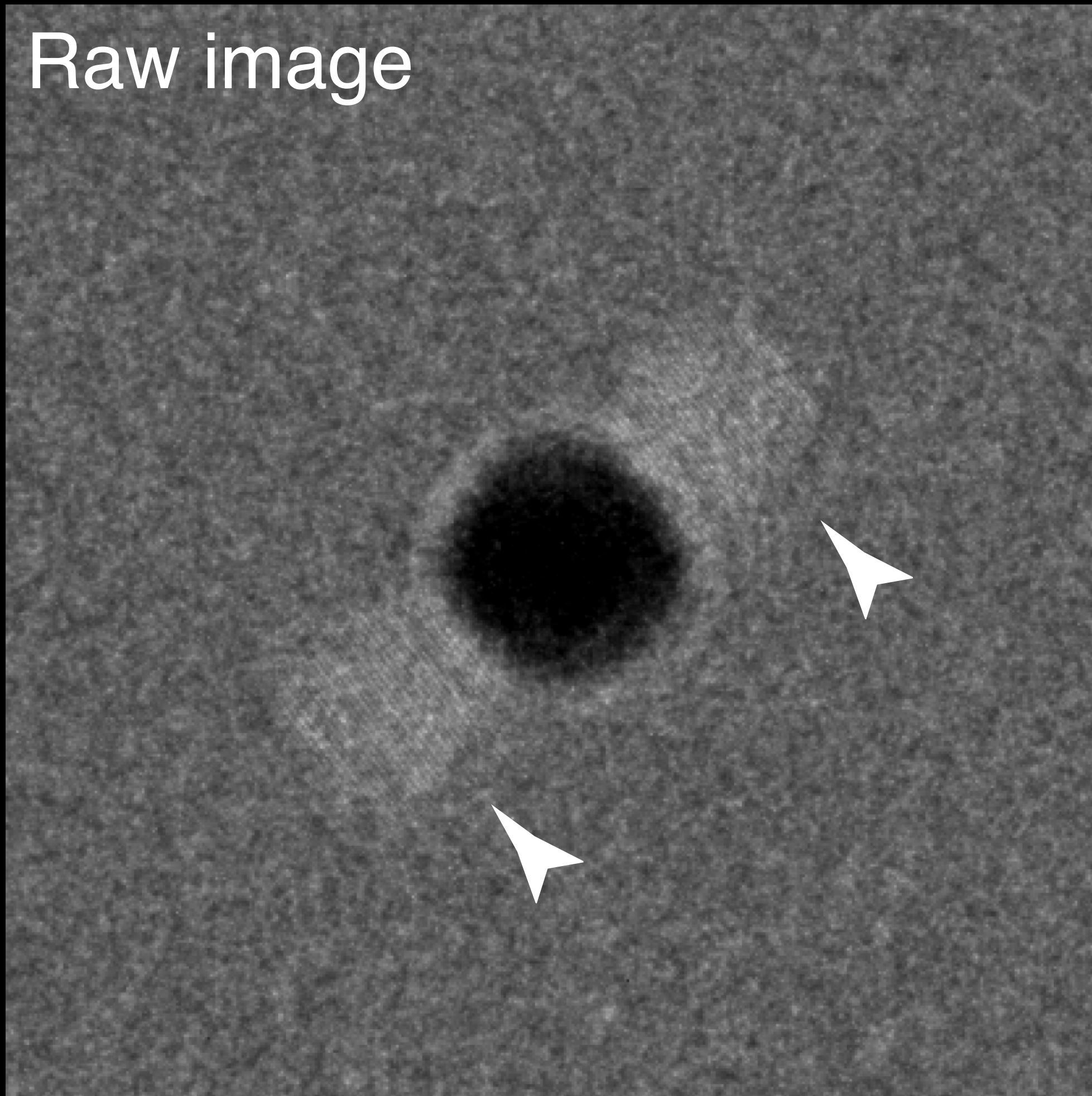


100 Å gold nanoparticle in ice
300 keV

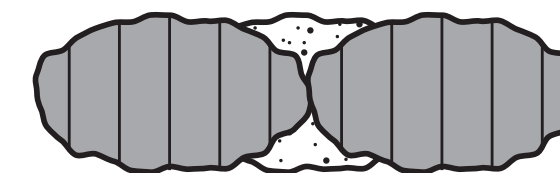
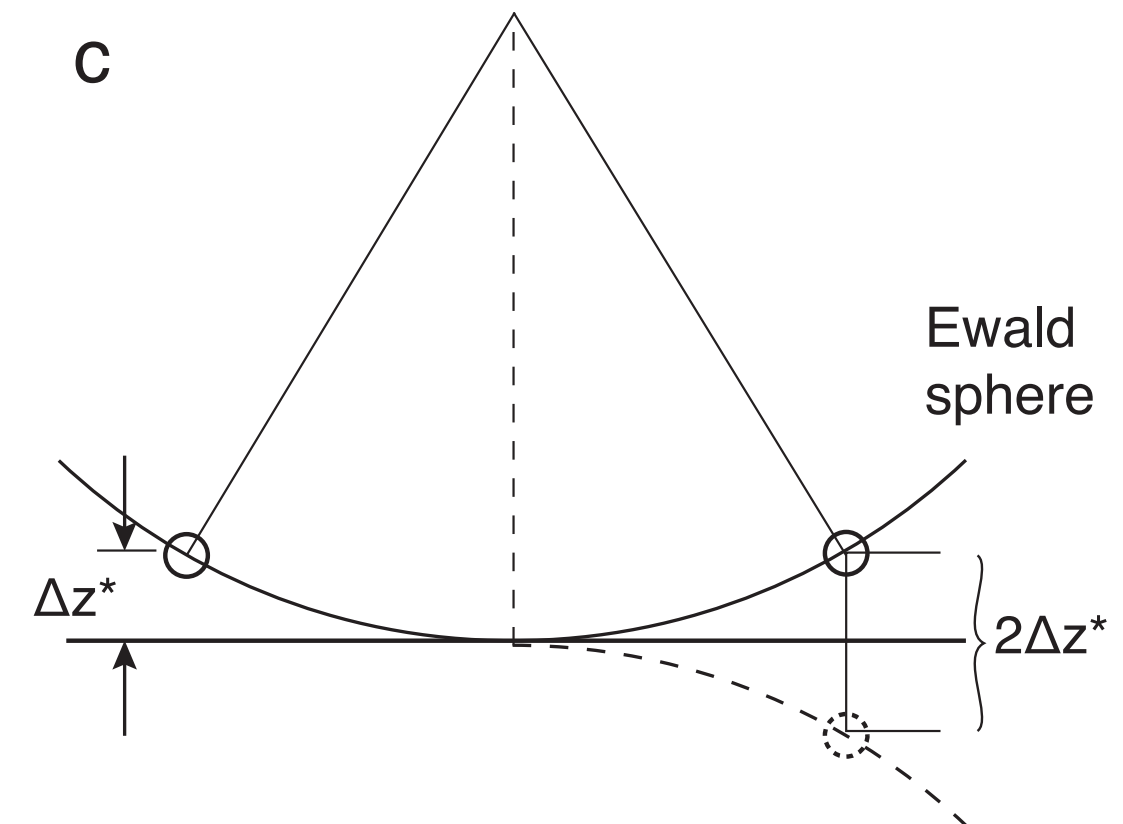


Russo & Henderson 2018c

Raw image

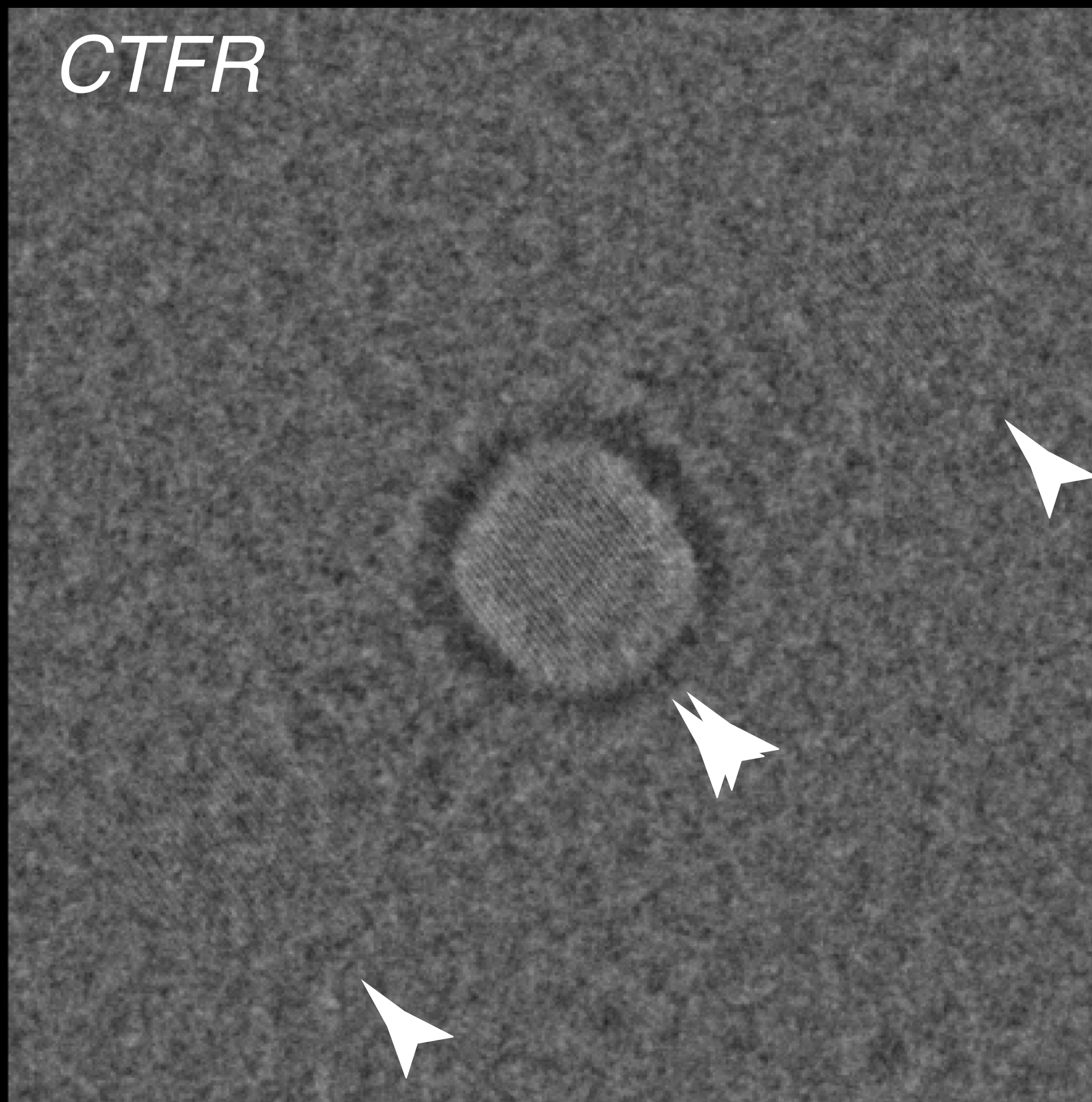


100 Å gold nanoparticle in ice
300 keV

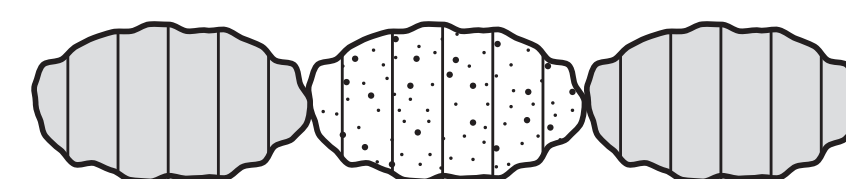
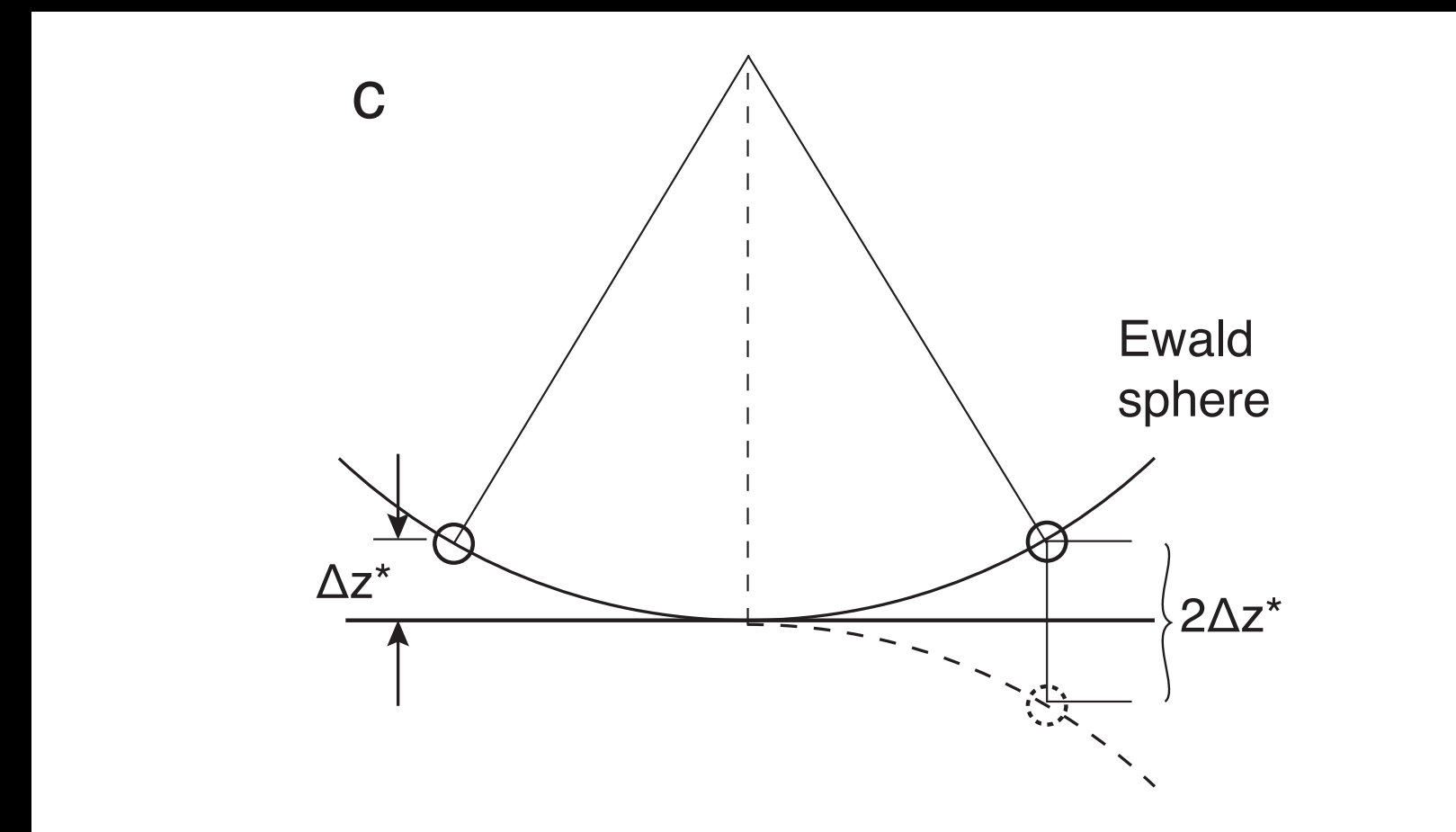


A in image

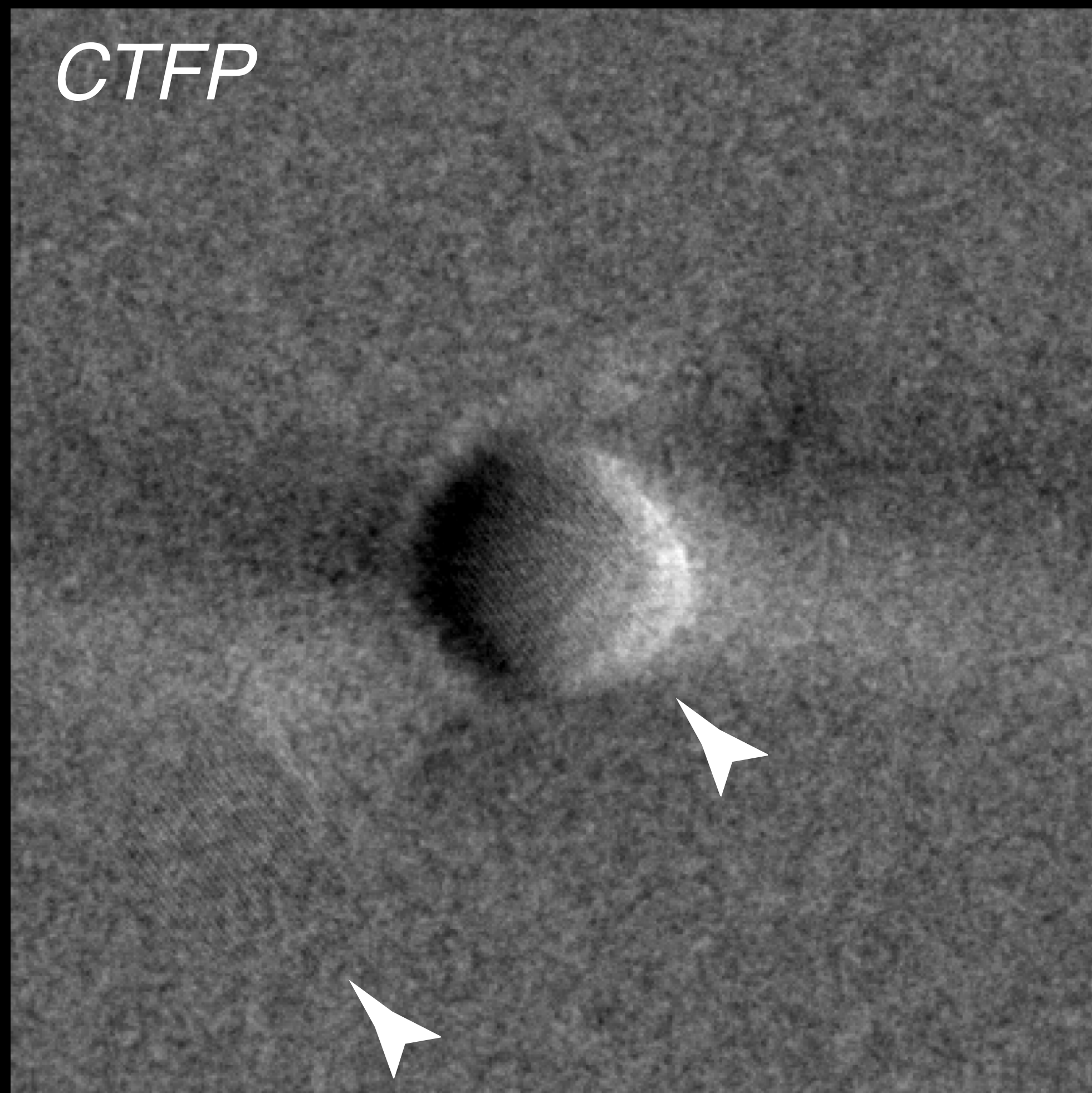
Russo & Henderson 2018c



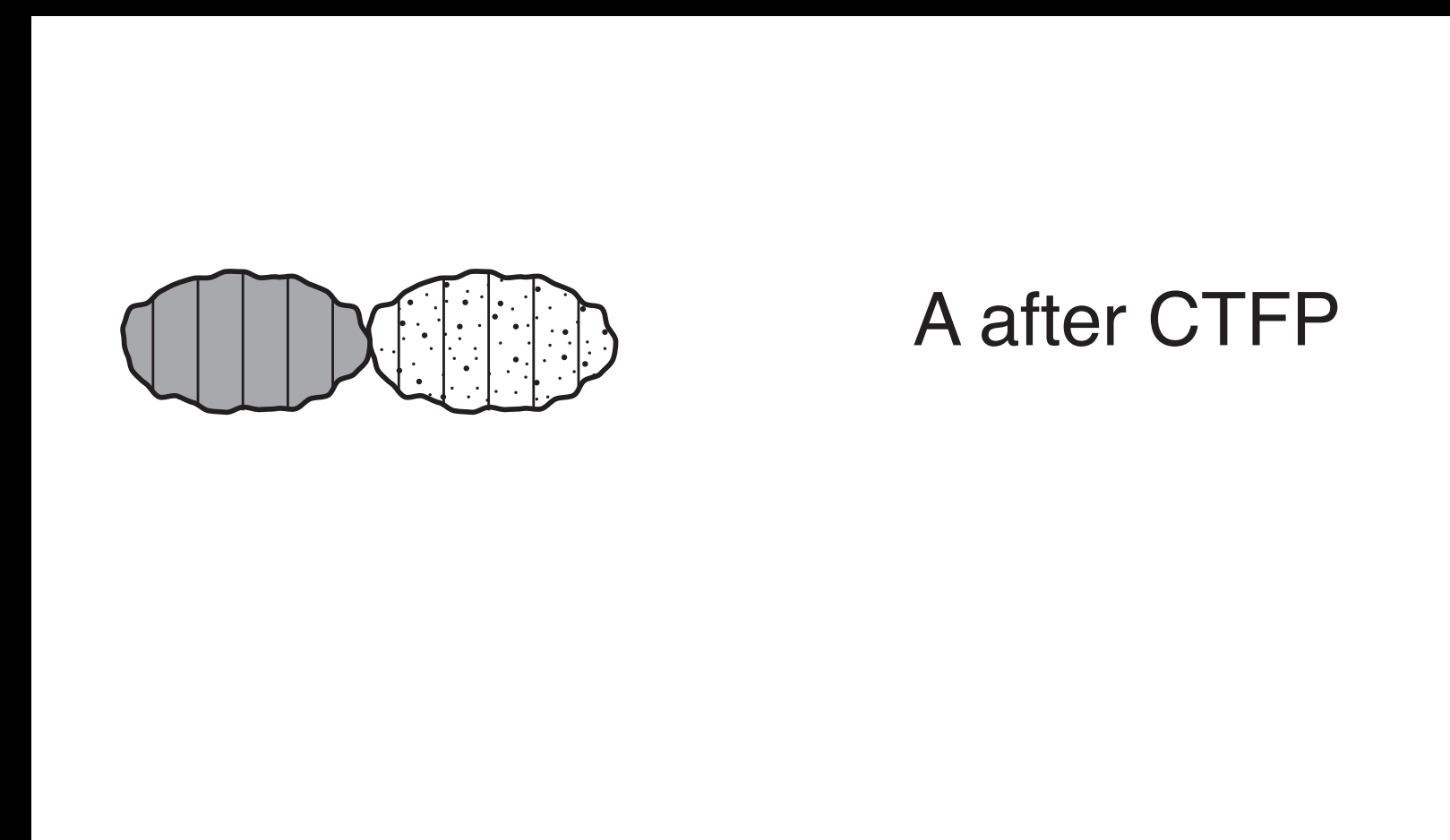
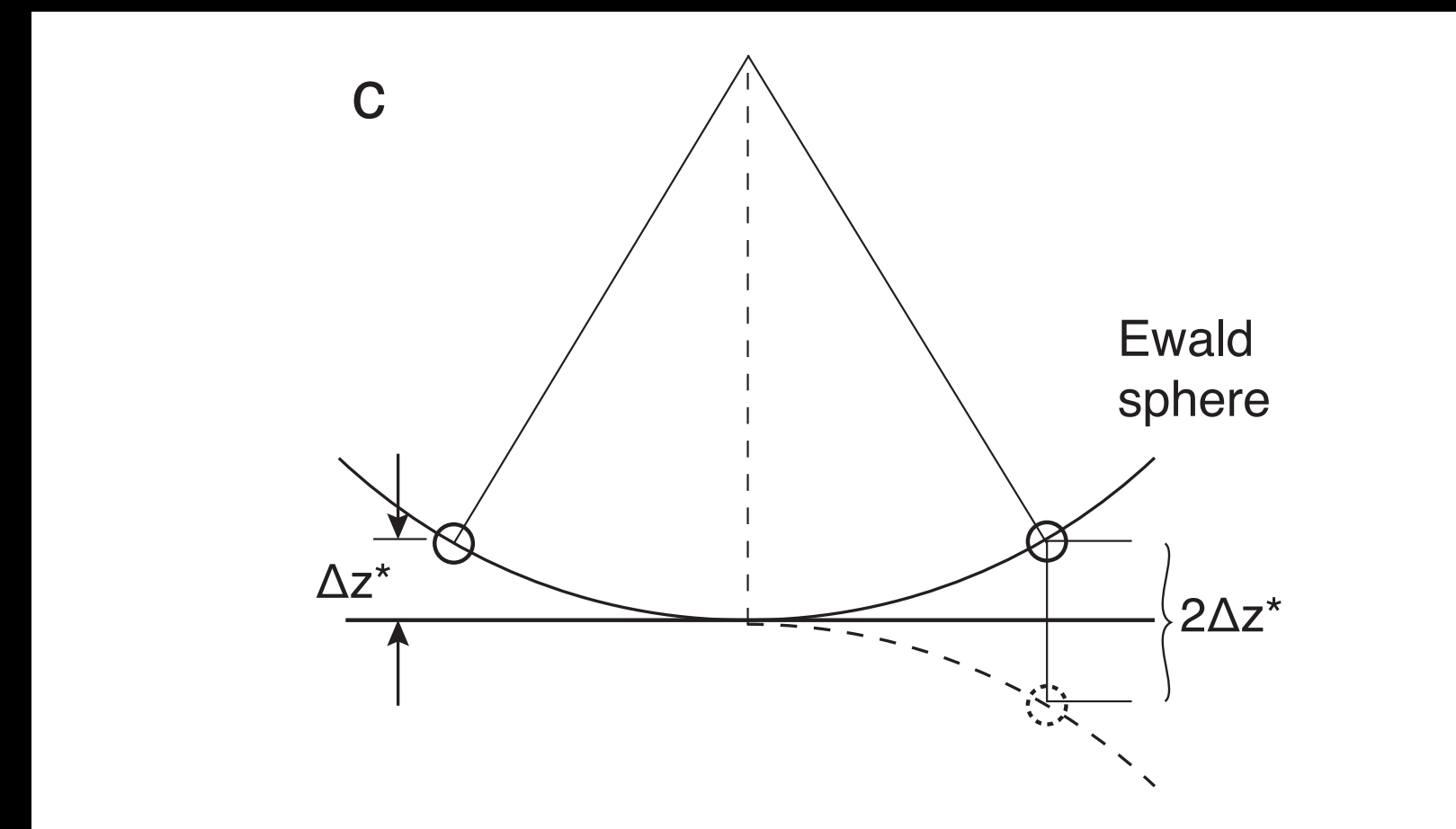
100 Å gold nanoparticle in ice
300 keV

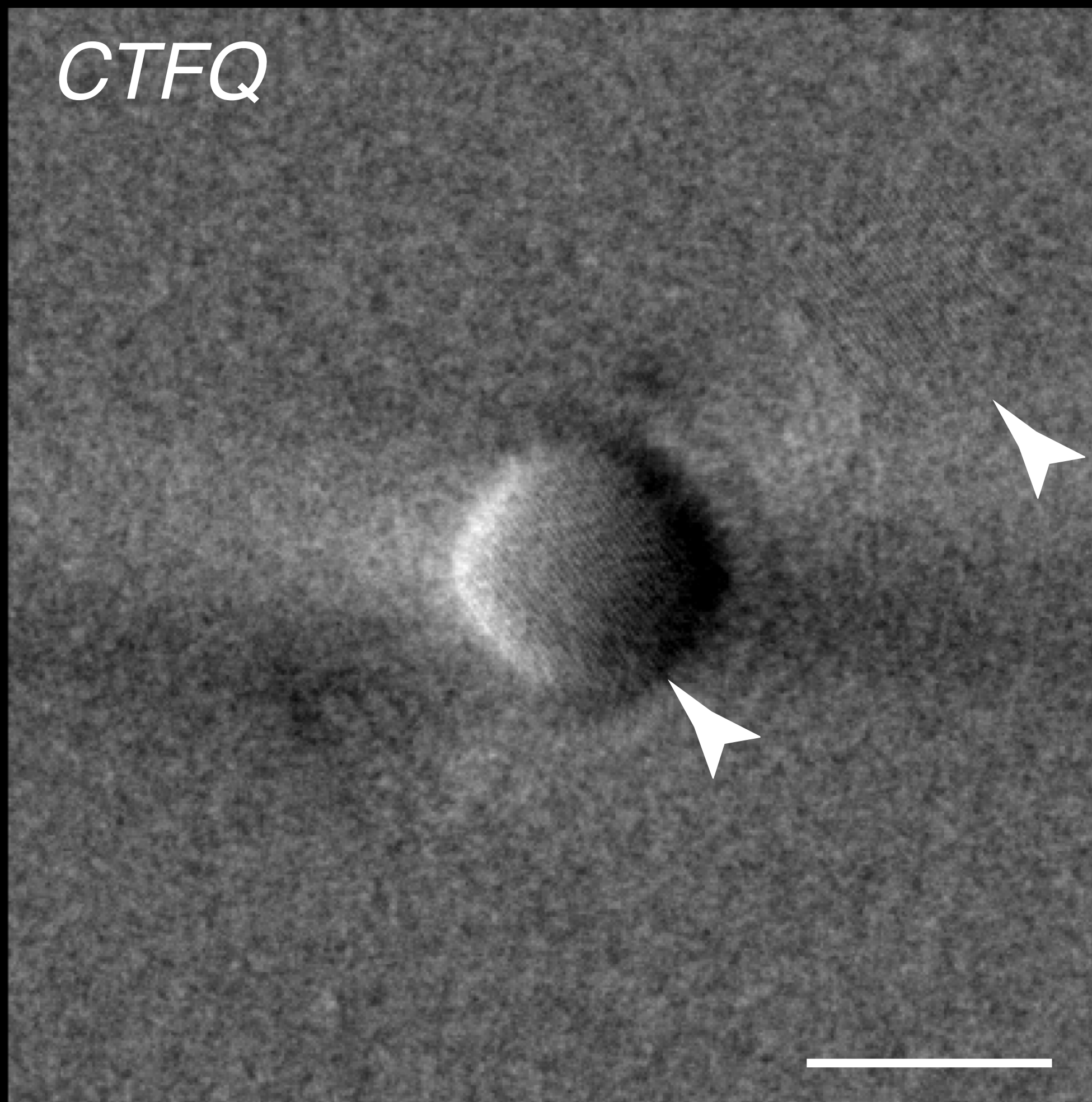


A after CTFR
= CTFP+CTFQ

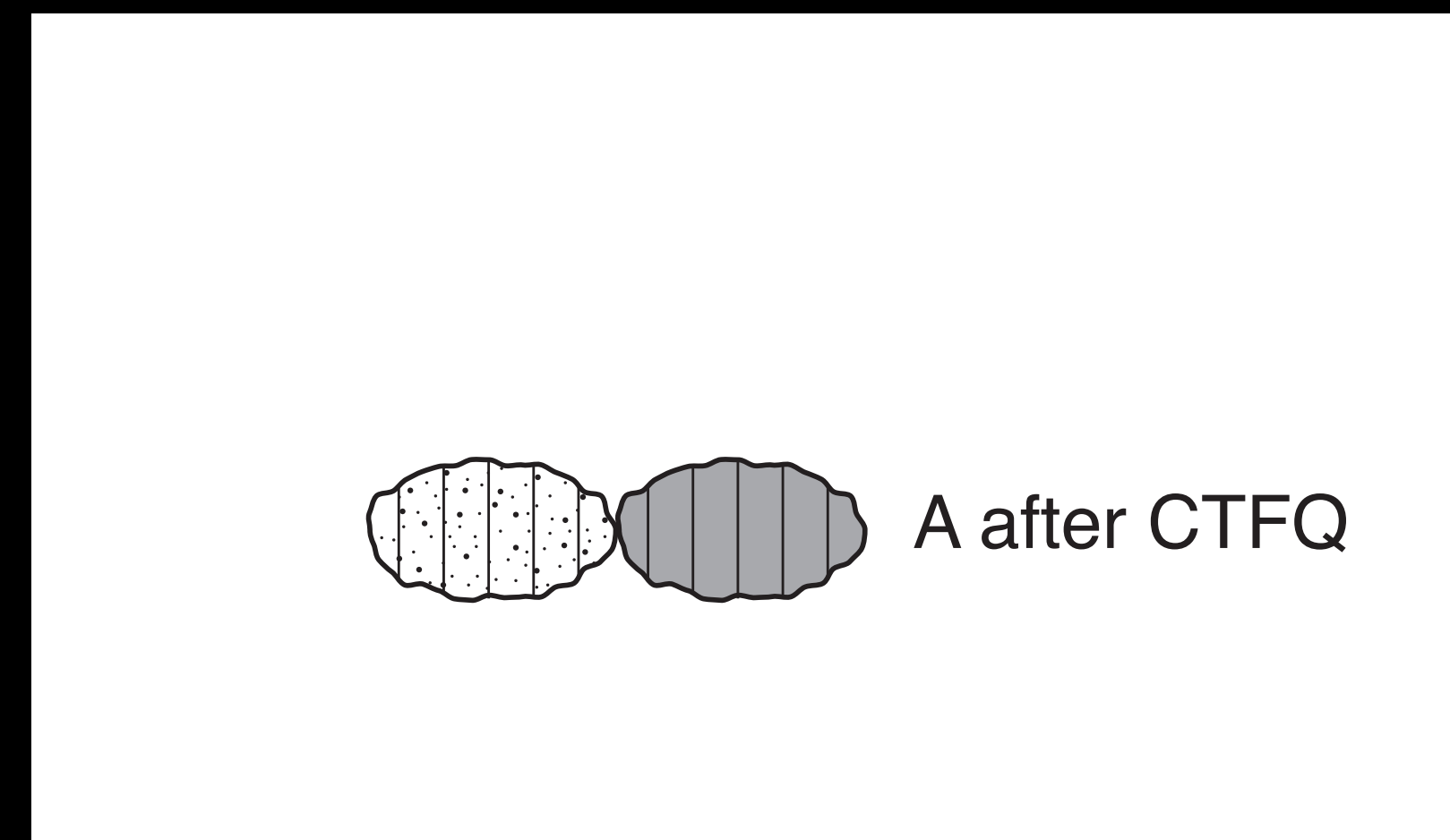
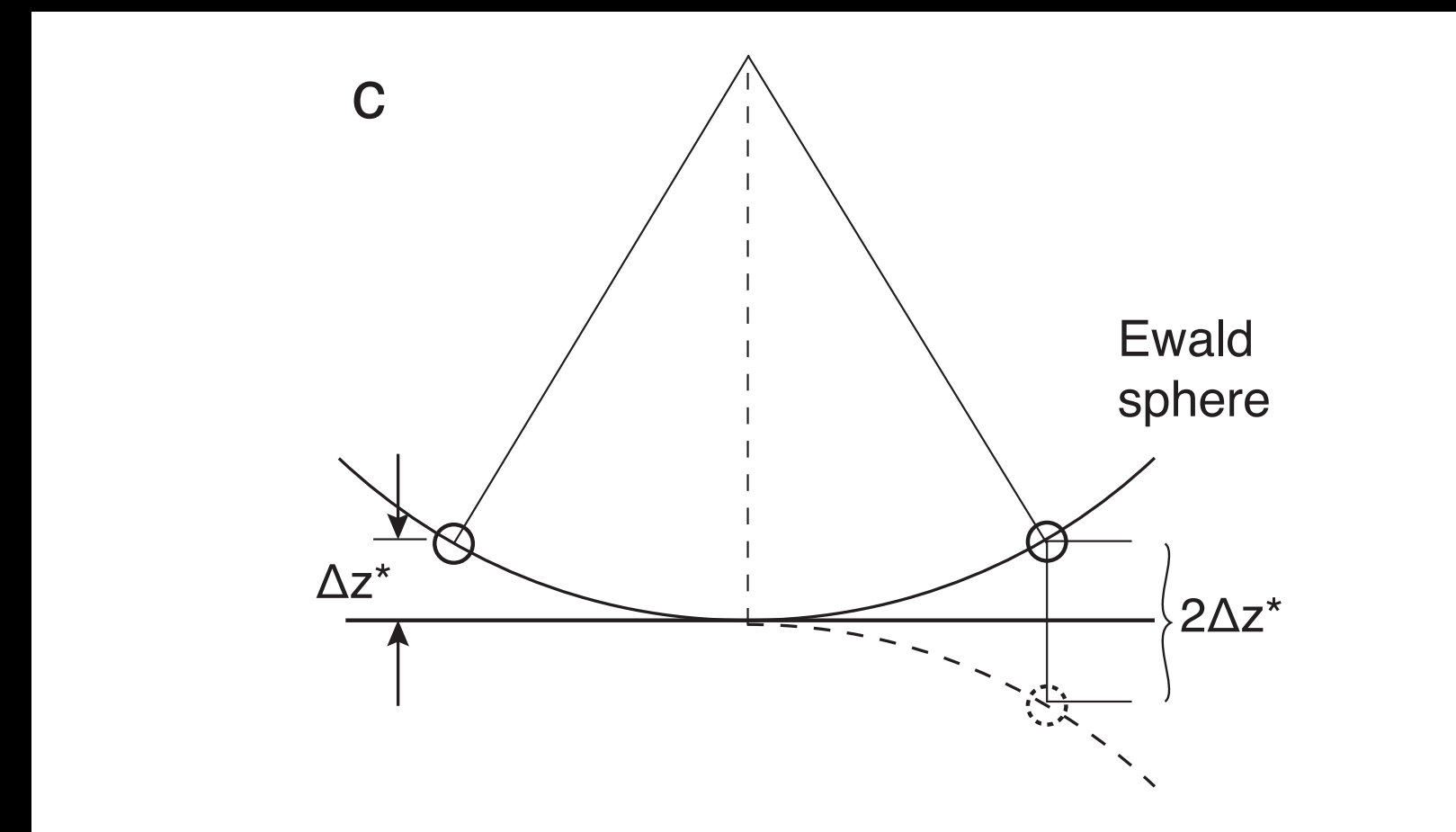


100 Å gold nanoparticle in ice
300 keV

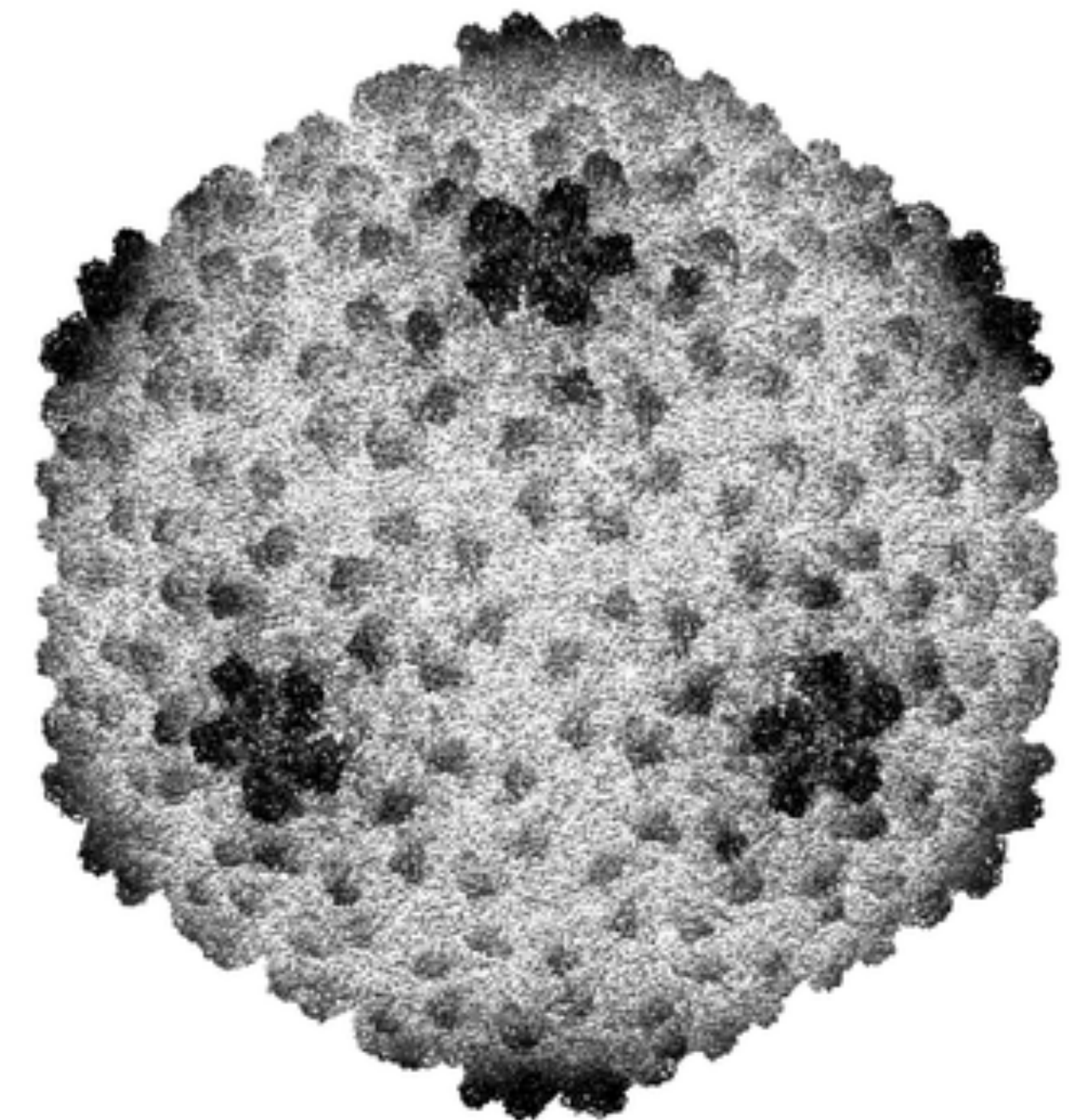
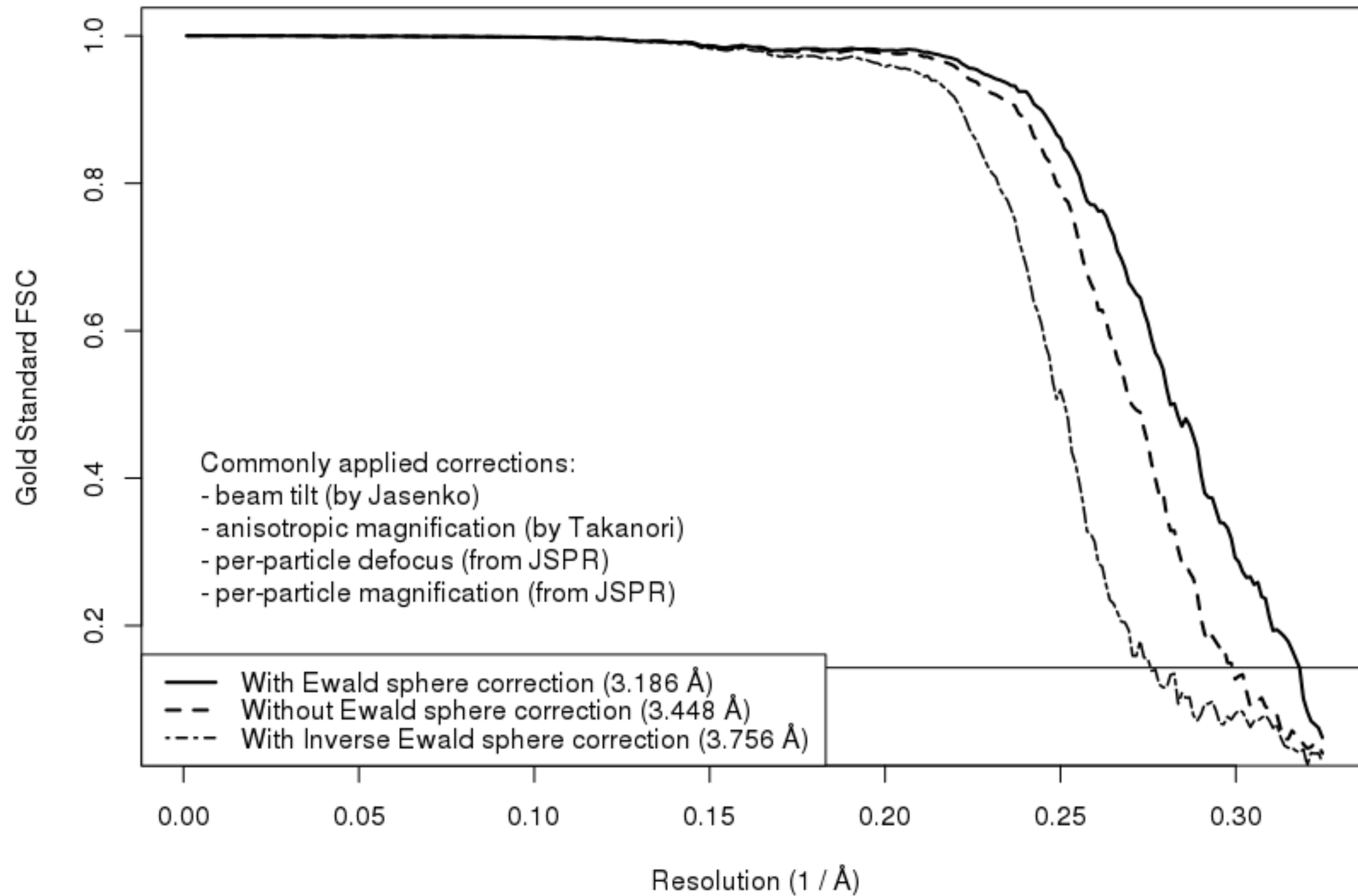




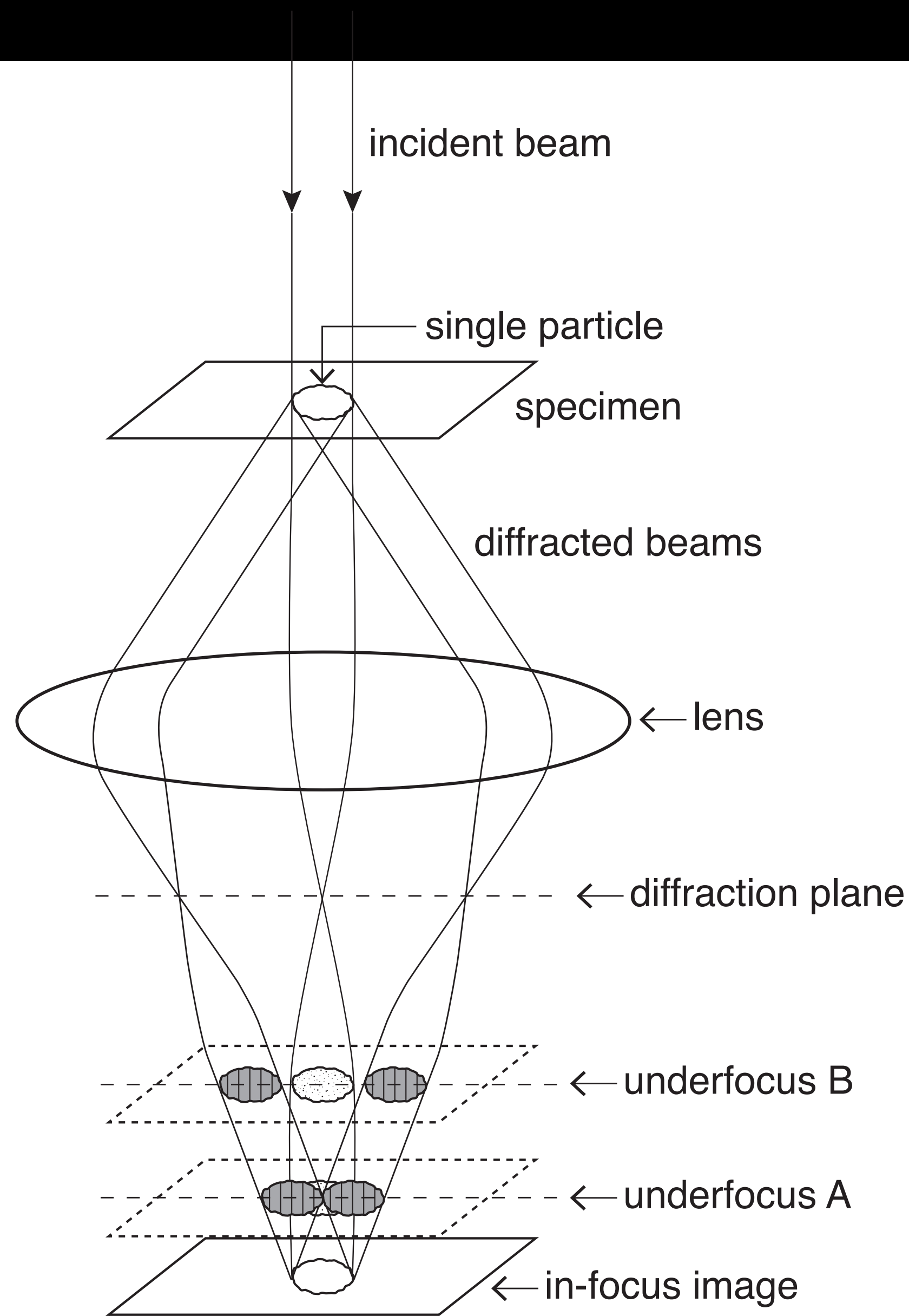
100 Å gold nanoparticle in ice
300 keV



P22 virion (EMPIAR 10083)



P22 virus structure
EMPIAR-10083

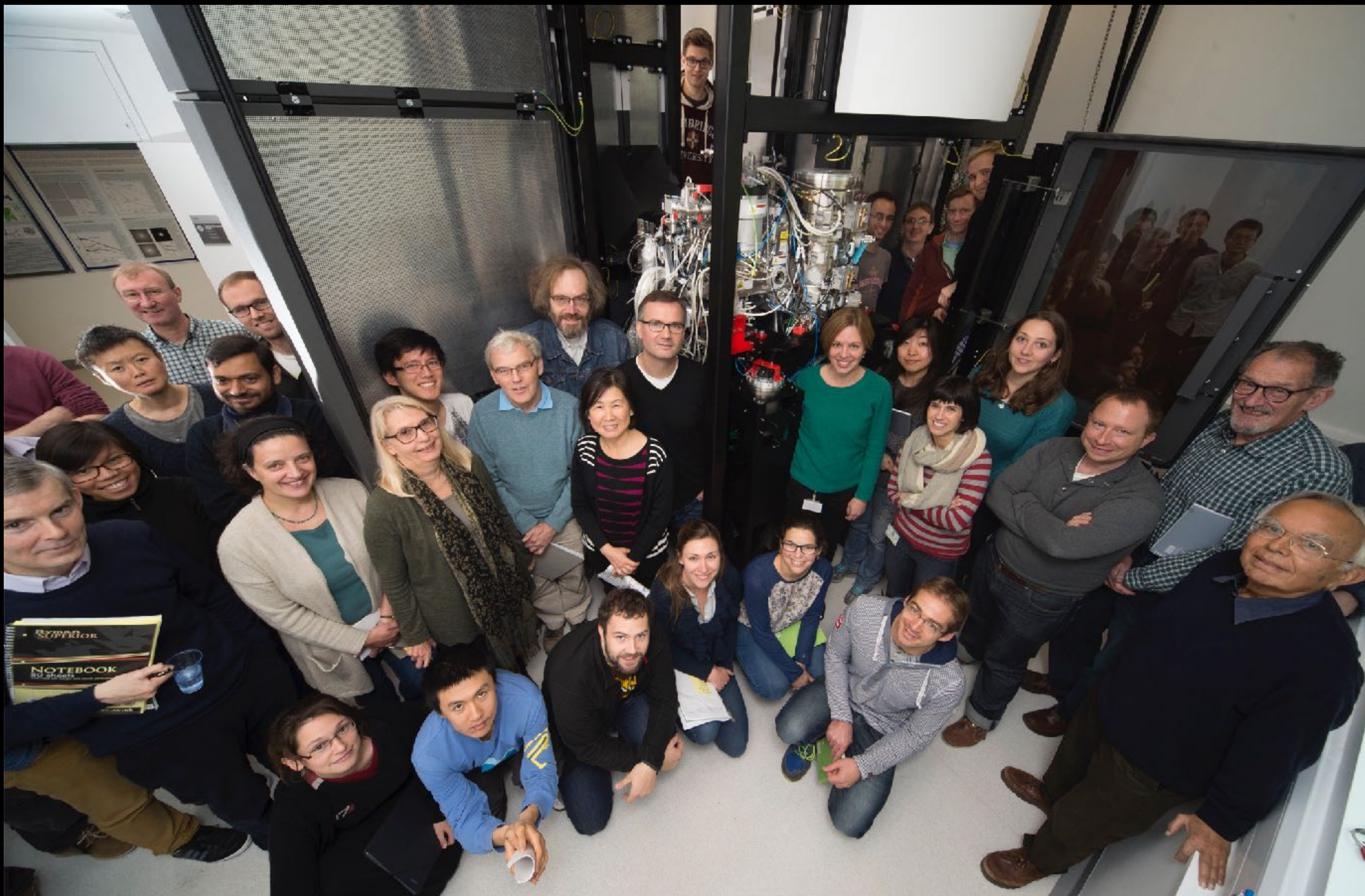


This correction method allows exact correction for Ewald sphere curvature in every micrograph

Collecting and processing images in this way will potentially improve the resolution of all cryoEM structures, particularly of those of large particles at high resolution

Perfect Ewald sphere correction will now allow the use of lower electron energies where the sphere is more curved without loss of high resolution information due to the incorrect assumption of a 2D projection

Thanks!



Greg McMullan
Wasi Faruqi
Shaoxia Chen
Christos Savva
Giuseppe Cannone
Tony Crowther
Lori Passmore
Nigel Unwin
Richard Henderson

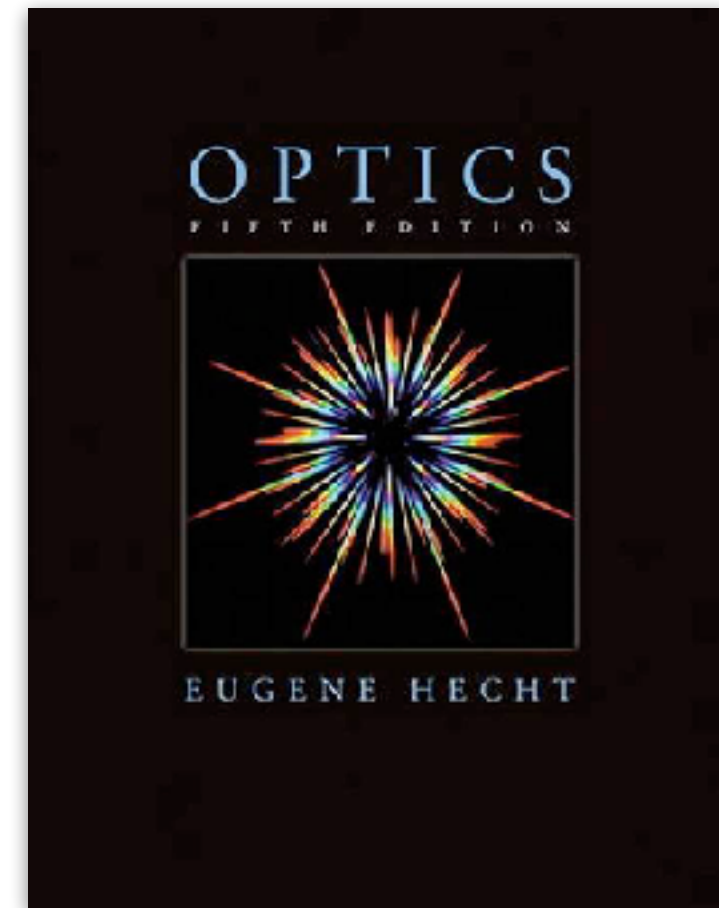
LMB workshops

**LMB Scientific
Computing**

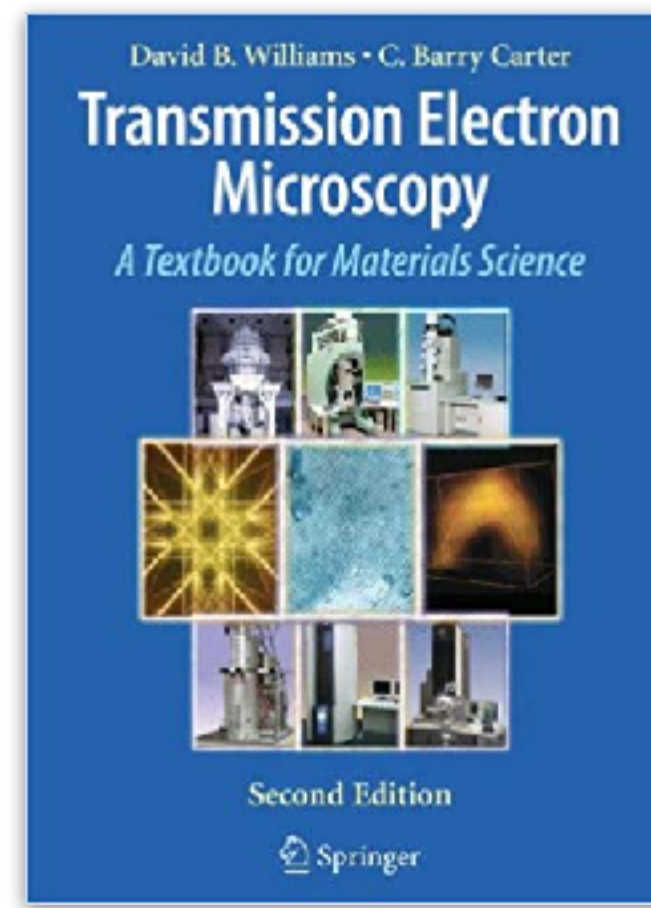
LMB IT

LMB Visual Aids

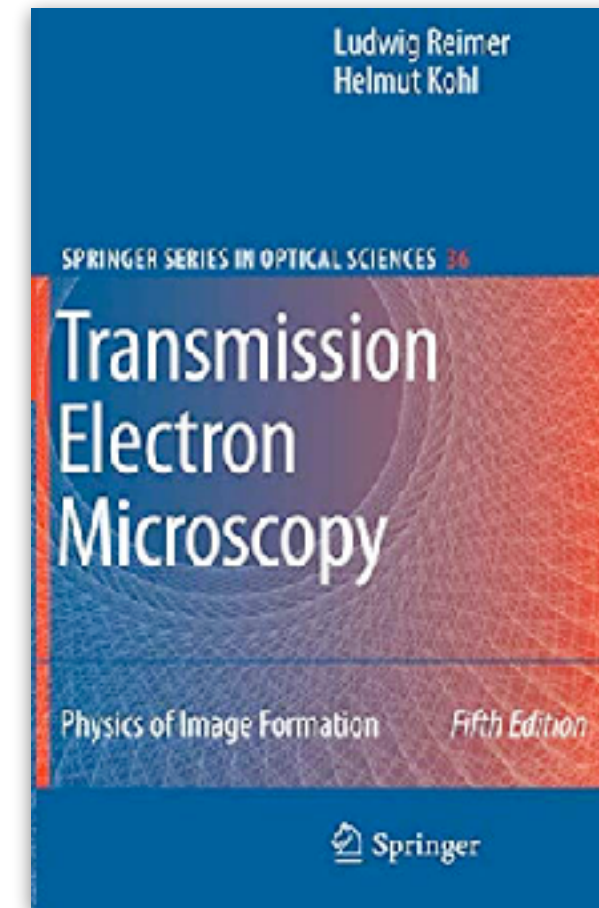
Some books you might want on your shelf



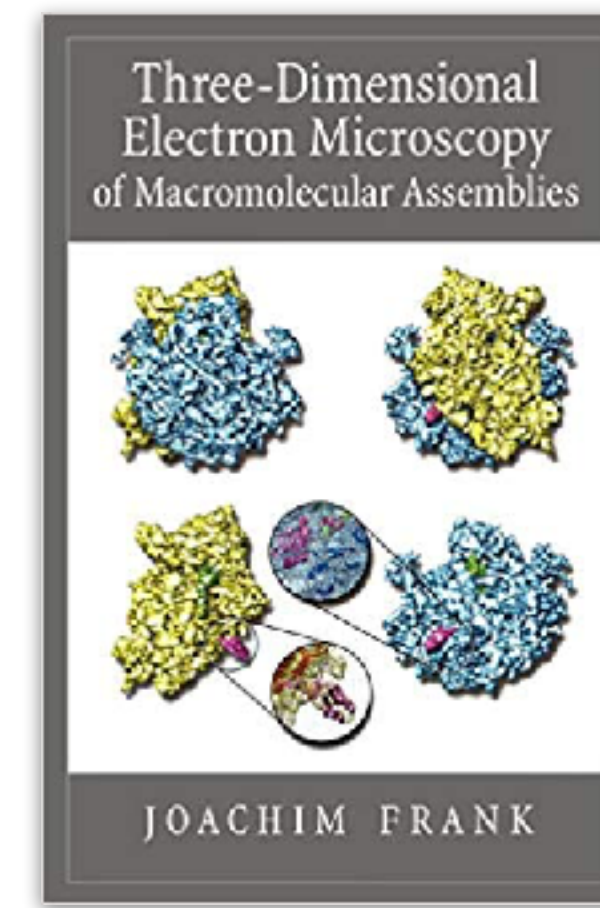
Hecht 3 - 5th ed.



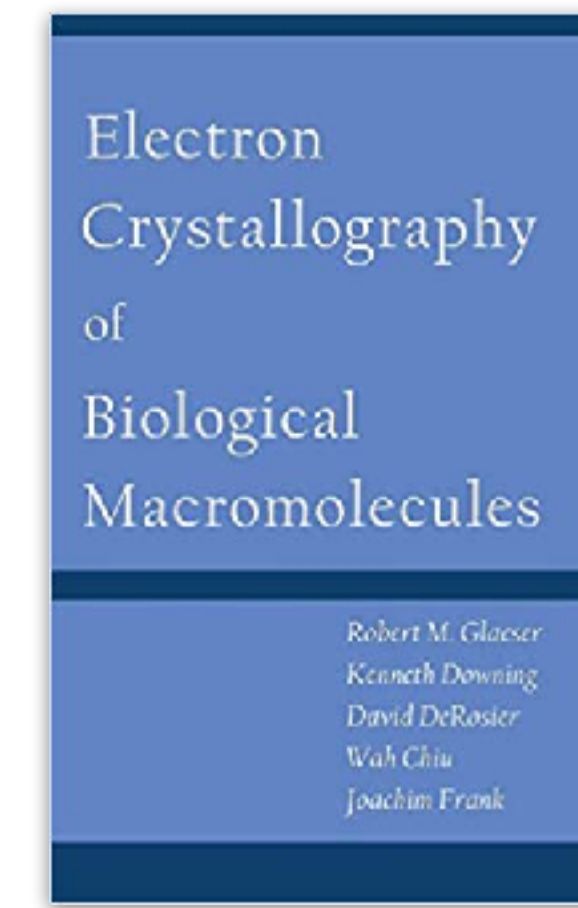
Williams and Carter 2nd or 3rd ed.



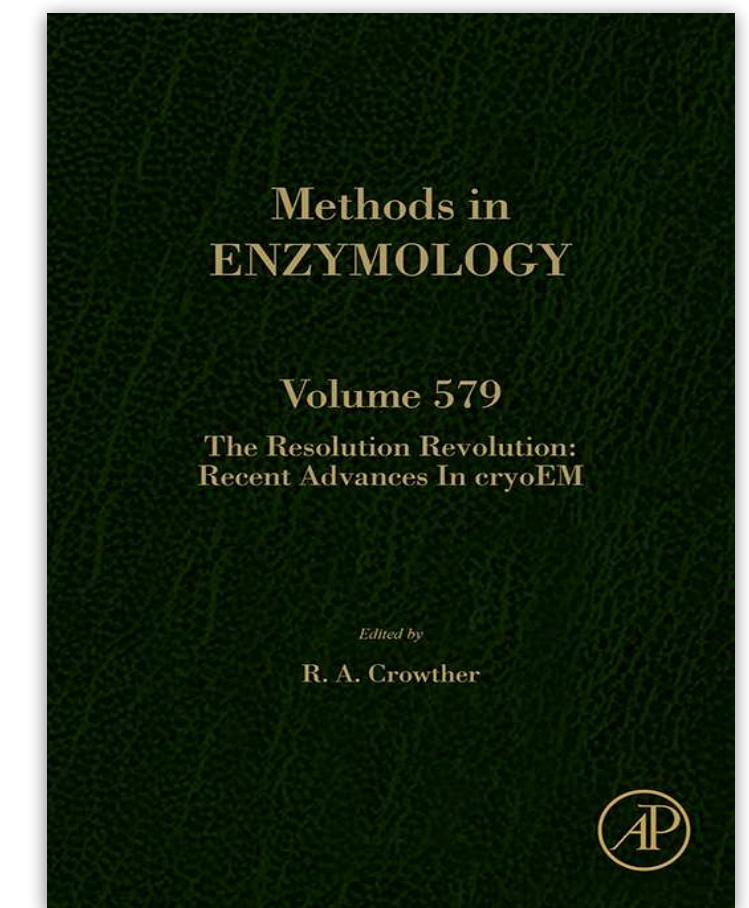
Reimer and Kohl 2008



Frank 2006



Glaser et al. 2007



MIE Volume 579 - Ed. RA Crowther

Copyright C. J. Russo, MRC Laboratory of Molecular Biology, 2019

All rights reserved.

The enclosed slides are provided for non-commercial, educational use only under the terms of The Creative Commons Attribution-NonCommercial 4.0 International License, and may contain reference to other material subject to copyright restrictions.

<https://creativecommons.org/licenses/by-nc/4.0/>